DYNAMIC PROCESSES IN MAGNETIC THIN FILMS

DOMAIN WALL MOTION AND FERROMAGNETIC RESONANCE

Thesis by

Carl E. Patton

In Partial Fulfillment of the Requirements

For the Degree of

Doctor of Philosophy

California Institute of Technology

Pasadena, California

1967

(Submitted April 5, 1967)

ii

ACKNOWLEDGEMENTS

Finally, the author wishes to gratefully acknowledge his wife Lois for her cheerful encouragement and support during his period of residence at the Institute and for her labors in the preparation of the final manuscript of this dissertation. Without her careful attention to the typing of the manuscript, as well as the numerous drafts, the appearance of this dissertation in final form would not have been possible.

ABSTRACT

The objective of the present investigation has been threefold:
(1) To characterize domain wall motion in thin ferromagnetic films
experimentally and to determine what film properties influence wall
mobility. (2) To investigate ferromagnetic resonance relaxation in
thin films over a wide range of temperature, frequency, and thickness
and to determine what physical relaxation processes contribute to the
resonance linewidth. (3) To correlate the losses for wall motion with
relaxation processes for ferromagnetic resonance.

Domain wall mobility for Ni-Fe alloy films has been measured as
a function of film thickness from 300 to 1650 $\mathring{A}$. Between 300 and 800 $\mathring{A}$,
the mobility decreases with increasing film thickness, ranging from
8×10^3 cm/sec·Oe at 300 $\mathring{A}$ to 3×10^3 cm/sec·Oe at 800 $\mathring{A}$. Between 900
and 1000 $\mathring{A}$, the mobility increases rapidly with increasing film thick-
ness to about 7×10^3 cm/sec·Oe. Above 1000 $\mathring{A}$, the mobility increases
slowly with film thickness. Predictions based on Lorentz microscopy
static wall shape measurements are in good agreement with the data for
a constant value of the Landau-Lifshitz damping parameter $\alpha = 0.014$.
Eddy-current losses are negligible. The crosstie and Bloch line
structures associated with domain walls in thin films do not appear to
influence the mobility. The sharp increase in mobility between 900 and
1000 $\mathring{A}$ is associated with a wall structure transition in this region.

Ferromagnetic resonance linewidth measurements have been made for films 150 to 3200 Å thick at frequencies from 1 to 9 Gc/sec and temperature from $2°K$ to $300°K$ with the static field in the film plane. Linewidths between 3 Oe (1 Gc/sec) and 50 Oe (9 Gc/sec) were observed. For fixed thickness, the $300°K$ linewidth increases monotonically with anisotropy dispersion. To eliminate dispersion, samples with the smallest linewidth (ΔH_{min}) were selected for each thickness. For thickness less than a critical thickness D_ω, ΔH_{min} is independent of thickness, but increases with thickness for $D > D_\omega$. The data are in good agreement with predictions based on two-magnon scattering between the uniform mode and degenerate magnons. Eddy-current losses are not important. The phenomenological damping varies from 0.005 (D = 400 Å) to 0.009 (D = 3200 Å) for the $300°K$ data. As a function of temperature, the linewidth exhibits a maximum at about $80°K$ which is generally larger in thinner films. The amplitude of the peak (as high as 15 Oe) is independent of frequency and the peak shifts to slightly higher temperatures with increasing frequency. Two annealing treatments at $150°C$, one in a vacuum and one in hydrogen or oxygen, indicate that the temperature dependence is associated with a surface oxide layer. Two mechanisms, valence exchange and exchange anisotropy, may be important.

Even though phenomenological damping parameters for the two processes, wall motion and resonance, are quite different (at $300°K$), there is a definite connection between the losses. Changes in the wall mobility between $300°K$ and $77°K$ have been measured for films exhibiting, to varying degrees, the above linewidth effect. From these mobility

and linewidth data, the losses for wall motion were found to be directly related to the losses for resonance from $300^{O}K$ to $77^{O}K$. There is a definite connection between the relaxation processes which are important for wall motion and those involved in resonance.

TABLE OF CONTENTS

Chapter 1. <u>INTRODUCTION</u>

Over the past decade, thin magnetic films have received consider-
able attention as potential computer memory elements which incorporate
the advantages of high speed, high packing density, and ease of fabri-
cation. A better understanding of the physical relaxation mechanisms
which control the magnetization motion during flux reversal is extremely
important if the greatest utility is to be realized from such memory
elements. Such an understanding has been the general objective of the
present investigation and is the subject of this report. The approach
has been to investigate two different extremes for magnetization motion:
(1) A large angle process, domain wall motion, which is directly rele-
vant to many memory devices, and (2) A small angle process, ferromagnet-
ic resonance, which is more amenable to fundamental interpretation.

The rate at which a moving domain wall can dissipate energy to the
lattice determines the magnitude of its velocity. Apart from eddy-
current losses, however, the energy dissipation mechanisms which limit
the wall velocity can best be described phenomenologically. Very
little information concerning physical relaxation processes can be
obtained. On the other hand, ferromagnetic resonance at low power
levels represents only a small perturbation on a system magnetized to
saturation. Some understanding of the resonance response of the system
in terms of fundamental physical processes is possible. Since both pro-
cesses simply represent different types of magnetization motion, it is

conceivable that the physical relaxation mechanisms which come out of

the resonance investigation may be directly applicable to wall motion

in particular and flux reversal in general.

Chapter 2. DOMAIN WALL MOTION

2.1 INTRODUCTION

The domain theory of Weiss (1907) provides the basis for under-
standing a large number of magnetic phenomena in ferromagnetic
materials. Weiss proposed that a ferromagnetic sample contains a
large number of small regions, called domains, within which the
magnetization $\overline{M}$ is constant in magnitude and direction. A change in
the total magnetization can occur at relatively low external fields
through an increase of the volume of those domains with $\overline{M}$ nearest the
field direction, at the expense of other domains. These Weiss domains
were observed experimentally by Bitter (1931) and the increase in
total magnetization at low fields was confirmed to occur by domain
growth as Weiss predicted.

Domain growth is associated with the motion of the transition
layer or wall between adjacent domains. The magnetization in adjacent
domains will lie along directions of lowest anisotropy energy (along
easy axes). In traversing the wall, the magnetization will not, in
general, lie along an easy direction and the domain wall will have an
associated anisotropy energy. The lowest anisotropy energy is
associated with a wall of zero width in which the magnetization
changes abruptly from one easy direction to another in traversing the
wall. All magnetization would then lie along some easy direction and

the anisotropy energy would be minimum. However, the exchange inter-
action between neighboring spins in the magnetic lattice gives rise to
an exchange energy which is proportional to the square of the angle
between adjacent spins and is minimum when all spins are aligned
parallel. If the wall had zero width and the magnetization changed
abruptly from one easy direction to another, the exchange energy
associated with the wall would be very large. Bloch (1932) was the
first to point out the importance of exchange in calculating the width
of the domain wall. The wall width in bulk material is determined
from a balance of the anisotropy energy (which is minimum for zero
width) and the exchange energy (which is minimum for infinite width).
A theory of the wall structure and a formula for its width and energy
was first worked out by Bloch (1932) and the domain wall is commonly
called the Bloch wall. Bloch, however, assumed that the magnetization
vanished at the center plane of the wall. The magnetization distribu-
tion which is usually associated with the Bloch wall is that proposed
by Landau and Lifshitz (1935) and shown in Fig.2-1 for the specific
case of a 180° Bloch wall separating antiparallel domains. The magni-
tude of $\overline{M}$ is constant but the magnetization turns about an axis perpen-
dicular to the plane of the wall (the axis defined by the tail positions
of the $\overline{M}$ vectors in Fig.2-1).

Under the influence of an applied field $\overline{H}$, domains with $\overline{M}$ oriented
nearest the field direction grow at the expense of other

-5-
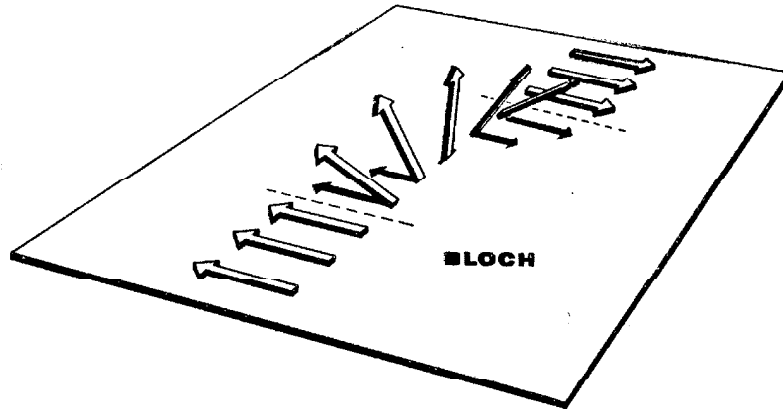
Fig.2-1. Magnetization distribution for Bloch walls. The magnitude of M is constant but the magnetization turns about an axis perpendicular to the plane of the wall (the axis defined by the tail positions of the M vectors). The magnetization remains in the plane of the wall.
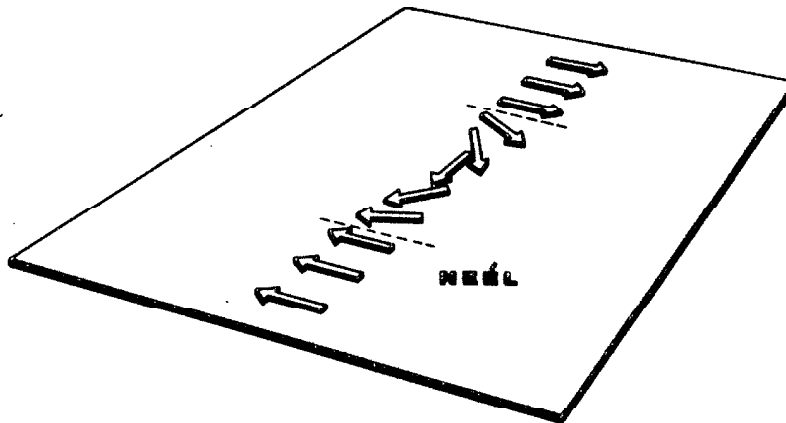
Fig.2-2. Magnetization distribution for Néel walls. The magnetization rotates in the plane of the film (represented by the flat plate).

domains and the total magnetic energy of the system ($-\overline{M} \cdot \overline{H}$ integrated over the volume of the system) is reduced. Domain growth occurs by the motion of Bloch walls and the associated energy loss must occur by energy dissipation within the walls during motion. Since the energy loss rate for the system will be determined by the velocity of the walls (wall motion controls how fast the domains oriented near the field direction can expand), the wall velocity will be limited by the rate at which energy dissipation can occur within the wall. If the wall is not capable of dissipating energy to the lattice by its motion, there will be no way for the system to lose magnetic energy and the walls will move with infinite velocity. (For a vanishingly small loss rate, the velocity is actually limited by the amount of wall distortion which can occur to produce the internal fields which move the wall. These internal fields, called Becker fields, will be discussed in section (2.2).) The domain wall velocity is loss limited and is controlled by the individual mechanisms by which energy is transferred from the magnetization motion within the wall to the lattice.

An understanding of the loss mechanisms by which the moving domain wall dissipates energy to the lattice is therefore an important prerequisite to any understanding of wall motion. Two loss mechanisms are of importance, relaxation losses and eddy-current losses. Relaxation losses denote those processes by which the magnetization motion is coupled directly to the lattice vibrations by various interactions

between the normal modes of the magnetic system (spin waves) and the normal modes of the lattice (phonons). Defined in this way the term "relaxation loss" can be adapted to include a large variety of physical interactions.. Eddy-current losses simply denote the joule heating of the system by the macroscopic eddy currents which are generated in the metal film because of the magnetization motion within the moving wall. Since both the spin-wave spectrum for the normal modes of the magnetic system and the eddy-current distribution depend on the magnetization distribution within the moving wall, the shape of the domain wall is expected to have a strong influence on both relaxation and eddy-current losses for wall motion. In order to understand these losses, a knowledge of the magnetization distribution associated with moving domain walls is required.

Thin ferromagnetic films are ideal structures for a study of domain wall motion for two reasons. Because of the thinness of the film, domain walls with their planes parallel to the film surface cannot occur and the domain configuration at the surface is representative of the whole film. For bulk material, the domain configuration deep inside the material cannot be determined with certainty. In addition, the magnetization distribution within domain walls (the wall shape) for thin films is understood in some detail. However, this information is for stationary walls in equilibrium (walls which are not moving) and in order to understand wall motion, a knowledge of the

magnetization distribution for moving walls is desirable. Since very little work has been done concerning moving walls, static wall shapes can be used as a starting point for the analysis of wall motion. If the static wall shape assumption is a poor one, the velocities predicted from the loss analysis based on static shapes may not be in agreement with experimental observations. On the other hand, if dynamic walls do not differ appreciably from static walls, the theoretical predictions and the experimental observations should be in agreement.

For thin films the domain wall energy is not determined solely from exchange and anisotropy as is the case for bulk material. If the rectangular plate in Fig.2-1 is taken to represent the film, it can be seen that the magnetization within the wall is discontinuous at the film surfaces. This discontinuity in magnetization at the film surfaces produces a magnetic field within the wall (usually called the stray field or demagnetizing field) and a resultant magnetostatic energy. For very thin films, when the film surfaces are separated by only several hundred angstroms, this magnetostatic energy density for the Bloch wall is quite large. Néel (1955) has pointed out that for extremely thin films (less than about 1000 Å thick for Ni-Fe alloy films with 80% Ni), there exists a completely new type of wall structure in which the magnetization is not discontinuous at the film surface. This structure is shown in Fig.2-2 and is usually called the

Néel wall. The magnetization rotates in the plane of the film instead of the plane of the wall. For thin films ($<$ 1000 Å thick), the stray field energy for Néel walls is lower than for Bloch walls.

Middelhoek (1961), Brown and LaBonte (1965) and others have calculated, with various degrees of accuracy, the detailed shapes for both Bloch and Néel walls in thin films. In addition, an extensive experimental investigation of the Néel wall shape for Ni-Fe alloy films (80% Ni) 100-800 Å thick has been carried out by Fuchs (1962) using the techniques of out-of-focus electron microscopy (Lorentz microscopy). This domain wall shape information is of extreme importance in understanding the losses associated with wall motion.

The first actual calculation of the domain wall velocity was carried out by Landau and Lifshitz (1935) for 180° Bloch walls separating antiparallel domains in bulk material by considering only relaxation losses which were treated in a phenomenological manner. The Landau-Lifshitz phenomenological equation of motion for the magnetization has been used extensively for a wide variety of problems involving magnetization dynamics. The Landau-Lifshitz treatment was extended by Galt (1952) to obtain the domain wall velocity for 180° walls in terms of an arbitrary magnetization distribution within the wall. Galt's result is particularly useful for calculating the relaxation-loss limited velocity in thin films where the wall shape and the type of

wall (Bloch or Néel) is dependent on the thickness of the film. The only calculation of the eddy-current loss-limited wall velocity is the analysis by Williams, Shockley, and Kittel (1950) in which the moving domain wall was approximated by a transition region of zero width. The calculation was carried out for a long rectangular bar. Ford (1960) has adapted their result to thin film geometry but the effect of the zero-width wall approximation on the calculation has not been considered.

Several experimental investigations have been reported, which undertake to characterize wall motion in terms of relaxation losses or eddy-current losses. Menyuk (1955) observed the reversal time in Permalloy tape cores varying in tape thickness from 3×10^4 to 3×10^5 Å. By observing the thickness dependence of the reversal time he concluded that eddy-current losses were negligible for tapes thinner than 3×10^4 Å and that wall velocity was relaxation-loss limited. Ford (1960), on the other hand, measured domain wall velocities for films 700-4000 Å thick which were consistent with predictions based on eddy-current losses and concluded that wall velocity was eddy-current loss limited. Recent wall motion measurements by Copeland and Humphrey (1963), Il'icheva and Kolotov (1965), Patton and Humphrey (1966a), and Middelhoek (1966) are at variance with Ford's data and indicate that the velocity is relaxation-loss limited.

Both the experimental results and the theoretical treatments for wall motion in thin films are in poor shape. The existing data for wall motion by various workers are not in agreement. No consistent interpretation of these data in terms of relaxation and eddy-current losses has been reported. In this chapter, wall motion in thin ferromagnetic films is examined both experimentally and theoretically. In the next section, the theoretical relaxation-loss limited velocity is calculated, taking advantage of existing theoretical and experimental wall shape information. In section (2.3), the eddy-current loss-limited velocity is calculated. Ford's extension of the Williams et al. result is improved by including the effect of the nonzero wall width and the stray field on the eddy-current distribution. Once these two loss mechanisms are understood, the wall velocity limited by both processes can be calculated. In section (2.4) an experimental technique for measuring wall velocity in thin films is described in detail and in section (2.5) the results of an extensive experimental study of wall motion in thin films are compared with the theoretical predictions based on relaxation and eddy-current losses. The results of the present investigation, theoretical and experimental, are summarized in section (2.6).

2.2 RELAXATION LOSSES

2.2.1 Phenomenological Formulation

Relaxation losses for wall motion have been defined in a very general way in terms of elementary interactions between the magnetic normal modes and the normal modes of the lattice. Such a definition is satisfying, from a fundamental point of view, inasmuch as it specifies the nature of the physical processes which are involved. In practice, however, this definition is of little utility. Calculations of relaxation losses for wall motion have all been phenomenological, not because there has been any clear connection between physical relaxation processes and a purely phenomenological formulation but because no technique for calculating relaxation losses from physical principles has yet been developed. The justification of a phenomenological formulation rests primarily in its mathematical simplicity.

The use of the phenomenological loss formulation in treating wall motion has not been consistent. In the absence of any real understanding of the physical processes involved, the choice as to what losses should be included in (or excluded from) such a formulation has been rather arbitrary. This is evident even in the first phenomenological treatment by Landau and Lifshitz (1935) who thought that the losses had a relativistic origin. Smith (1963) has worked backwards, by reducing eddy-current losses (a well understood physical concept) to

a phenomenological formulation. Middelhoek (1966) has included the
effects of macroscopic film imperfections and impurities on wall motion
in defining the phenomenological losses.

For the present purpose of understanding wall motion, phenomeno-
logical will be taken to denote those processes which cannot be calcu-
lated (or at least understood) in terms of basic physical principles.
Eddy-current losses are excluded since they can be calculated from
electromagnetic theory. The losses which result from the interaction
of the walls with macroscopic film imperfections and impurities are
excluded because such losses can be qualitatively understood from
magnetostatic considerations and can be eliminated experimentally by
careful sample preparation.

The spirit of the phenomenological approach to relaxation losses
can be obtained by considering a very simple viscous damping model for
wall motion. For purposes of calculation, consider the simple domain
geometry and co-ordinate system shown in Fig.2-3. The ferromagnetic
film specimen possesses a uniaxial anisotropy along the z-axis (the
anisotropy energy is minimum when $\overline{M}$ is along the z-axis). A single
isolated domain wall is located in the film aligned with the easy axis,
separating two antiparallel domains (labeled I and II). A magnetic
field of amplitude H is applied along the anisotropy axis (easy-axis)
causing domain I to become larger at the expense of domain II. The
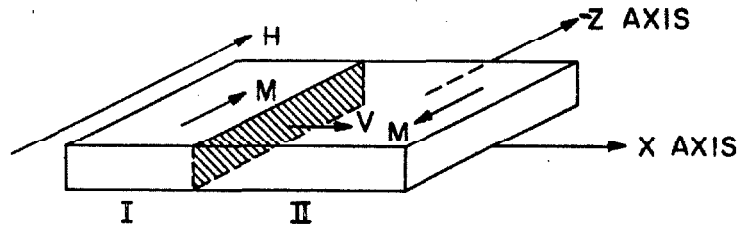
Fig.2-3. Domain geometry for wall motion. The domain wall is oriented with its plane parallel to the easy-axis (z-direction) and moves at a constant velocity v in the x-direction under the influence of an easy-axis field H.
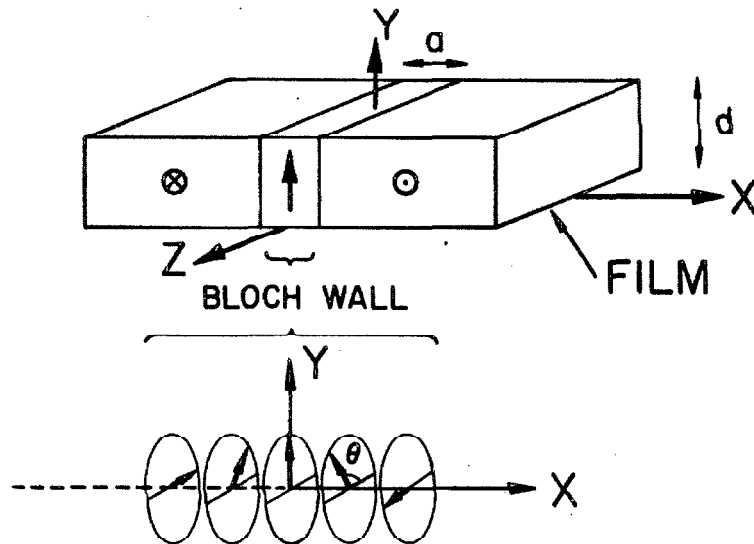
Fig.2-4. Bloch wall structure and co-ordinate system for calculating the losses associated with wall motion. The wall is moving in the x-direction and is shown at the instant when the center of the wall coincides with the y-z plane.

growth of I occurs by the displacement of the wall in the positive

x-direction with some velocity v. All interactions between the domain

wall and the edges of the film are neglected. More complicated

situations are possible in which the domain wall does not lie along the

easy-axis or the velocity is not at right angles to the wall plane.

Figure 2-3, however, describes the simplest situation which can be

obtained experimentally.

Details of the Bloch wall structure for this geometry are shown in

Fig.2-4, at the instant (t = 0) when the center plane of the wall

coincides with x = 0. For Néel walls, the magnetization rotation would

be confined to the x:z plane (film plane) instead of the y:z plane

(wall plane). Consider the magnetization of a small volume ΔV ini-

tially in domain II. As the wall moves past this volume, the magneti-

zation will rotate from its initial position in the z-direction at

$\theta = \pi$ to a final position in the negative z-direction at $\theta = 0$ (corre-

sponding to domain I). If this rotation is viewed as the simple motion

of a physical vector in a viscous fluid, the viscous torque associated

with the motion can be written as $-C(d\theta/dt)\Delta V$, where C is a viscous

damping constant. In rotating from $\theta = \pi$ to $\theta = 0$, the magnetization

loses energy equal to $2MH\Delta V$ per unit volume. The viscous damping

energy loss is given by the integral of $C(d\theta/dt)\Delta V$ from $\theta = 0$ to $\theta = \pi$.

Since the magnetostatic energy decrease $(-2MH\Delta V)$ can only occur by energy

dissipation within the wall due to the viscous torque,

$$2MH = \int_{\pi}^{o} C(d\theta/dt)d\theta \qquad (2.1)$$

If the wall is situated as shown in Fig.2-4, for the magnetization within the wall at an angle θ with the negative z axis, $d\theta/dt$ is equal to $-v(d\theta/dx)$. With this substitution in Eq.(2.1), the domain wall velocity can be seen to be

$$v = (2MH/C)\left[\int_{o}^{\pi}(d\theta/dx)_{t=0}d\theta\right]^{-1}. \qquad (2.2)$$

An important assumption implicit in the previous derivation concerns the shape of the moving wall. In the same way that a physical mass moving under the influence of gravity in a viscous fluid falls with a constant velocity due to the balance of the viscous force against the gravitational force, the rotating magnetization vector in the moving wall can be considered to represent a dynamic equilibrium situation, in which all the torques acting on the magnetization sum to zero. The exchange, anisotropy, and stray field energy of the wall each have an associated torque. The viscous torque has already been considered and the field torque is given by $(\overline{M} \times \overline{H})$. Equation (2.2) can also be derived by assuming a balance between the field torque and the viscous torque. Since for dynamic equilibrium the total torque

must vanish, the sum of the exchange, anisotropy, and stray field torques must also vanish. This static equilibrium between the exchange, anisotropy, and stray field torques is precisely the criteria for determining the static domain wall shape corresponding to a stationary wall with minimum energy. Therefore, this analysis makes the implicit assumption that the moving wall has the same magnetization distribution as a static wall. In general, an exact balance between the field torque and the viscous damping torque cannot be obtained for static wall shapes. However, the exchange, anisotropy, and stray field torques are usually much larger than the field or viscous damping torques for the wall motion which is of interest here and the above conclusions are quite accurate.

Two other important properties of this derivation should be pointed out. The velocity is a linear function of the applied field and is inversely proportional to the viscous loss parameter C. Both of these properties are a result of the quadratic dependence of the energy dissipation rate on velocity which can be demonstrated by multiplying both sides of Eq.(2.1) by v. Then

$$2MHv = Cv^2 \int_0^\pi (d\theta/dx)d\theta \qquad (2.3)$$

using the substitutions noted above. The left hand side (L.H.S.) represents the rate at which a unit area of wall moving at velocity v reduces the energy of the system. The right hand side (R.H.S.)

balances this energy reduction rate with the dissipation rate for the moving wall. The linear dependence of velocity on H and the inverse dependence on C follow directly from Eq.(2.3). In passing, it is worthwhile to note that the form of Eq.(2.3) is similar to that which will be obtained for eddy-current losses in section (2.3). Only the coefficient of v^2 on the R.H.S. will be different. This similarity will simplify considerably the final calculation of the velocity.

The velocity in Eq.(2.2) is a linear function of the H. For this situation, a convenient approach is to characterize the wall motion by a field independent parameter, the wall mobility, which can be defined as the rate of change of velocity with respect to the applied easy-axis field, $G = \partial v/\partial H$. As derived from the viscous damping model and the static wall shape assumption, the wall mobility is independent of field and depends only on the magnetization of the sample, the viscous damping parameter and the domain wall shape (which is needed to evaluate the integral in Eq.(2.2)). The mobility, then, is determined by the material properties of the sample and film thickness (which influences the wall shape).

The foregoing analysis has been developed on the basis of a simple viscous damping model. This model is useful in illustrating the basic assumptions and results which come out of the phenomenological formulation. The standard phenomenological treatments, however, do not

utilize this simple approach. These treatments start with the usual

undamped equation of motion of the magnetization

$$(d\overline{M}/dt)_{precession} = -\gamma(\overline{M} \times \overline{H}_i) \qquad (2.4)$$

where $\overline{H}_i$ is the total internal field acting on $\overline{M}$ and γ is the gyromag-

netic ratio (taken to be positive for electrons). A number of

phenomenological damping terms are in common use. These are terms

which are added to the R.H.S. of Eq. (2.4) to account for losses in the

magnetic system. One form, proposed by Landau and Lifshitz (1935)

puts the equation of motion into a form:

$$d\overline{M}/dt = -\gamma(\overline{M} \times \overline{H}_i) + (\alpha\gamma/M)\ \overline{M} \times (\overline{M} \times \overline{H}_i) \quad . \qquad (2.5)$$

The damping term represents a relaxation of $\overline{M}$ toward $\overline{H}_i$ with the magni-

tude $|\overline{M}|$ unchanged. The damping motion for the Landau-Lifshitz

equation is proportional to only the precession component of $d\overline{M}/dt$

($\overline{M} \times \overline{H}$ in the last term of Eq.(2.5)). In the spirit of the viscous

damping model, the damping motion should be proportional to the total

$d\overline{M}/dt$ such that

$$d\overline{M}/dt = -\gamma(\overline{M} \times \overline{H}_i) + (\alpha/M)(\overline{M} \times d\overline{M}/dt). \qquad (2.6)$$

This equation of motion is in the form originally proposed by Gilbert (1955). If the damping parameter α is small, $(d\bar{M}/dt)$ will be nearly equal to $(d\bar{M}/dt)_{precession}$ and the differences between Eq.(2.5) and (2.6) will be negligible.

Equation (2.5) has been applied to the analysis of domain wall motion (Galt, 1952), with results which are similar to those obtained from the simple viscous damping model. The mathematical details are not of prime importance here but the results are relevant to this discussion. From the magnetization distribution inside the wall (see Fig.2-4), for an applied field in the z-direction Eq.(2.5) clearly does not predict the magnetization rotation in the y-z plane (for Bloch walls) assumed in the viscous damping analysis. Equation (2.5) predicts, instead, that $\bar{M}$ will tip out of the wall plane, with an x-component normal to the wall. This tendency of $\bar{M}$ in a Bloch wall to have a component normal to the wall for an applied easy-axis field (first pointed out by Becker, 1951) gives rise to a demagnetizing field in the x-direction, commonly called the Becker field. The magnetization rotation in the wall plane about the x-axis, assumed in the viscous damping analysis, results from the magnetization precession about this x-directed Becker field. From Eq.(2.4) the magnetization precession rate in the moving wall, $d\theta/dt = v(d\theta/dx)$, requires that

$$\bar{H}_{Becker} = -(\bar{v}/\gamma)(d\theta/dx). \qquad (2.7)$$

The most important result of the Becker field treatment is that for wall motion to occur, some distortion of the static wall shape is required in order to produce the internal field necessary for magnetization rotation during wall motion. For undistorted walls, there are no such internal fields which can act on $\bar{M}$. Without a component of $\bar{M}$ along the wall normal (for Bloch walls), the Becker field is zero and no rotation can take place. This requirement appears to be in complete contradiction with the earlier static wall shape assumption for the viscous damping treatment. This apparent contradiction can be partially resolved by noting that $4\pi M$ for ferromagnetic materials is usually quite large ($\approx 10^4$ Oe for Ni-Fe alloys with 80% Ni) and large Becker fields (≈ 100 Oe) can be produced by extremely small x-components of $\bar{M}$. This wall distortion is extremely important in a physical interpretation of wall motion in terms of Eq.(2.5), but is so small that the static wall shape assumption is still approximately valid.

The energy dissipation rate per unit volume within the moving wall ($\bar{H} \cdot d\bar{M}/dt$) can be calculated from Eq.(2.5) and is approximately equal to $(\alpha \gamma M)H_{Becker}^2$, if $H_{Becker} >> H$ (Galt, 1951). By integrating this dissipation rate over the wall, a rate-balance equation identical to Eq.(2.3) with $C = M\alpha/\gamma$ is obtained. With this substitution, the

relaxation-loss limited mobility G_α can be written as

$$G_\alpha = (2\gamma/\alpha) \left[\int_0^\pi (d\theta/dx)_{t\,=\,0} d\theta \right]^{-1} \qquad (2.8)$$

using the above expression for $\overline{H}_{Becker}$ and $G = \partial v/\partial H$. Equation (2.8) will be used extensively to calculate the relaxation-loss limited mobility. The foregoing discussion has been concerned with Bloch wall motion. For Néel wall motion, a similar analysis is possible (H_{Becker} in the z-direction) and the results are identical. The damping parameter α (usually called the Landau-Lifshitz damping parameter) is a phenomenological measure of the relaxation losses for wall motion.

As evident from Eq.(2.8), the two particulars of the magnetic system which are required in order to calculate the domain wall mobility are the damping parameter α and the wall shape $\theta(x)$. The damping is phenomenological and can only be determined experimentally. If relaxation losses could be calculated explicitly, it would not be necessary to resort to a phenomenological analysis in the first place. In fact, the determination of this parameter for wall motion is one of the important results of this investigation.

The other important particular is the wall shape, $\theta(x)$. In the previous discussion it has been assumed that the magnetization orientation in the wall is only a function of distance along the wall normal

and that $\bar{M}$ remained either in the wall plane (Bloch walls) or in the film plane (Néel walls). Even with these simplifying assumptions, the problem of calculating wall structure is a complicated one. For some situations, the problem is simplified by the possibility of experimental determinations of wall structure. In any case, wall structure information is an important prerequisite to any real understanding in relaxation losses for wall motion. The problem of wall structure in thin films and its relation to the wall mobility will be considered in the next part of this section.

2.2.2 Wall Shape Considerations

The conceptual problems connected with the phenomenological treatment of relaxation losses has been considered in detail and the importance of wall shape in this treatment has been pointed out. Without a knowledge of wall structure, the mobility expression for C_α in Eq.(2.8) is of little use. In the remainder of this section, the present day understanding of static wall structure in thin films will be reviewed and this knowledge will be used in a further discussion of Eq.(2.8) and the relaxation-loss limited wall mobility. It is important to keep in mind the fact that the static wall shape assumption is not a trivial one, and that it can serve only as a starting point for treating relaxation losses for wall motion. The test of the validity of this assumption can come only from comparison with experiment.

The Bloch wall energy and shape $\theta(x)$ for bulk material is deter-
mined by the balance between exchange and anisotropy energies, but in
thin films a magnetostatic energy term is also of importance. The
origin of this energy term can be understood in terms of a conceptual
magnetic charge density defined by $\rho_m = -\nabla \cdot \overline{M}$, by analogy with electro-
statics where $\rho = -\nabla \cdot \overline{P}$ ($\overline{P}$ is the electric polarization). In the same
way that electric fields are associated with an electrostatic charge
density, magnetic fields are associated with ρ_m. For a Bloch wall,
$\nabla \cdot \overline{M} = 0$ everywhere except where the wall intersects the surface of the
material. For bulk material the magnetostatic field is large only
near the surface and has little effect on the energy of walls deep
within the material. For films, however, all of the material is near
the surface. For the wall and film geometry of Fig.2-4, the positive
magnetostatic charge density at the upper film surface
$\rho_m(y = D) = M \sin\theta$ and the negative density on the opposite lower
surface $\rho_m(y = 0) = -M \sin\theta$ produce a magnetostatic stray field within
the wall which has considerable influence on the wall energy and shape.
The magnetostatic charges associated with the wall intersections with
the film surfaces correspond to + signs and - signs on the upper
and lower film surfaces in Fig.2-4. For the Bloch wall in Fig.2-4, the
largest component of the stray field (H_{stray}) is in the negative
y-direction. The magnetostatic stray field energy density of the wall

(per unit area of wall surface in the y:z plane) is given by

$$E_{stray} = - \int_{-a/2}^{+a/2} \overline{H}_{stray} \cdot \overline{M} \, dx \qquad (2.9)$$

if a is taken to be the width of the wall centered at the origin. For Bloch walls, it should be emphasized that the stray field results from a surface charge density and is negligible (i.e. E_{stray} is negligible) when the film thickness is large (D $\gg$ a).

If the stray field energy is neglected, the Bloch wall energy and shape, determined by a balance between exchange and anisotropy, are the same as for bulk material and a $\approx \pi\sqrt{A/K}$ (Landau and Lifshitz, 1935). For typical values of 10^{-6} erg/cm for the exchange constant A and 10^{3} erg/cm^{3} for the uniaxial anisotropy constant K in 80% Ni-20% Fe films, a $\approx$ 13,000 Å. The effect of the stray field on Bloch wall shapes for thin films can be qualitatively understood in terms of a simple model based on Eq.(2.9) and Fig.2-4. If $\theta(x)$ is approximated by

$$\theta = \pi(x/a + 1/2) \qquad -a/2 < x < a/2 \qquad (2.10)$$

and H_{stray} is approximated by

$$\overline{H}_{stray} = -(\text{Const}) \{a/(a + D)\}\overline{e}_{y} \qquad -a/2 < x < a/2 \qquad (2.11)$$

so that $H_{stray} \approx 0$ for $D >> a$ (the bulk limit), E_{stray} is proportional to $a^2/(a + D)$. In Eq.(2.11), $\bar{e}_y$ is a unit vector in the y-direction. The stray field energy for Bloch walls in thin films has an effect similar to the anisotropy energy in reducing the wall width as discussed in section (2.1).

Because of exchange, the wall width cannot go to zero and for sufficiently thin films there is a sizeable stray field energy due to the finite Bloch wall width. As mentioned in section (2.1), the Néel wall configuration of Fig.2-2 does not have the large E_{stray} associated with Bloch walls in thin films. In Fig.2-4, if the magnetization were constrained to rotate in the x:z plane instead of the y:z plane, there would be no ρ_m associated with the wall intersection at the film surface (since $\rho_m = -\nabla \cdot \bar{M}$, both M_y and $\partial M_y/\partial y$ are zero). However, since M_x is non-zero $\partial M_x/\partial x$ is also non-zero ($\theta = \theta(x)$) and there will be a volume distribution of magnetostatic charge associated with the Néel wall configuration (in contrast with the surface charge for Bloch walls). If the rotation of $\bar{M}$ in the x:z plane of Fig.2-4 were such that $M_x > 0$, this volume distribution of ρ_m could be indicated by putting + signs in the wall for $0 < x < a/2$ and - signs in the wall for $-a/2 < x < 0$. Since a volume charge distribution is now involved, as $D \longrightarrow 0$ the charges vanish and the stray field energy is zero. For Néel walls in thin films in the limit $D \rightarrow 0$, the wall energy and shape $\theta(x)$ are determined only by exchange and anisotropy

with results identical to those for Bloch walls in bulk material (i.e. a $\approx$ 13,000 $\overset{o}{A}$). For Néel walls, the stray field expression analagous to Eq.(2.11) is

$$\overline{H}_{stray} = -(Const)\{D/(a + D)\}\overline{e}_x \qquad (2.12)$$

which vanishes as $D \longrightarrow 0$, in line with the above reasoning. In Eq.(2.12), $\overline{e}_x$ is a unit vector in the x-direction. From Eqs.(2.10) and (2.12), an argument can be developed for Néel walls which is very similar to that for Bloch walls. For Néel walls, however, $E_{stray} \approx aD/(a + D)$ which vanishes for $D = 0$ instead of for infinite thickness (bulk). The wall narrows (as E_{stray} increases) with increasing thickness.

The first calculation of the thickness dependence of the energy and width for Bloch and Néel walls was done by Néel (1955). This initial calculation used the linear wall shape trial function of Eq.(2.10) (θ is a linear function of x) and the stray field approximations of Eqs.(2.11) and (2.12). Exchange, anisotropy, and magnetostatic energy terms were included in the calculation. More recently, this calculation has been repeated by Middelhoek (1961), using a slightly different constant in Eq.(2.11) and (2.12). Middelhoek presented numerical results evaluated using material constants typical of the films of experimental interest (80-20 Ni-Fe

films, A = 10^{-6} erg/cm, K = 10^3 erg/cm^3, 4πM = 10^4 Gauss). His results

for Bloch and Néel wall width as a function of film thickness are

shown in Fig.2-5 by the solid lines. As discussed, the Néel wall width

is about 13,000 Å (the Landau-Lifshitz result for Bloch walls in bulk)

for zero thickness and narrows with increasing film thickness. The

Bloch wall narrows with decreasing thickness. Middelhoek's results

for the wall energy are not shown but Bloch walls are predicted for

D < 400 Å and Néel walls are predicted for D > 400 Å.

The change in wall structure as a function of film thickness and

the existence of both Bloch and Néel walls can be understood in terms

of the simple one-dimensional θ = θ(x) wall models which have been

considered. The models, however, have been very restrictive, permitting

the magnetization to rotate only in the y:z or the x:z plane with the

θ = θ(x) only. It is entirely possible that more complicated

magnetization distributions will result in a lower stray field energy

(and wider walls) than the simple distributions discussed above. The

solid lines in Fig.2-5, then, represent a lower limit for the wall

width in thin films. If other magnetization distributions result in

reduced E_{stray}, the walls will be wider. The upper limit of 13,000 Å

for E_{stray} = 0 is, of course, still valid. Even for the simple one-

dimensional model discussed here, wall shape and energy calculations

are extremely complicated and usually must be done using numerical

methods. Several workers have carried out this same calculation using

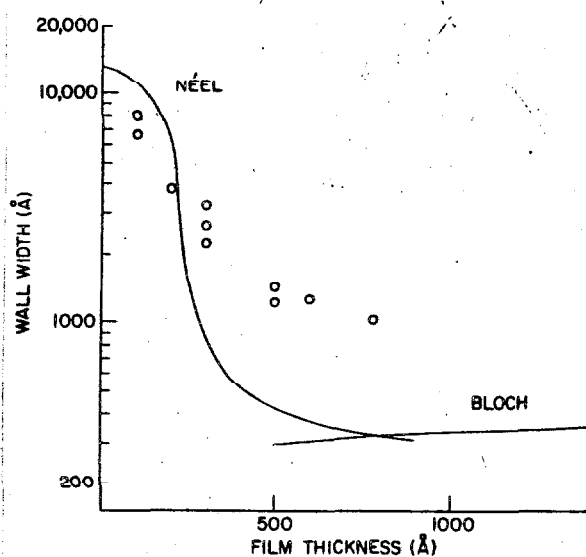Fig.2-5. Domain wall width as a function of film thickness for 80-20 Ni-Fe alloy films with a uniaxial anisotropy constant of 10^3 erg/cm^3, an exchange constant of 10^{-6} erg/cm, and a saturation flux density ($4\pi M$) of 10^4 gauss. The solid lines are after Middelhoek (thesis, University of Amsterdam, Holland (1961)) and the open circles are after Fuchs (Z.Angew. Phys. 14, 203 (1962)).

more sophisticated $\theta(x)$ trial functions and different approximations

for H_{stray} (Behringer and Smith, 1961; Dietze and Thomas, 1961; Brown

and LaBonte, 1965). These calculations, however, give essentially the

same results as the linear wall model. Very little progress has been

made with models which are capable of describing the magnetization

distribution in the wall more accurately than the simple one-dimensional

model. LaBonte (1966) has performed a two-dimensional calculation

with $M = Mf(x,y)$ in which the Bloch wall shape was found to change

with penetration depth into the film. No other multidimensional

calculations for thin films have been reported. On the other hand,

several powerful experimental techniques have been used to actually

examine wall structure in thin films. The results of these investiga-

tions indicate that the simple one-dimensional Bloch and Néel models

are reasonably good approximations to real wall structures. The

deviations of the actual wall structures from these simple models can

be qualitatively understood in terms of the magnetostatic stray field

energy.

An indication of wall structure can be obtained using the tech-

nique, first reported by Bitter (1931), of depositing a drop of

colloidal suspension of very fine magnetite (Fe_3O_4) particles on the

surface of a magnetic specimen. Due to Brownian motion, the particles

move in the suspension until they are captured by the magnetic stray

fields which are associated with domain walls. A visible picture of

the surface domain wall arrangement results. In Fig.2-6, photographs
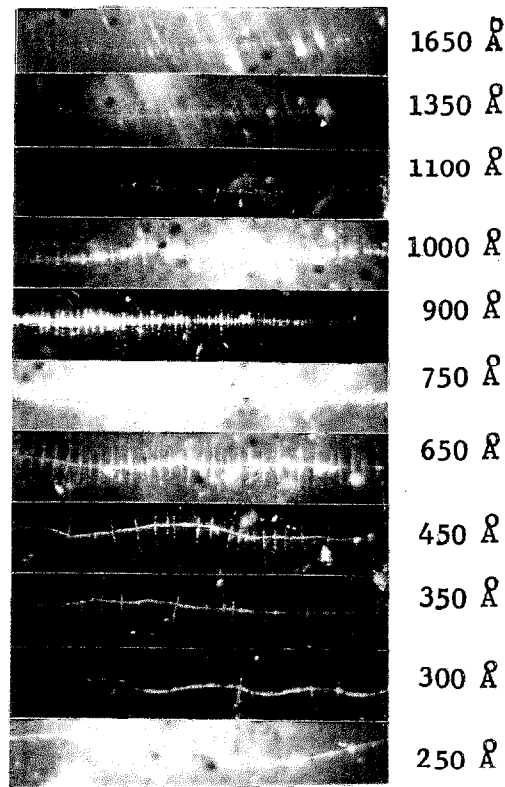
Fig.2-6. Photographs of Bitter patterns for domain walls in films
250 - 1650 Å thick. Each photograph corresponds to a wall section
approximately 300 µ long.

of these magnetite distributions around domain walls (called Bitter

patterns) are shown for films 250-1650 $\mathring{A}$ thick. For film thickness

between 250 $\mathring{A}$ and 1000 $\mathring{A}$, additional structures (usually called

crossties) appear at regular intervals along the wall length. The

crosstie spacing decreases with increasing thickness. For thicker

films, the Bitter patterns are very faint. The abrupt change in the

Bitter pattern intensity at about 1000 $\mathring{A}$ film thickness has been

associated with a Bloch-Néel transition (Methfessel et al., 1960)

qualitatively expected from the magnetostatic stray field energy

considerations. Since the magnetic charge distributions for Bloch

walls in thin films (surface charge distribution) are very different

from those for Néel walls (volume charge distribution), the surface

stray fields and the associated Bitter colloid accumulation should

also be very different. The intensity reduction for Bloch walls in

thick films has been qualitatively explained by Middelhoek (1961) in

terms of flux closure for the different Bloch and Néel stray field

configurations.

The Bloch-Néel transition, however, appears to occur at $D \approx 1000$ $\mathring{A}$

instead of 400 $\mathring{A}$ as predicted for the one-dimensional wall models.

This unexpectedly large transition thickness is due to the existence of

the crossties and their influence on the stray field energy of Néel

wall. The crosstie structure was first observed by Huber et al. (1958)

for 600 $\mathring{A}$ thick films. They suggested that the crossties separated

Néel wall sections with alternating senses of rotation. For the Néel

wall configuration in Fig.2-2, $\overline{M}$ could rotate counterclockwise as well as clockwise in going from the upper to the lower domain. The previous discussion did not depend on a particular sense of rotation. As calculated by Middelhoek (1961), this alternation reduces the magnetostatic stray field energy of the wall and results in an increase in the Bloch-Néel transition thickness to about 900 $\mathring{A}$. The crosstie density decreases with film thickness (as $E_{stray} \longrightarrow 0$) as expected. Qualitatively, the effect of the alternation in reducing E_{stray} is also expected to result in a widening of the Néel wall sections. Using electron microscopy techniques, Fuchs (1962) has performed observations on thin Ni-Fe films 100-800 $\mathring{A}$ thick and obtained $\theta = \theta(x)$ experimentally for the Néel wall sections between crossties. Fuchs' method is based on the Lorentz deflection force experienced by electrons in passing through a magnetic material. The $\theta(x)$ observed by Fuchs for films 100-800 $\mathring{A}$ thick is sketched in Fig.2-7. His determination is in good qualitative agreement with the linear rotation model (Eq.(2.10)) in the center of the wall but deviates markedly near the wall edges $(0 < \theta < \theta_c$ and $\pi-\theta_c < \theta < \pi)$. For these edge regions, $d\theta/dx \approx 0$. The wall width for these data can be conveniently defined as $a^* = \pi(d\theta/dx^{-1})_{x = 0}$. His results are indicated by the open circles in Fig.2-5. As expected (for 200 $\mathring{A} < D < 800 \mathring{A}$), the experimental widths are larger than predicted from the one-dimensional model due to the reduction in E_{stray} because of the crosstie structures.
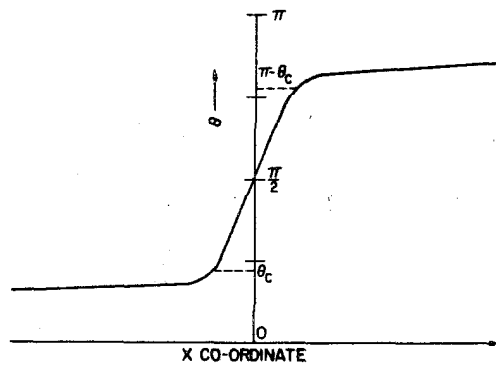
Fig.2-7. Typical Néel wall shape observed in thin films, 300-800 Å thick (E. Fuchs, Z.Angew. Phys. 14, 203 (1962)). The magnetization orientation angle θ with respect to the easy-axis is plotted as a function of distance along the wall normal (x = 0 corresponds to the center of the wall).

-35-

If the alternation of Néel sections reduces the stray field energy,
the alternation of Bloch wall sections should have the same effect for
Bloch walls in thicker films. (For the Bloch wall configuration in
Fig.2-1, $\overline{M}$ could also rotate clockwise in going from the upper to the
lower domain.) Methfessel et al. (1960) have pointed out that the
flux closure between alternating Néel sections must occur in the film
(producing crossties) while the flux closure between alternating Bloch
wall sections must be in the space above (and below) the film. There-
fore no structures analogous to crossties separate alternating Bloch
wall sections in thick films. Smaller structures called Bloch lines
(which do not extend away from the wall for large distances) have been
observed in iron whiskers (DeBlois and Graham, 1958) and recently in
1200 $\overset{o}{A}$ Ni-Fe films using Lorentz microscopy (Torok et al., 1965). This
configuration (alternating Bloch wall sections separated by Bloch lines)
reduces the stray field energy and results in wider walls than
predicted by the one-dimensional model. Because Bloch walls occur in
thick films (D $>$ 1000 $\overset{o}{A}$), Lorentz microscopy measurements of $\theta(x)$ for
Bloch walls are difficult. Torok's observations were only qualitative
insofar as no attempt to analyze the images to obtain $\theta(x)$ was made.
No Bloch wall data similar to Fuchs' Néel wall data have been reported.

After this brief review of the present day understanding of static
wall structure in thin films, it is worthwhile to summarize the various
points concerning static wall shapes, which are of importance for
calculating the relaxation-loss limited mobility of Eq.(2.8). (1) The

Bloch and Néel wall models, for which Eq.(2.8) is valid, represent reasonable approximations to actual wall shapes in thin films. (2) Calculations based on one-dimensional Bloch or Néel wall models, however, can only establish lower limits on the wall width. Actual structures consist of wall sections with alternate rotation senses which further reduces E_{stray} and widens the walls. (3) Experimental measurements of $\theta(x)$ for Néel walls in films 100-800 Å thick have been reported which can be used directly in Eq.(2.8). No similar data for Bloch walls in thick films exists.

For future reference, Equation (2.8) can be converted into an expression for G_α directly in terms of the wall width a for the linear rotation model of Eq.(2.10).

$$G_\alpha = 2\gamma a/\pi^2 \alpha. \qquad (2.13)$$

The relaxation-limited mobility is directly proportional to the wall width so that the wall width curves of Fig.2-5 can be converted to mobility by multiplying by $(2\gamma/\pi^2 \alpha)$. For Fuchs' Néel wall shape data, $d\theta/dx \approx 0$ for $0 < \theta < \theta_c$ and $(\pi - \theta_c) < \theta < \pi$ (see Fig.2-7). For this wall shape, G_α can be expressed as

$$G_\alpha = 2\gamma a^*/\{\pi(\pi - 2\theta_c)\alpha\}. \qquad (2.14)$$

The dependence of θ_c on film thickness can be obtained from the 3-parameter wall shape calculation developed by Feldtkeller and Fuchs (1964) for comparison with Fuchs' electron microscopy data. These θ_c values are small (Feldtkeller, 1965) and represent only a small correction to the G_α of Eq.(2.13).

It is important to emphasize that the relaxation-loss limited mobility calculation summarized in Eq.(2.8) and described by the above equations does not include the effect of crossties (separating Néel wall sections) or Bloch lines (separating Bloch wall sections) on the mobility. If these localized transition structures along the length of the wall do influence the mobility, the extent of this influence can only be determined from experiment.

The list of assumptions in the present calculation of the relaxation limited mobility G_α is growing long. In summary, they are: (1) Relaxation losses can be described phenomenologically using a viscous damping model. (2) Wall shapes for moving walls are very nearly equal to static wall shapes. (3) The crossties and Bloch lines which are present in actual wall structures do not influence G_α and only the shapes of the Bloch or Néel wall sections comprising the wall are of importance. The test of the validity of these assumptions will lie in the experimental mobility data to be presented in section (2.5).

2.3 EDDY-CURRENT LOSSES

In contrast with relaxation losses for wall motion, the eddy-current losses can be calculated explicitly, without resorting to a phenomenological formulation. From Maxwell's equations and the wall shape information discussed in section (2.2), the eddy-current distribution about a moving wall and the resultant losses can be calculated in terms of known physical parameters for the material, with no adjustable phenomenological constants. As was the case for relaxation losses, the static wall shape assumption is used. However, this assumption is necessary only for the final evaluation since some specific wall shape must be used in order to obtain numerical results. It is not necessary in order to calculate the current or loss expressions. For relaxation losses, the static wall shape assumption was implicit in the initial derivation. For eddy-current losses this is not the case.

As mentioned in the introduction, section (2.1), such calculations have been made but may be in error because the wall width was assumed to be zero. The original calculation was carried out by Williams, Shockley, and Kittel (1950), for a moving domain wall of zero width in bulk material. Their predictions were in agreement with wall velocity measurements in single crystal silicon iron. The effect of nonzero wall width on the eddy-current losses was neglected because the sample dimensions were much greater than the wall width. Ford (1960), however,

extended the Williams et al. result to films on the order of 1000 Å
thick, where the wall width (also ≈ 1000 Å) is comparable to the film
thickness. (Refer to the extensive discussion of wall shape in
section (2.2)). The Williams et al. result adapted to thin films
predicts that the current density will fall off exponentially with
distance from the wall, with decay lengths which are the same order of
magnitude as known wall widths (Fuchs, 1962). Ford's use of the zero-
wall-width approximation can hardly be justified under these circum-
stances. On the other hand, no calculation has been reported which
includes the effect of finite wall width on the eddy-current losses
for wall motion in thin films. The purpose of the present section is
to present such a calculation. The current distributions associated
with both Bloch and Néel walls in thin films are calculated, including
the effect of the stray demagnetizing fields associated with these wall
structures. Using the calculated current density, the energy dissipa-
tion rate is evaluated and used to predict the eddy-current limited
wall velocity. The calculation for Bloch walls has been summarized in
a recent article by Patton et al. (1966b).

Maxwell's equations provide the basis for calculating the current
density associated with a moving domain wall. Assuming no charge sepa-
ration and neglecting displacement currents in a conducting medium,

Maxwell's equations may be written

$$\nabla \cdot \overline{J} = 0, \tag{2.15a}$$

$$\nabla \times \overline{H}_{total} = (4\pi/c)\overline{J}, \tag{2.15b}$$

$$\nabla \times \overline{J} = -(\sigma/c)(\partial/\partial t)(\overline{H}_{total} + 4\pi\overline{M}), \tag{2.15c}$$

$$\nabla \cdot \overline{H}_{total} = -4\pi\nabla \cdot \overline{M}, \tag{2.15d}$$

where the current density $\overline{J}$ is equal to the conductivity σ multiplied by the electric field. Gaussian units are employed throughout. An exact solution for $\overline{J}$ using Eqs.(2.15a-d) and the proper boundary conditions is extremely complicated. The field $\overline{H}_{ec}$ produced by $\overline{J}$ must be included, in addition to the applied field and the stray demagnetizing $\overline{H}_{stray}$, in the $\overline{H}_{total}$ appearing in Maxwell's equations. Since $\overline{J}$ is not known beforehand (the purpose of the calculation is to obtain $\overline{J}$), $\overline{H}_{ec}$ is not known. However, if H_{ec} is assumed to be small compared to $4\pi M$, the $\nabla \cdot \overline{J}$ and the $\nabla \times \overline{J}$ equations can be used to obtain an approximate solution for $\overline{J}$ within the film. This approximate solution for $\overline{J}$ and the $\nabla \times \overline{H}_{total}$ equation can be used to calculate $\overline{H}_{ec}$ (only $\overline{H}_{ec}$ contributes to the curl of $\overline{H}$) and this $\overline{H}_{ec}$ can be used in the $\nabla \times \overline{J}$ equation to obtain a correction to the first current solution due to the eddy-current generated fields. However, if $H_{ec} << 4\pi M$,

such a correction will be small and the current solution obtained

neglecting $\overline{H}_{ec}$ can be taken as an accurate representation of the

actual distribution.

The film and wall geometry for the calculation are the same as in

Fig.2-3 and discussed in section (2.2). A single isolated domain wall

is aligned along the easy-axis (z-axis) separating antiparallel domains.

The film is assumed to have infinite extension in the x- and z-directions.

From translational symmetry along the easy axis, $\partial \overline{J}/\partial z = 0$. Under the

influence of an applied easy-axis field H, the domain wall is displaced

in the positive x-direction with velocity v. The Bloch wall magnetiza-

tion distribution corresponding to this domain configuration (Fig.2-3)

at the instant when the center plane of the wall coincides with x = 0

can be conveniently described as shown in Fig.2-4 and discussed in

section (2.2). For Néel walls, the magnetization rotates in the film

(x:z) plane instead of the wall (y:z) plane. For the co-ordinate

system and geometry of Fig.2-4, the following equations summarize the

Bloch and Néel wall shape information which is necessary in order to

calculate $\overline{J}$ from the $\triangledown \times \overline{J}$ equation (neglecting the $\overline{H}_{ec}$ contribution to

$\overline{H}_{total}$).

$$\overline{M}(Bloch) = -(M \cos\theta)\overline{e}_z + (M \sin\theta)\overline{e}_y, \qquad (2.16a)$$

$$\overline{M}(Néel) = -(M \cos\theta)\overline{e}_z + (M \sin\theta)\overline{e}_x. \qquad (2.16b)$$

Here $(\overline{e}_x, \overline{e}_y, \overline{e}_z)$ denote unit vectors. The one-dimensional wall model

$\theta = \theta(x)$ used extensively in section (2.2), will also be used in the present development, and $d\theta/dt = v(d\theta/dx)$. The justification for using $\theta = \theta(x)$ rests primarily in the fact that it provides a reasonably accurate description of real domain walls (see section (2.2)).

The z-component of the magnetization is the same for both Bloch and Néel walls (as shown by Eqs.(2.16a, b)). Since neither wall has a significant $\overline{H}_{stray}$ component in the z-direction ($\overline{H}_{stray}$ is y-directed for Bloch walls and x-directed for Néel walls), the z-component of the $\nabla \times \overline{J}$ equation is the same for both structures and involves only J_x and J_y. This component of Eq.(2.15c) is:

$$\partial J_y/\partial x - \partial J_x/\partial y = -J_o(d\theta/dx)\sin\theta,$$

where $J_o = 4\pi \cdot (\sigma vM/c)$. From $(\nabla \times \overline{J})_z$ and $\nabla \cdot \overline{J} = 0$ (which also involves only J_x and J_y, since $\partial \overline{J}/\partial z = 0$), the uncoupled differential equations for J_x and J_y can be obtained. They are:

$$\partial^2 J_x/\partial x^2 + \partial^2 J_x/\partial y^2 = 0, \tag{2.17a}$$

and

$$\partial^2 J_y/\partial x^2 + \partial^2 J_y/\partial y^2 = f(x), \tag{2.17b}$$

with

$$f(x) = -J_o\{(d^2\theta/dx^2)\sin\theta + (d\theta/dx)^2\cos\theta\} \quad .$$

The necessary boundary conditions for the solution of Eqs.(2.17a, b) are

that J_x and J_y vanish at large distances from the wall, $J_y = 0$ at the film surfaces (current cannot flow out of the film), and

$$(\partial J_x/\partial y)_{\text{film surfaces}} = J_o(d\theta/dx)\sin\theta = h(x).$$

It is important to emphasize the fact that these two uncoupled equations for J_x and J_y and their boundary conditions are valid for both Bloch and Néel wall motion. These two current density components will have the same mathematical expressions for both structures. Equation (2.17a) for J_x (current normal to the wall plane) was solved using Fourier techniques while Eq. (2.17b) for J_y (current normal to the film) was solved using Green's functions. The details for both solutions are given in the appendix. Still for an arbitrary magnetization distribution within the wall (no specific $\theta(x)$ has yet been chosen), these components are given by:

$$J_x = (1/2\pi) \int_{-\infty}^{+\infty} \left[\{\cosh(\zeta y) - \cosh(\zeta(y-D))\}/(\zeta\sinh(\zeta D)) \right] \cdot$$

(2.18a)

$$\int_{-\infty}^{+\infty} h(x')e^{-i\zeta x'}dx'\,e^{ix\zeta}d\zeta,$$

$$J_y = \sum_{\text{odd } n} (2D/n^2\pi^2)\sin(n\pi y/D)Y_n(x,D). \tag{2.18b}$$

$$Y_n(x,D) = e^{-n\pi x/D} \int_{-\infty}^{+\infty} f(x')e^{n\pi x'/D}dx'$$
$$+ e^{n\pi x/D} \int_{-\infty}^{+\infty} f(x')e^{-n\pi x'/D}dx'.$$

These solutions do not yet assume any specific one-dimensional wall shape; $\theta(x)$ is an arbitrary function of x. For any specific $\theta(x)$, J_x and J_y for moving Bloch or Néel walls can (in concept) be calculated.

The z-component of the current can be obtained directly from the x- and y-components of the $\nabla \times \bar{J}$ equation, Eq.(2.15c), and the requirement that $J_z(x = \pm\infty) = 0$. From the simple discussion of section (2.2), $\bar{H}_{\text{stray}}$ has either a large x-component (for Néel walls) or a large y-component (for Bloch walls). It is, therefore, no longer possible to neglect $\bar{H}_{\text{stray}}$ in Eq.(2.15c) as in the solution for J_x and J_y. Including stray fields, the x- and y-components of $\nabla \times \bar{J}$ are given by:

$$\partial J_z/\partial y = (\sigma v/c)(d/dx)\{H_x(\text{stray}) + 4\pi M_x\} \tag{2.19a}$$

and

$$\partial J_z/\partial y = (\sigma v/c)(d/dx)\{H_y(\text{stray}) + 4\pi M_y\}. \tag{2.19b}$$

For Néel walls, $H_y(\text{stray})$ and M_y are approximately zero so $\partial J_z/\partial x = 0$

and $J_z = J_z(y)$. From the condition $J_z(x = \pm \infty) = 0$, $J_z = 0$ everywhere for Néel walls. For Bloch walls, H_x(stray) and M_x are approximately zero, so $\partial J_z/\partial y = 0$ and

$$J_z = J_z(x) = -\sigma v/c \int_{-\infty}^{x} \{H_y(x) + 4\pi M_y\} dx.$$

From section (2.2), $\overline{H}_{stray}$ for Bloch walls can be written as $\overline{H}_{stray} = -\text{Const}\{a/(a+D)\}e_y$. In the limit $a >> D$, $\overline{H}_{stray}$ is equal to $-4\pi M \cdot \sin\theta$ ($\rho_m = \pm M \sin\theta$ on the upper and lower film surfaces) so that the next higher order approximation to $\overline{H}_{stray}$ is

$$\overline{H}_{stray} = -4\pi M \sin\theta\{a/(a+D)\}\overline{e}_y$$

and J_z can be evaluated as

$$J_z(\text{Bloch}) = \{J_o D/(a+D)\} \int_{-\infty}^{x} (d\theta/dx)\cos\theta dx. \tag{2.20}$$

In order to obtain explicit expressions for the current distribution about a moving wall, it is necessary to assume some specific functional dependence for $\theta(x)$. As discussed in section (2.2), the linear wall shape trial function

$$\theta = \pi(x/a+1/2) \tag{2.10}$$

describes the magnetization rotation in Bloch and Neel walls

reasonably well. As mentioned previously, sophisticated wall shape

calculations yield results very similar to predictions based on the

so-called linear wall model. The eddy-current solutions represented

by Eqs.(2.18a,b) and Eq.(2.20) can be reduced to explicit algebraic

current expressions by using the θ dependence of Eq.(2.10). For the

linear wall, $d\theta/dx = \pi/a$ within the wal $(-a/2 < x < a/2)$ and

$d\theta/dx = 0$ for $x > a/2$. As a result, $h(x)$ and $f(x)$ simplify

considerably and the integrals of Eqs. (2.18a,b) can be evaluated

explicitly. The results are:

$$J_x/J_o = F(x,y) - (4/\pi) \sum_{\text{odd } n} \{\cos(n\pi y/D)/n(1+n^2 a^2/D^2)\}Q_n(x)$$

$$(2.10a)$$

$$F(x,y) = \{\cosh(\pi y/a) - \cosh(\pi(y-D)/a)\}/\sinh(\pi D/a) \qquad 0 < x < a/2$$

$$F(x,y) = 0 \qquad\qquad x > a/2$$

$$Q_n(x) = \cosh(n\pi x/D)e^{-n\pi a/2D} \qquad\qquad 0 < x < a/2$$

$$Q_n(x) = \cosh(n\pi a/D)e^{-n\pi x/2D} \qquad\qquad x > a/2$$

$$J_y/J_o = -(4/\pi)\sum_{\text{odd } n} \{\sin(n\pi y/D)/n(1+n^2 a^2/D^2)\}S_n(x) \qquad (2.10b)$$

$$S_n(x) = \sin(\pi x/a) - e^{-n\pi a/2D}\sinh(n\pi x/D) \qquad 0 < x < a/2$$

$$S_n(x) = e^{-n\pi x/D}\cosh(n\pi a/2D) \qquad x > a/2$$

These expressions are valid for $x > 0$, J_x is odd in x and J_y is even in x. The expression for J_z (for Bloch walls) becomes:

$$J_z/J_o = \{D/(a+D)\}\cos(\pi x/a) \qquad x < a/2$$

$$\qquad (2.22)$$

$$J_z/J_o = 0 \qquad x > a/2$$

For Néel walls, $J_z = 0$ everywhere.

This solution can be used to estimate the magnitude of $\overline{H}_{ec}$ in order to examine the validity of the assumption, $H_{ec} << 4\pi M$, on which the present analysis is based. Equations (2.21a,b) and Eq.(2.22) indicate that the magnitude of $\overline{J}$ is on the order of $J_o - 4\pi\sigma vM/c$. Consider the wall cross section in the x:y plane defined by the area between $x = \pm a/2$, $y = 0$, and $y = D$. From the $\nabla \times \overline{H}$ equation, Eq.(2.15b), and Stoke's theorem, the circuital integral of $\overline{H}_{ec}$ around the perimeter of the cross section is equal to the area integral of J_z

over the cross section and

$$H_{ec} \approx (2\pi\sigma v/c^2)\{aD/(a+D)\}4\pi M.$$

For typical values, $\sigma = (16\mu\Omega\text{-cm})^{-1} = 0.57 \times 10^{17} \text{ sec}^{-1}$, $a = D = 10^{-5}$cm, and $v = 10^4$cm/sec, the result is that $H_{ec} \approx 4\pi M \times 10^{-5}$. The initial assumption that $H_{ec} << 4\pi M$ is therefore a reasonable one. The current solutions and Eq.(2.15b) could be used to calculate $\bar{H}_{ec}$ for substitution back into the $\nabla \times \bar{J}$ equation, Eq.(2.15c), in order to get the eddy-current field correction to $\bar{J}$ but since $H_{ec} \approx 4\pi M \times 10^{-5}$ this correction would be negligible.

The eddy-current solution expressed by Eqs.(2.21a,b) and Eq.(2.22) has been evaluated numerically. The wall width was taken to be the static width calculated by Middelhoek (1961) and discussed in section (2.2). The static wall shape assumption is important in calculating the eddy-current losses, just as it is in calculating relaxation losses. The shapes for moving walls are assumed to be approximately equal to static wall shapes (the wall distortion which produces the Becker field for wall motion is small). Providing that the static wall assumption is a good one, it is important to note that the linear wall calculation predicts only a lower limit for the width of actual walls. Depending on whether the eddy-current losses for wall motion increase or decrease with wall width, the present calculation will represent a lower or upper limit on the losses. The results of the numerical

evaluation for all three components of $\overline{J}$ for Bloch walls are shown by the solid lines in Figs.2-8, 2-9, and 2-10. The current components are normalized to J_o and the normalized magnitudes are plotted as a function of the x-coordinate (normal distance from the center of the wall) with film thickness D as a parameter. The dotted lines represent solutions for the limit a = 0 (the zero width approximation used by Ford (1960)). For Bloch walls in the 400-2000 Å thickness range corresponding to the curves in Figs.2-8 and 2-9, the wall width is about 500 Å (see Fig.2-5). The present results are clearly different from the predictions of the zero-width approximation and exhibit the effect of a nonzero wall width on the current distribution. The J_x distribution in Fig.2-8 (plotted for y = 0) deviates markedly from the zero-width prediction for x < a/2 and approaches this prediction for large x. The J_y distribution in Fig.2-9 (plotted for y = D/2; at y = 0 or D, J_y = 0) exhibits a maximum near x = a/2 and goes to zero for x = 0, quite different from the zero-width prediction. The J_z distribution in Fig.2-10 (valid only for Bloch walls) exhibits a cos($\pi x/a$) dependence within the wall and is zero for x > a/2 (for Néel walls, J_z = 0 everywhere).

The nonzero width has a definite effect on the current distribution for the moving Bloch or Néel walls and it is expected that the eddy-current losses for wall motion will also be influenced singifi- cantly by the wall shape. The energy loss rate per unit volume is

Fig.2-8. Eddy-current component J_x at the film surface
(y = 0, D) as a function of x (normal distance from wall center) with
D (film thickness) as a parameter. Dotted curves represent the results
for zero wall width.
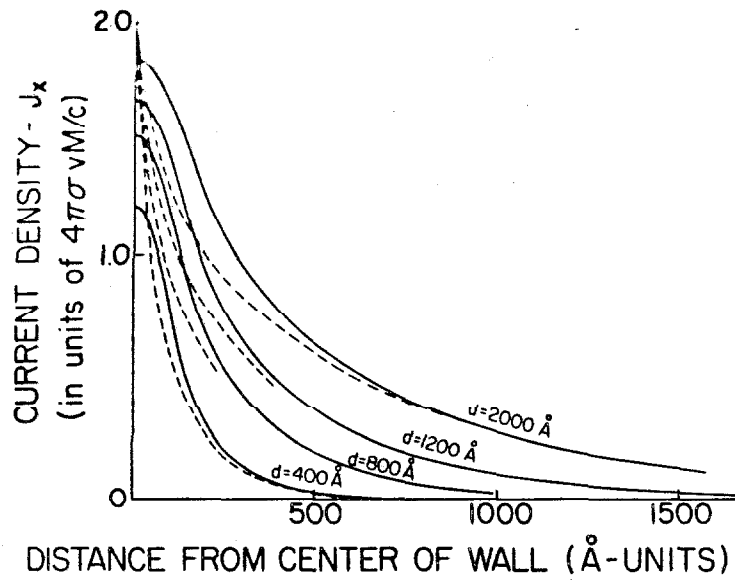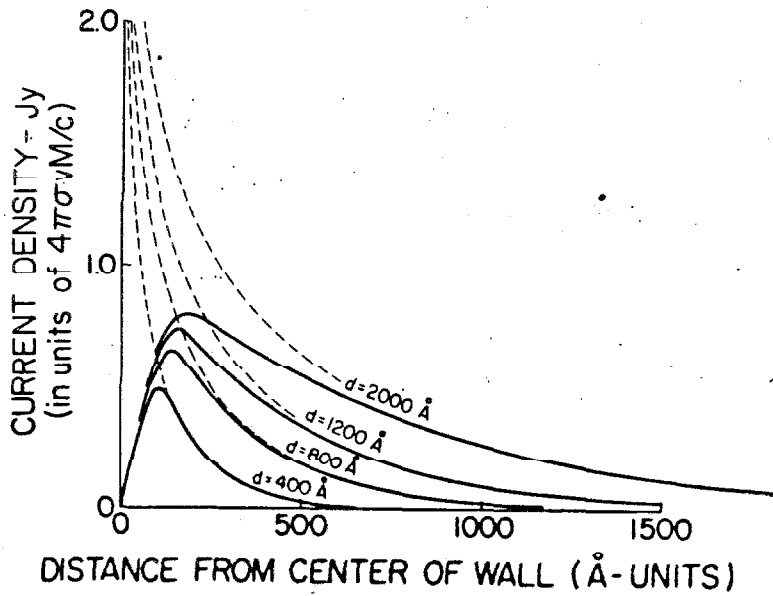

Fig.2-9. Eddy-current component J_y at the film center plane
y = D/2, as a function of x (normal distance from wall center) with
D (film thickness) as a parameter. Dotted curves represent the
results for zero wall width.
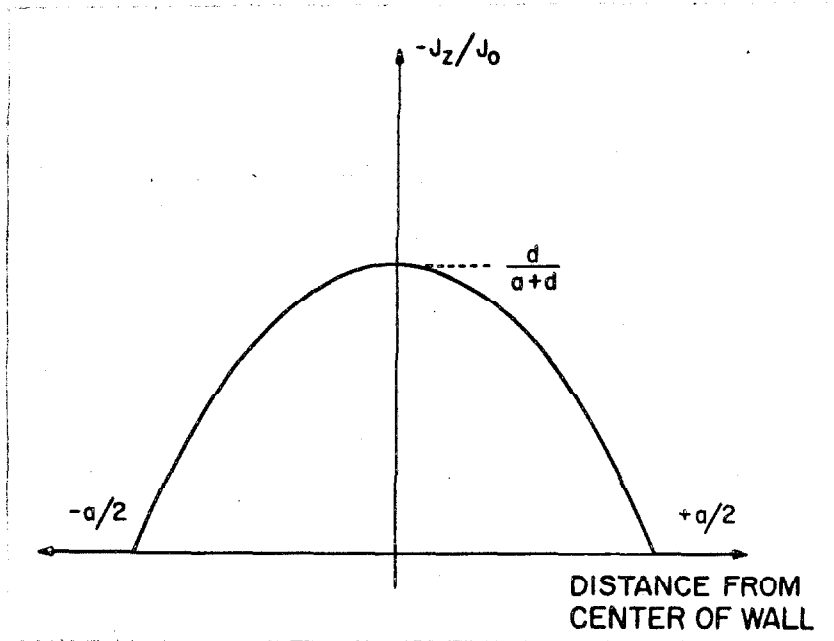
Fig. 2-10. Eddy-current component J_z within the linear Bloch wall including demagnetizing field effects. For zero wall width, $J_z \approx 0$ everywhere.

$-\bar{E} \cdot \bar{J} = -J^2/\sigma$. ($\bar{E}$ is the electric field) and the eddy-current losses per unit length can be calculated using

$$W_{eddy} = (1/\sigma) \int_0^D dy \int_{-\infty}^{+\infty} dx J^2. \tag{2.23}$$

The integrand in Eq.(2.23) can be formed from J_x and J_y from Eqs.(2.21a, b) and J_z from Eq.(2.22) ($J_z = 0$ for Néel walls). The integration region is such that all the losses associated with a unit length of wall are included in W_{eddy}. The losses are given by:

$$W_{eddy} = (1/\sigma)(4\pi\sigma vM/c)^2 \{I_{sq}(a,D) + I_{zsq}(a,D)\}$$

where

$$I_{sq}(a,D) = (d^2/\pi^3) \sum_{odd\ n} \{\pi R_n(1+R_n^2)+2(1+e^{-\pi R_n})\}/\{n^3(1+R_n^2)^2\} \tag{2.24b}$$

for both Bloch and Néel walls ($R_n = na/D$),

$$I_{zsq}(a,D) = (Da/8)\{D/a+D)\} \tag{2.24c}$$

for Bloch walls, and $I_{zsq}(a,D) = 0$ for Néel walls. For a $180°$ domain wall moving with a velocity v in an easy-axis field H, the rate of energy decrease for the system (the two antiparallel domains and the moving wall) per unit length of wall is 2DvMH. If the system energy

decrease is due only to eddy-current dissipation, $W_{eddy} = 2DvMH$ and the eddy-current limited domain wall velocity is

$$v = HDc^2/\{32\pi^2\sigma M(I_{sq}+I_{zsq})\}$$

As was the case in the relaxation loss analysis, the dissipation rate is quadratic in velocity and the velocity is a linear function of the applied easy-axis field. The wall mobility, $G = \partial v/\partial H$, is field independent. The eddy-current limited mobility is given by

$$G_e = Dc^2/\{32\pi^2\sigma M(I_{sq}+I_{zsq})\}. \qquad (2.25)$$

It is a function of the material constants of the film and the film thickness. No phenomenological damping parameter appears. There are no adjustable constants.

The mobility expressed by Eq.(2.25) is plotted in Fig.2-11 as a function of thickness for Bloch walls (i.e. $I_{zsq}(a,D)$ is calculated from Eq.(2.24)). The resistivity used is typical for Ni-Fe alloy films with 80% Ni (16$\mu\Omega$-cm, corresponding to $= 0.57 \times 10^{-17}\text{sec}^{-1}$). The solid line in Fig.2-11 was obtained by using the wall width a for the one-dimensional linear Bloch wall model discussed in section (2.2). The dotted line is the result obtained by letting $a = 0$. The differences between the two results are not large; they are certainly much less than expected on the basis of the large differences in the
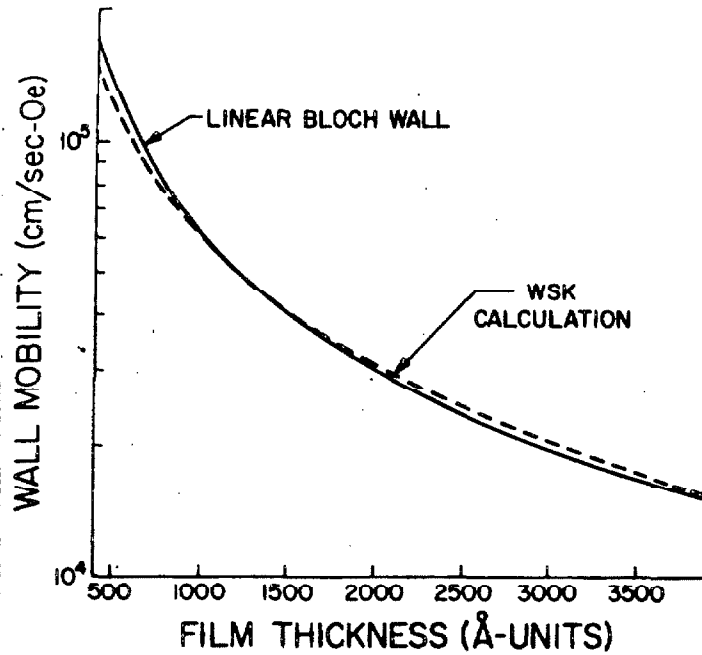
Fig.2-11. Eddy-current-loss limited wall mobility as a
function of film thickness, calculated using linear Bloch walls.
The material parameters were taken as those appropriate for
80-20 Ni-Fe alloy films.

current distributions which have been pointed out. A detailed analysis indicates that the increase in losses due to J_z for the non-zero width wall calculation (J_z and $I_{zsq}(a,D)$ are zero for a = 0) nearly compensate for the reduced J_x and J_y losses, resulting in a mobility which is not significantly different from the earlier a = 0 result. For Néel walls, J_z = 0 everywhere, and the mobility corresponding to the solid line in Fig.2-11 would be larger. However, Néel walls are only important in very thin films (D < 1000 Å). In this thickness range, J_z for Bloch walls (proportional to D/(a+D)) is negligible so that the solid line is also a good representation of the Néel wall mobility for D < 1000 Å.

For fixed film thickness, G_e increases with increasing wall width. Since the calculation has incorporated theoretical wall widths which represent only lower limits for actual wall widths (due to magneto-static energy considerations as discussed in section (2.2)), the mobility shown in Fig.2-11, as calculated from Eq.(2.25), represents a lower limit on the actual eddy-current loss limited mobility. Since real walls are wider than predicted from the linear model (due to the existence of crossties or Bloch lines and a reduced magnetostatic stray field energy), the actual eddy-current limited mobility should be larger than calculated.

In this section, the eddy-current losses associated with a moving domain wall in a thin ferromagnetic film have been considered in detail.

The present treatment includes the effect of nonzero wall width on the current distribution and the eddy-current losses, taking into account the stray demagnetizing fields associated with domain walls as well. It was found that the current distribution is essentially the same as previously calculated outside the wall, but inside the wall the current components normal to both the wall plane and the film plane are reduced significantly. There is an additional component, along the length of the wall, which is zero for the $a = 0$ calculation. Even though the current distribution is dependent on the width of the moving wall, the reduced losses due to the smaller current components in the plane normal to the wall and the film compensate for the increased losses due to the nonzero current component normal to this plane and produce an eddy-current limited mobility which is not significantly different from the earlier $a = 0$ prediction.

2.4 EXPERIMENTAL DETERMINATION OF WALL MOBILITY

2.4.1 Introduction

Relaxation losses and eddy-current losses for domain wall motion in thin ferromagnetic films have been considered in detail in the last two sections. In these treatments a number of assumptions have been necessary. As these assumptions were made, it was pointed out that the test of their validity could come only from a comparison of the theoretical mobility predictions with experiment. In order to compare the results of the previous two sections with experiment, two things are

necessary. First,it is necessary to obtain a theoretical prediction of the wall mobility, limited by both relaxation and eddy-current losses. Second, it is necessary to measure the domain wall velocity for thin films as a function of easy-axis field amplitude H and use these velocity data to obtain the empirical wall mobility. In deciding how the wall velocity should be measured and in establishing standards as to what measurements are meaningful, conceptual problems arise. (1) If the wall distorts during its motion or if the motion is impeded by macroscopic imperfections which visibly inhibit wall motion in localized regions of a film, are the velocity determinations meaningful in terms of the previous theoretical discussion? (2) Can the wall velocity be determined only by using time-of-flight techniques (extremely difficult) and observing the wall during its motion, or is a velocity determination based on the transit time between two static wall positions (a quasistatic technique) equally valid? In the first part of this section, these questions will be considered and aspects of the quasistatic technique relevant to them will be discussed. In the second part, the instrumentation which was used for quasistatic velocity measurements will be described in detail. In the third part, actual velocity data will be presented and used to justify the experimental technique, and the manner in which the velocity data are used to determine the empirical mobility will be discussed.

2.4.2 Conceptual Problems

In this part, two points will be considered. First, a theoretical prediction of the wall mobility, limited by both relaxation and eddy-current losses, will be obtained in order that a later comparison of theoretical and experimental mobility determinations will be possible. This comparison will be done in the next section, section (2.5). Second, the conceptual problems which arise in making accurate and meaningful velocity determinations will be discussed. The first of these conceptual problems, concerning wall distortion during motion and the effects of macroscopic film imperfections on wall motion, will involve film preparation and selection procedures. The second problem, concerning the validity of the quasistatic technique, will involve physical questions (such as the acceleration time to bring a static wall to its loss-limited velocity) as well as instrumentation problems (such as techniques for observing domain walls). A discussion of this second problem will therefore involve a description of the experimental technique. Since the emphasis here, however, is on the conceptual rather than the practical aspects of the technique, a description of hardware will be postponed until the next part (2.4.3).

The wall mobility limited by both eddy-current and relaxation losses can be expressed in terms of G_α and G_e, the mobilities calculated on the basis of relaxation losses only and eddy-current losses only. As mentioned previously, both the relaxation loss rate and the

eddy-current loss rate are quadratic in velocity. Since the rate of
energy decrease per unit length of wall is given by 2MHDv (as before),
the total loss rate equation can be written as

$$2MHDv = (K_\alpha + K_e)v^2 \qquad\qquad (2.26)$$

where K_α and K_e are coefficients characterizing eddy-current and relax-
ation losses. If there were no eddy-current losses (i.e. $K_e = 0$), the
relaxation-loss limited mobility is given by $G_\alpha = 2MD/K_\alpha$. Similarly,
$G_e = 2MD/K_e$. The mobility for Eq.(2.26) is given by $G = 2MD/(K_e + K_\alpha)$
and satisfies the relation

$$1/G = 1/G_e + 1/G_\alpha. \qquad\qquad (2.27)$$

Therefore, the wall mobility, limited by both relaxation and eddy-
current losses, can be calculated in terms of the individual mobilities
for each type of losses. It is this total mobility which should be
consistent with mobility determinations from the wall velocity measure-
ments for thin films, if the theoretical assumptions of the last two
sections are valid.

The theoretical development of the last two sections depended on
the assumption that an isolated straight domain wall aligned along the
easy-axis of a uniaxial film moves at a uniform velocity in a direction
perpendicular to its length under the influence of a uniform easy-axis

field. If any meaningful comparison of theory with experiment is to be made, this assumption must be satisfied experimentally. Wall motion compatible with the above description is extremely difficult to obtain. The demagnetizing fields at the film edges have considerable influence on the walls near the edges and inhibit uniform wall motion. In addition, films contain large numbers of internal imperfections and non-magnetic inclusions which may inhibit wall motion in localized regions of a film. All of these interactions tend to destroy the simple wall geometry which has been assumed in the calculations of the last two sections. Only by careful film preparation, could the above wall motion criteria be satisfied.

Before considering the mobility data, it is appropriate to briefly summarize the technique used to prepare the samples for which the data were taken. The film samples were vacuum evaporated from a melt of 80% nickel and 20% iron onto glass substrates heated to $300^{\circ}C$ in a moderate vacuum of 10^{-6} Torr. During evaporation, a uniform magnetic field of 40 Oe was applied in the plane of the glass substrate in order to determine the direction of the uniaxial anisotropy. Film composition was determined to be about 77% Ni using x-ray fluorescence techniques. For films with a nickel content of about 83%, the magnetostriction is zero and the mechanical strains in the film due to the high temperature evaporation and subsequent cooling to room temperature do not appreciably affect the magnetic properties of the films. The particular recipe for film preparation described above was used primarily because

the resultant films exhibited reasonable wall motion properties. It is important to emphasize the fact that the ability to obtain reproducible and consistent wall velocity data depends, to a large degree, on the ability to make films which satisfy three requirements. (1) The films must be free of internal imperfections which inhibit wall motion. (2) The films must be capable of supporting only a few domain walls so that the number of walls moving simultaneously does not interfere with measurements on a single wall. (3) The film edges must not distort the wall significantly from linearity. (Some wall distortion near the edge always exists. If the distortion is small, wall sections far from the edges will still be straight and move uniformly.) The most effective (and inefficient) way to satisfy these requirements was by evaporating a large number of films and simply selecting those films (few in number) which satisfied the above wall motion criteria. Out of approximately 300 films which were prepared and examined, only 60 exhibited wall motion which was sufficiently uniform for accurate measurement.

In the next section, the film thickness will be an important parameter in discussing the wall motion data. An accurate determination of the thickness is therefore extremely desirable. Two methods were used to determine film thickness, flux measurements and Tolansky multiple beam interferometry (Tolansky, 1948). The amplitude of the hysteresis loop for thin films is proportional to the total amount of reversed flux, which increases with thickness. When calibrated properly, the hysteresis loop amplitude can be used to determine film thickness. The

Tolansky interferometry technique is based on the fringe shift caused
by a step in a mirror coating on the film because of the film edge.   By
using an aluminum coating on the film the fringes can be made extremely
sharp and the shift can be used to determine thickness to ± 20 Å.

The basis for the experimental mobility determinations is the
observation of domain walls and the measurement of their velocity.   The
second conceptual problem concerns the method of velocity measurement.
Before considering this problem, however, a discussion of the technique
used to observe the wall in the first place is in order.   Observation
of domain walls is based on the Kerr magneto-optic effect first used
by Fowler and Fryer (1955) for the observation of domain walls in
thin films.   When linearly polarized light is reflected by a ferro-
magnetic sample, the polarization direction is rotated through an
angle which depends on the magnetization direction in the sample with
respect to the direction of incidence for the light.   For uniaxial
thin films consisting of antiparallel domains, an analyzer can be
adjusted in such a way that the light reflected from one kind of
domain is extinguished (after passing through the analyzer) but the
light reflected from the antiparallel domains is not completely
extinguished.   Adjacent antiparallel domains will be light and dark
respectively, and the domain wall will be indicated by the light-
dark boundary.   In Fig.2-12, a typical arrangement for the Kerr
magneto-optic observation of domain walls in thin films is sketched.
Light from the source (high intensity) is converted into a parallel
beam by the condenser lens, is polarized, and is reflected by
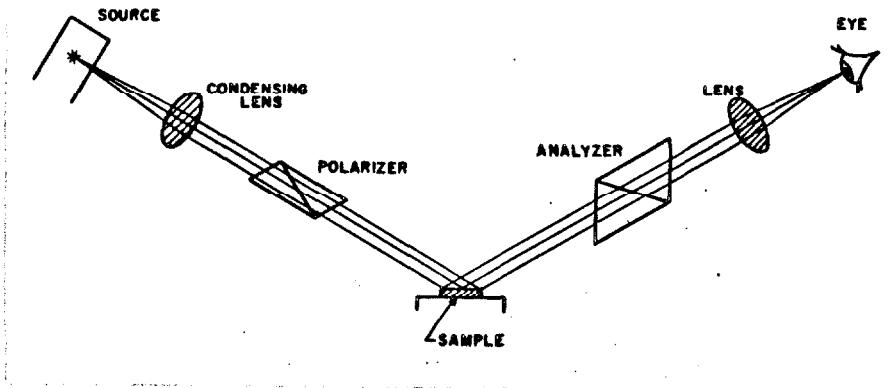
Fig.2-12. Typical arrangement for the Kerr magneto-optic observation of domains in thin films.
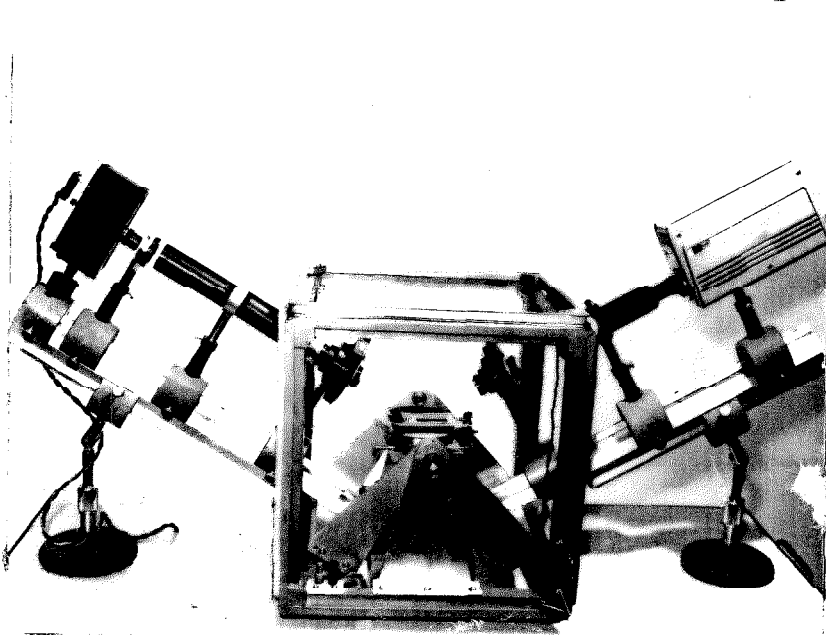
Fig.2-13. Instrumentation for the Kerr magneto-optic observation of domains in thin films.

the film. The magnetization in the film rotates the plane of polariza-
tion in a sense depending on the domain structure. The reflected light
passes through the analyzer as well as a focusing lens, and is displayed
as a picture of the domain structure of the film (sensed by the eye in
Fig.2-12).

With the domain configuration displayed conveniently, the problem
of measuring the wall velocity as it moves under an applied easy-axis
field can now be considered. As will be shown later, wall velocities
in thin films are on the order of 10^4 cm/sec (for 80-20 Ni-Fe alloy
films less than 2000 Å thick). Direct velocity measurements for moving
walls, using time-of-flight techniques, would be the most straight-
forward procedure. However, for the velocity magnitudes involved, such
a procedure would require photographic techniques with megacycle per
second framing rates and nanosecond exposure times. Two factors make
this technique impractical, the short exposure times required and the
low light intensity. In using the Kerr effect for domain viewing, the
analyzer and polarizer are adjusted for almost complete light
extinction for one type of domain. The emerging light corresponding to
the other antiparallel domains is of low intensity because of the small
polarization rotation angles (a few degrees at most) obtained using the
Kerr effect. No standard light source is strong enough to give good
photographs for low intensity Kerr effect images and nanosecond
exposure times. If valid, a much simpler and more practical quasistatic
technique can be used to measure the domain wall velocity. By suitable

display of the domain image obtained with the Kerr effect, static domain

wall positions can be measured with high accuracy. If the wall is

moved using a short duration rectangular easy-axis field pulse, the

wall displacement produced by the pulse can be accurately determined

by measuring the wall position before and after the pulse. If the wall

is assumed to move at a constant velocity during the pulse, this

velocity is simply the wall displacement divided by the pulse duration.

This simple procedure constitutes the quasistatic technique. The

remainder of the present discussion will be concerned with the criteria

for its validity in wall velocity determinations. After a discussion

of the instrumentation for making quasistatic velocity determinations

in the next part (2.4.3), velocity data will be presented and the

quasistatic technique will be shown to be valid. The successful use of

this technique for velocity measurements represents the main experi-

mental accomplishment presented in this chapter.

The criteria for the validity of the quasistatic technique for

making wall velocity measurements can be obtained by examining the

details of the wall motion from the time before the application of the

easy-axis field pulse when it is at rest in its initial position to the

time after the pulse when it is at rest in its final position. A

detailed mathematical description is possible but is not necessary here.

The quasistatic technique is valid for determining the loss-limited

domain wall velocity only for rectangular field pulses of sufficient

duration so that most of the displacement occurs at the loss-limited

velocity. If this condition is not satisfied, the velocity determination will be lower than the loss-limited velocity (the wall will not have time to respond to a short field pulse). If the quasistatic technique is not valid, the velocity determinations will exhibit a dependence on pulse length T_p and the validity of the technique can be checked by measuring velocity as a function of pulse duration. If the measurements really correspond to the true loss-limited velocity, v will be independent of the pulse duration. In the next part, instrumentation for performing quasistatic velocity measurements will be discussed. In the last part, the velocity dependence on τ_p and other aspects of the velocity data will be considered. The quasistatic technique will be shown to be valid.

2.4.3 Instrumentation for Velocity Measurements

Conceptually, the quasistatic technique for measuring the domain wall velocity is very simple. The position of a stationary domain wall is observed before and after the application of a field pulse of known duration. Several steps are required to accomplish the measurement. First, the film sample is placed in the Kerr magneto-optic apparatus so that the domain pattern can be conveniently observed. Then external fields are utilized to form a straight, isolated domain wall in the film, away from the film edges and aligned along the easy-axis. Finally, an easy-axis field in the form of a rectangular pulse is applied to the film, the domain wall is displaced, and the velocity is

determined from the wall displacement and the pulse duration. Such a procedure is straightforward and the instrumentation is standard. A detailed description of the instrumentation is included in this part for one reason and one reason only. For the first time, the quasistatic technique has been used to obtain meaningful velocity measurements for domain wall motion in thin films; the author has used this technique successfully where others have failed (Ford, 1960; Copeland and Humphrey, 1963). This success has been due, in part, to careful attention to sample preparation and selection. The main reason for success, however, was the careful attention to the various details of the instrumentation and the experimental technique, and to the taking and analysis of the data. For this reason, a description of the instrumentation and the measurement technique is appropriate. (It should be noted that, simultaneously with the present research, two other workers, Il'icheva and Kolotov (1965) and Middelhoek (1966), were able to obtain meaningful velocity data using modifications of the same technique.) This discussion can conveniently be divided into two parts, one concerning the Kerr magneto-optic instrumentation for viewing the domain structure and measuring the wall displacements, and one concerning the instrumentation for producing the proper fields which influence or produce wall motion.

The use of the Kerr magneto-optic effect for viewing the domain structure in thin films was discussed in the last part and is schematically shown in Fig.2-12. The actual instrumentation corre-

sponding to Fig.2-12 is shown in Fig.2-13. A high pressure short arc

mercury vapor lamp (PEK Labs, Inc. type 110) was used as a light

source. The lamp was mounted in a housing (L.H.S. of Fig.2-13) and

its position could be adjusted for proper alignment with the rest of

the optics. In the order shown in Fig.2-13, the items mounted on the

optical bench to the left of the sample platform tilted 30° to the

horizontal are: light housing and condensing lens, iris, light tube,

iris and polarizer prism. The polarized light is reflected from the

sample on the platform in the center of Fig.2-13, passes through the

analyzer prism, iris, focusing lens, and light tube, to the image

plane of a closed circuit television camera. The film image is then

displayed on a television screen remote from the Kerr apparatus.

Using this Kerr effect instrumentation, high contrast domain

observations on thin films are possible. In Fig.2-14, two photographs

of domain patterns on circular films 1 cm in diameter, obtained using

the Kerr effect, are shown. Domain walls are indicated by the

boundaries separating light and dark regions. The high contrast which

can be obtained between antiparallel domains makes the determination

of domain wall position extremely accurate. Figure 2-14 is included to

demonstrate the Kerr magneto-optic viewing of domains. Of course, none

of the wall configurations shown in Fig.2-14 consist of the single

isolated walls oriented along the easy-axis (vertical in Fig.2-14)

which are necessary for velocity measurement. With the domain config-

uration displayed conveniently on the closed circuit television screen,

-69-

Fig.2-14. Photographs of domain patterns on circular films 1 cm in diameter, obtained using the Kerr effect. Domain walls are indicated by the boundaries separating light and dark regions.
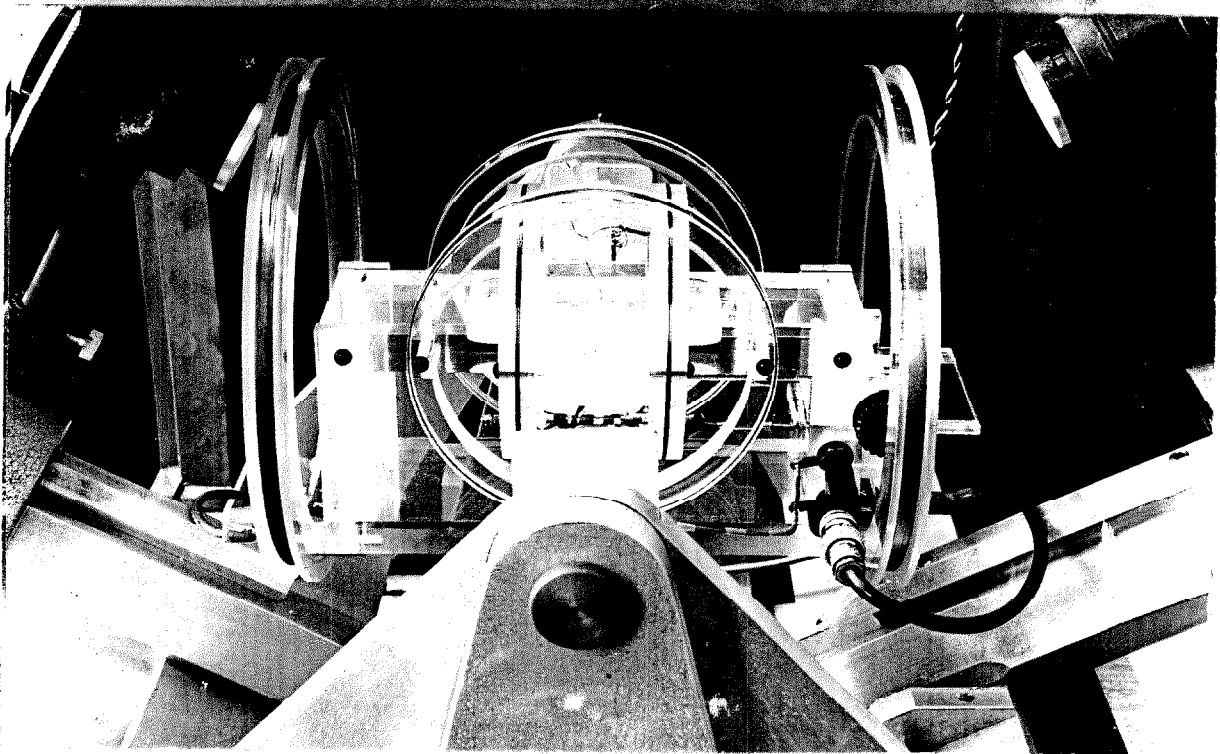

Fig.2-15. The coil assembly used to produce the required applied fields for velocity measurements while the sample was under observation using the Kerr apparatus. The polarizer and analyzer prisms can be seen in the upper corners of the photograph. (A) Coils for canceling the earth's magnetic field. (B) Hard-direction field coils. (C) Easy-direction field coils.

a calibrated traveling microscope was suspended in front of the screen and used to measure the domain wall positions accurate to about $\pm$ 0.05 mm on films 1 cm in diameter. The domain wall displacement, Δx, for the velocity determination, could be determined to about 1%.

The next phase of the instrumentation concerns the apparatus for producing and measuring the required magnetic fields. As will be seen shortly, the fields at which wall motion can be measured using the quasistatic technique are from about 1-5 Oe, depending on the properties of the film. The earth's magnetic field, which is about 0.3 Oe, can therefore cause a considerable discrepancy between the value of the applied easy-axis field and the total field which influences wall motion. By arranging a set of six square coils in the shape of a cube to produce crossed fields, as shown in Fig.2-13, the earth's magnetic field can be effectively cancelled out at the sample position by proper adjustment of the coil currents. The coil assembly shown in Fig.2-15 was used to produce the required applied fields at the sample position (center of apparatus) while it was under observation using the Kerr magneto-optic apparatus. The polarizer and analyzer prisms can be seen in the upper corners of the photograph. The smallest center Helmholtz coil pair was used to produce the easy-axis field pulses for wall motion. The other details of the apparatus will be discussed shortly in connection with film alignment.

A block diagram of the field instrumentation is shown in Fig.2-16. This instrumentation is divided into two sections, (1) the electronics for producing the easy-axis field pulses for wall motion, and (2) the electronics for measuring the easy-axis field amplitude and the pulse length τ_p for wall displacement. The easy-axis field must be applied in such a way that the optical access to the film required for use of the Kerr effect is preserved. An easy solution is to use a Helmholtz coil pair, as mentioned above and shown in Fig.2-15. Helmholtz coils, however, present a problem. A coil pair with small dimensions is desirable in order to get the most field from the available current sources but large dimensions are required in order that the field be homogeneous over the film sample. If large coils are used for field homogeneity and the number of turns is increased to provide the necessary field strength, the increased inductance degrades the rise time of the field pulse. Clearly a compromise is necessary. The present design incorporated a Helmholtz pair with a radius (and separation) of 2 inches, so that the homogeneity over the 1 cm diameter film sample was better than ± 0.1 %. Using two turns per coil, the field calibration was 0.36 Oe/amp and the risetime was 0.1 μsec with the coils in series with 50 Ω. The current source consisted of a triggered Rutherford pulse generator with a minimum risetime of 15 nsec and an output voltage of 50 volts into 50 Ω, driving either a one stage transistor power amplifier or a grid-controlled electron multiplier tube driver (Tung-Sol type 8428). Using the transistor driver, useful field pulses with
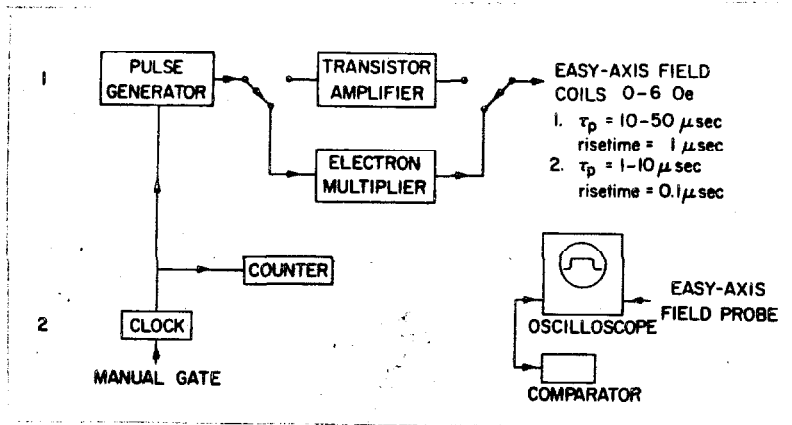
Fig.2-16. Block diagram of the field instrumentation.

amplitudes from 0-6 Oe, pulse lengths from 10-50 μsec, and risetimes of 1 μsec could be obtained. Using the grid-controlled multiplier tube, useful field pulses with amplitudes from 0-10 Oe, pulse lengths from 1-10 μsec, and risetimes of 0.1 μsec could be obtained. Using these pulses, the quasistatic technique can be tested for τ_p from 1 to 50 μsec.

For measurements using the shorter pulse lengths ($\approx$ 1 μsec) and low field amplitudes, the displacements caused by a single pulse were usually not large enough for accurate measurement. For this reason, a number of pulses was applied (N pulses, for example) and the quasistatic velocity was determined from the total displacement. A clock, controlled by a manual gate, was used to trigger the pulser, and a decade scaler was used to count the number of pulses. The individual pulses were monitored on an oscilloscope from which the pulse duration τ_p was determined. By operating the oscilloscope with high vertical gain, the pulse amplitude could be determined to $\pm$ 0.01 Oe using a high gain differential comparator. From the total wall displacement Δx during the pulse sequence, the number of pulses N, and the pulse duration τ_p, the velocity was determined from $v = \Delta x / (N \tau_p)$ as a function of easy-axis field amplitude H and pulse duration.

In this discussion of instrumentation and measurement technique, it has been tacitly assumed that the easy-axis of the film was aligned with the field direction for the easy-axis field pulse. Since film

alignment might conceivably be very important (the theory assumed an easy-axis field only), a definite procedure for film alignment was established. The technique used for film alignment is based on the sketch in Fig.2-17. The larger Helmholtz pair in Fig.2-15 was used to produce a hard-direction field in the plane of the film but perpendicular to the easy-axis field from the smaller coil pair, and a 20 turn pickup coil was mounted on the rotatable film platform. In Fig.2-17, the coil is shown as a winding around the film, sensitive to the time rate of change of the magnetization component in the easy direction. In practice, the coil was wound in the shape of a figure eight (after Oguey, 1960) and mounted below the film so that the winding would not interfere with the Kerr observations. In the alignment procedure, the film was first saturated in the approximate hard-direction. When the hard-direction field is turned off, the magnetization in the film relaxes to the easy-direction and induces a voltage in the coil. If the easy-axis of the film were aligned precisely in the easy-axis field direction, after the hard-direction saturation exactly half the total magnetization would relax toward one easy-direction and half would relax toward the other. For an aligned film, therefore, the induced voltage in the pickup loop would be zero. By rotating the film platform until zero induced pickup voltage is observed during the easy-direction relaxation, the easy-axis of the film can be precisely aligned ($\pm$ 0.1$^{\text{o}}$) with the easy-direction field. Initially, great care was taken in this alignment procedure since the sensitivity of the velocity data to film
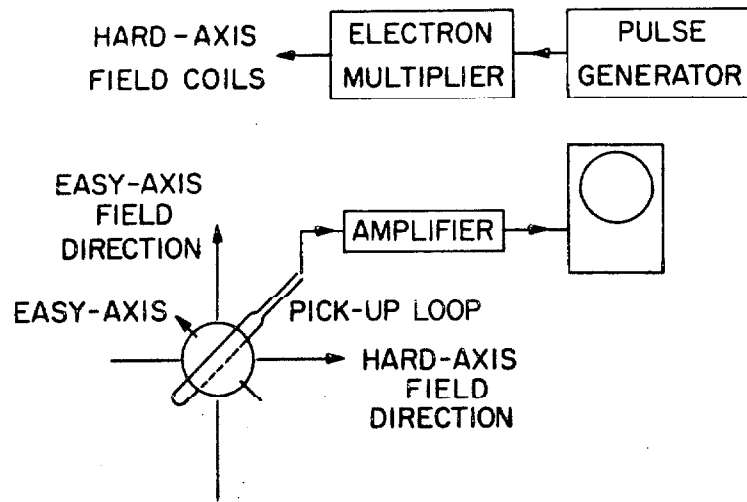
Fig.2-17. Sumarry of the technique used for film alignment.

alignment was not known. However, it was later found that alignment was not critical and that visual alignment using the Kerr image was usually sufficient.

2.4.4 Conceptual Problems Resolved

The conceptual problems concerning quasistatic velocity measurements have been discussed and the instrumentation for quasistatic measurements has been described in detail. From the four experimental parameters Δx, τ_p, N and H, the wall velocity as a function of easy-axis field amplitude can be obtained. In the last part of this section, velocity data will be presented and used to determine: (1) The validity of the quasistatic technique. (2) The validity of the concept of wall mobility for characterizing wall motion.

Wall velocity determinations were made by pulsing the film (once a single, isolated domain wall was formed, aligned along the easy-axis) with a series of N easy-axis field pulses, measuring the total displacement Δx and pulse duration τ_p, and calculating $v = \Delta x/(N \tau_p)$. In Fig. 2-18, a series of domain wall photographs are shown. Wall positions are shown after successive applications of a sequence of ten easy-axis field pulses with $\tau_p = 2.6$ µsec. From the initial to final wall position, a total of 70 pulses was applied. The film region shown in each photograph was about 5 mm wide (horizontal direction in the figure), and is not near the edges of the film. The easy direction
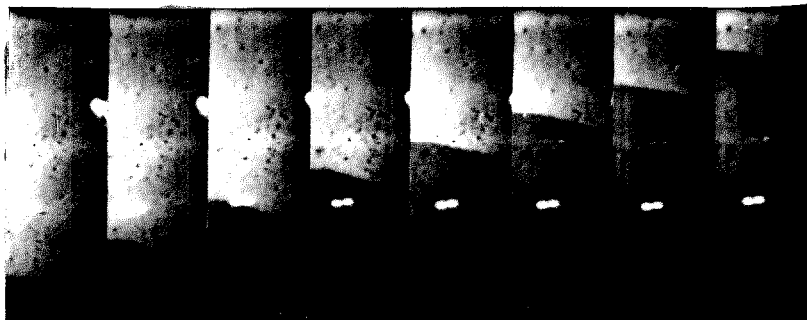
Fig.2-18. Kerr effect observations of the simple wall configura-
ations and the systematic wall displacements obtained after successive
application of seven field pulse sequences. Each sequence was identi-
cal, consisting of ten pulses, 2.6 μsec long, with amplitudes of
2.5 Oe.
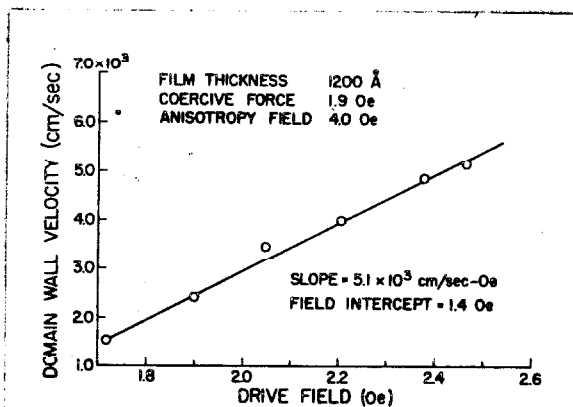
Fig.2-19. Domain wall velocity as a function of applied easy-
axis field. These data are typical for Ni-Fe alloy films in the
300-1650 Å thickness range.

is vertical. Even though the film used for Fig.2-18 exhibited reason-
ably straight walls and uniform motion, some wall distortion (both in
orientation and linearity) can be seen to occur as the wall is
displaced. Such distortion certainly introduces some error into the
data. As mentioned previously, one of the biggest experimental
problems involved the preparation and selection of films which exhibited
smooth, uniform, undistorted wall motion. The wall configuration and
displacements shown in Fig.2-18 are typical of the films for which
reproducible and consistent velocity determinations could be made. As
mentioned previously, wall position could be measured to $\pm$ 0.05 mm, so
that for Δx = 5.0 mm, the accuracy was about 1%.

The quasistatic technique for wall velocity determinations, for
which the instrumentation of the last part was developed, assumed that
most of the wall displacement Δx measured experimentally takes place at
the loss-limited wall velocity. This assumption is not a trivial one.
In fact, both Ford (1960) and Copeland and Humphrey (1963) have
reported that the quasistatic technique of inferring wall velocity from
static wall position measurements did not yield consistent or reproduc-
ible velocity determinations. Neither worker, however, was able to
directly observe the domain walls as the velocity determinations were
made. It is entirely possible (and probable) that the walls were not
straight and undistorted and that the wall motion was not uniform. The
present application of the quasistatic technique, performed according
to the procedures outlined in the previous parts of this section, was

found to yield consistent and reproducible velocity data. The velocity

measurements were found to be independent of the easy-axis field pulse

duration τ_p for τ_p between 1 and 50 μsec. Velocities were the same

within 5% for the same field amplitude and the same region of a film.

Therefore, the criteria for the validity of the quasistatic technique

are satisfied and $v = \Delta x/(N\tau p)$ can be taken as a good measure of the

loss-limited domain wall velocity.

In connection with the theoretical discussion, the quantity of

interest is the domain wall mobility, or the increase in wall velocity

per unit increase in field. From the theoretical discussion, the

velocity is expected to vary linearly with easy-axis field amplitude

according to $v = GH$ where G is the field independent wall mobility.

Velocity determinations for wall motion in a single film as a function

of easy-axis field amplitude are shown in Fig.2-19. As predicted, wall

velocity is a linear function of field amplitude so that the wall

mobility as defined above is a meaningful quantity. However, the

velocity-field data appear to fit a curve of the form $v = G(H - H_w)$,

not $v = GH$. In other words, some threshold field exists, below which

wall motion does not occur. In light of this unexpected effect, a new

problem arises. Does this threshold field modify the interpretation of

the velocity-field data in terms of a wall mobility, as calculated in

the previous two sections? If G, as defined and calculated, is to

remain a meaningful quantity, the empirical velocity-field dependence

$v = G(H - H_w)$ must be consistent with the total loss rate equation,

Eq.(2.26). The threshold field for wall motion can be interpreted in

terms of an additional loss term in the total loss rate equation so that

$$2MHDv = (K_\alpha + K_e) v^2 + 2MH_w Dv$$

or

$$2MDv(H - H_w) = (K_\alpha + K_e)v^2. \qquad (2.27)$$

The physical origin of the additional loss term is not completely understood and represents an interesting aspect of wall motion which is not of direct interest here. For the present purposes, it is only necessary to consider H_w as an effective field opposing the applied easy-axis field. The previous mobility definition $G = \partial v/\partial H$ is not modified by the additional loss term.

This section will be concluded with a short discussion of the manner in which the velocity-field data were used to obtain an empirical determination of the wall mobility. Since G is the slope of the line defined by the v vs H data (see Fig.2-19), velocity measurements should be obtained over a sufficient range of field values to determine this slope accurately. Consistent and reproducible velocity determinations could only be made for a small range of easy-axis field amplitude. A definite lower limit is set by H_w. For $H < H_w$, there is no wall motion. The practical lower limit is actually higher than H_w. For fields

nearly equal to H_w, the wall velocity is quite small (less than

0.5×10^3 cm/sec for the data in Fig.2-19), the wall motion is not very

uniform over the film, and velocity measurements are difficult. An

upper limit is set by the requirement that measurements be made on

single, isolated domain walls. For high fields, additional walls form

at the film edges and inside the film which obscure the uniform motion

of the individual wall under observation. The upper limit on the field

amplitude for meaningful velocity determinations was usually about

1 Oe greater than H_w. For higher fields, isolated straight walls could

not be moved intact and undistorted over an appreciable distance in the

film. They combined with other walls to form complicated domain

structures which did not satisfy the requirements for wall velocity

determination. Once reproducible velocity determinations have been

made over the field range just discussed, the field dependence of the

velocity can be fitted to $v = G(H - H_w)$ and the wall mobility G can be

obtained. The velocity-field data were fitted to $v = G(H - H_w)$ using

the method of   least squares and a chi-squared test for the

probability of a linear fit was performed in each case. For the sixty

films for which reproducible velocity determinations could be made, the

probabilities were all greater than 0.9. These determinations of the

domain wall mobility can then be compared to the theoretical prediction

of the loss-limited mobility calculated from $1/G = 1/G_e + 1/G_\alpha$ and the

previous two sections.

2.5 MOBILITY AND LOSS MECHANISMS FOR WALL MOTION

In the last section, an experimental technique for determining the mobility for wall motion in thin films was described in detail. In this section, the empirical mobility values obtained using this technique are presented, discussed, and compared with predictions based on the previous theoretical development concerning relaxation and eddy-current losses. Such a comparison makes it possible to obtain several important conclusions concerning (1) the losses limiting wall motion and (2) the influence of wall shape on the mobility. These conclusions go hand in hand since the relaxation-loss limited mobility is sensitive to the wall shape (which is in turn determined by the film thickness and the material parameters of the film) while the eddy-current-loss limited mobility is relatively insensitive to changes in wall shape but decreases monotonically with film thickness. A very efficient comparison, therefore, is one based on the thickness dependence of the mobility, since each of the two loss mechanisms considered result in a different mobility-thickness dependence. On this basis, in the film thickness range $D = 100$ $\overset{o}{A}$ to 1650 $\overset{o}{A}$, the mobility will be shown to be limited almost entirely by relaxation losses. The eddy-current losses are negligible. The relaxation-loss limited mobility can be fitted to the data using a constant value of the damping parameter and the static wall shape data discussed in the section on relaxation losses. On the basis of this fit, it appears that: (1) The cross-tie structures

associated with Néel walls in thin films with D < 900 Å do not contrib-

ute directly to the wall mobility, and (2) walls for films with

D > 1000 Å are much wider than predicted for Bloch walls. The present

discussion is divided into two parts. The first part will be limited

to a discussion of the experimental results and the second part will

correlate these results with the previous theoretical discussion. This

work has been summarized in a recent publication by Patton and Humphrey

(1966c).

For the limited number of films which exhibited uniform wall

motion, the quasistatic technique discussed in the last section was

used to determine the domain wall mobility. Mobilities were determined

for films ranging in thickness from 300 Å to 1650 Å. As discussed

previously, film thickness was determined magnetically, using a 20-cps

hysteresis loop tracer, and optically, using the Tolansky multiple

beam interference technique (Tolansky, 1948). In Fig.2-20, the experi-

mentally determined mobilities are displayed as a function of film

thickness. Earlier data by Copeland and Humphrey (1963) for very thin

films are also shown. Between 100 and 800 Å, the mobility decreases

with increasing film thickness, ranging from 8 x 10^3 cm/sec-Oe at 300 Å

to 3 x 10^3 cm/sec-Oe at 800 Å. Between 900 and 1000 Å, the mobility

increases rapidly with increasing film thickness to about

7 x 10^3 cm/sec-Oe. Above 1000 Å, the mobility increases slowly with
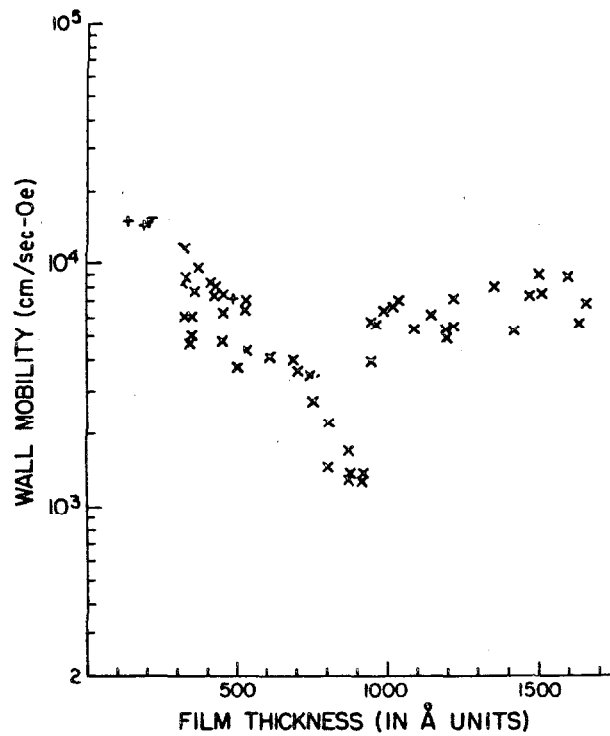
film thickness.

Fig.2-20. Domain wall mobility as a function of film thickness
for Ni-Fe alloy films with 80% Ni evaporated onto glass substrates
at 300°C in a vacuum of 10⁻⁶ Torr. Data for very thin films (+)
after J.A. Copeland and F.B. Humphrey, J. Appl. Phys. 34, 1211
(1963).

These data are in qualitative agreement with the recent mobility

measurements (also using a quasistatic technique) by Il'icheva and

Kolotov (1965) and Middelhoek (1966). The mobility data of Il'icheva

and Kolotov, however, consist of only a few points and are lower than

the present results by a factor of five. Middelhoek's data are pre-

sented as a mobility band and actual data points are not shown.

Middelhoek indicates that the mobility minimum occurs at $D = 600 \overset{o}{A}$,

not $D = 900 \overset{o}{A}$. Later in this section, it will be shown that the

present data are consistent with the theoretical predictions. The

present investigation improves on these two previous works in two ways.

First, the quality of the data is such that the quantitative dependence

of mobility on film thickness is obtained, in contrast to the data of

Il'icheva and that of Middelhoek. Second, the data are successfully

correlated to theoretical predictions based on eddy-current and

relaxation losses and available wall shape information.

Two points concerning the data are of interest, the nature

of the velocity-field dependence from which the mobility was determined,

and the origin of the scatter in the mobility data. Consider the first

point. Most of the sixty films had a wall velocity-field dependence as

shown in Fig.2-19 and discussed in the last section. The velocity

increases linearly with applied easy-axis field, and extrapolates to

$v = 0$ at a threshold field H_w for wall motion. However, a number of

films exhibited a different type of velocity-field dependence, as shown

by the velocity vs field curve in Fig.2-21. At the higher field values,

the velocity departs unexpectedly from the simple linear dependence
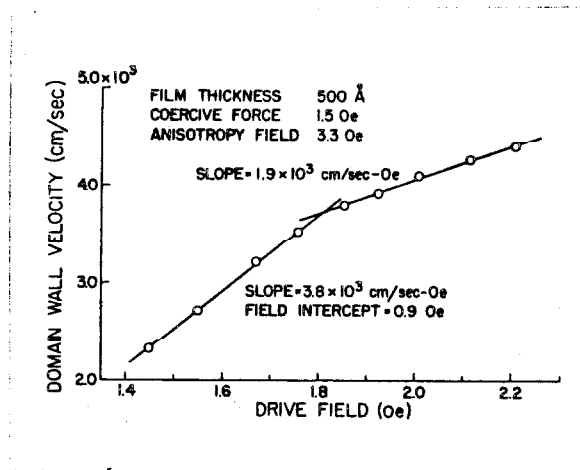
Fig.2-21. Domain wall velocity as a function of applied easy-axis field observed for several Ni-Fe alloy films. The break in the curve shown here was not observed for most of the samples.

$v = G(H - H_w)$. The velocity remains linear with field but the slope of the curve is reduced significantly. It should be emphasized that most films did not exhibit this effect. The break in the linear v vs H curve was observed for only five or six films. A similar effect has been reported by Middelhoek (1966) for a large number of Ni-Fe alloy films with thickness from 100 to 3000 $\mathring{A}$. Il'icheva and Kolotov (1965), however, reported no such behaviour for any of their velocity data. A more extensive investigation of domain wall motion for fields at least several oersteds greater than the threshold for wall motion is necessary before any serious explanation can be attempted. In any case, the wall mobility plotted in Fig.2-20 was extracted from the low field v vs H curve for films exhibiting this effect.

The other point of interest concerns the scatter in the mobility data, evident from Fig.2-20. The origin of the scatter is also relevant to the data interpretation in terms of the loss mechanisms discussed previously. As shown in Fig.2-20, there is considerable scatter in the observed mobilities for films of the same thickness. Using the techniques of the previous section, the reproducibility in the mobility for wall motion in a given region of a specific film was well within 5%, so that the scatter is not due to the experimental technique. The same problem that plagued the efforts toward obtaining velocity data in the first place, sample preparation, also degrades the reproducibility of the mobility determinations from film to film. It should be remembered, that for most of the original 300 films, imperfections notice-

ably impeded wall motion to such an extent that meaningful velocity measurements could not be performed in the first place. The selection process was only designed to separate good films which exhibited reasonably uniform wall motion (as shown in Fig.2-18) from bad films which showed erratic wall motion. Even for the 60 films which exhibited reasonably uniform wall motion, and for which mobility determinations were made, film imperfections still influenced the wall motion to some degree. These film imperfections introduce an additional loss term for wall motion and since the imperfection content varies from film to film, this loss term will cause a scatter in the mobility from film to film. From this explanation, the upper bound of the experimental mobility data can be taken to represent wall motion unimpeded by film imperfections, limited only by eddy-current and relaxation losses. It should be pointed out that in section (2.2) relaxation losses were very carefully defined in such a way as to exclude the losses caused by imperfections.

From Fig.2-20, it can be seen that the mobility exhibits a distinct minimum in the vicinity of 900 $\overset{o}{A}$ film thickness. In the section on relaxation losses, it was pointed out that the transition from Bloch walls to Néel walls with crossties occurred at approximately this same thickness. It is logical to associate the mobility minimum with the Bloch-Néel wall structure transition. Since the eddy-current limited mobility is relatively insensitive to the wall structure, such an association leads to the immediate conclusion that relaxation losses

contribute most heavily to the losses limiting wall motion. The sharp

increase in the mobility as the thickness increases from 900 Å to 1000 Å

also has some surprising implications concerning the wall width. The

large increase in mobility for D = 1000 Å as compared to that for

D = 900 Å indicates that the Bloch wall structure (D = 1000 Å) is much

wider than the Néel wall structure (D = 900 Å). In the discussion on

wall width in section (2.2) and Fig.2-5, the Bloch structure was calcu-

lated to be slightly narrower than the Néel structure. A cursory

examination of the present mobility data therefore indicates that:

(1) Relaxation losses are most important in limiting the wall motion,

and (2) Bloch walls are much wider than expected. Both of these

implications will be discussed further as the data of Fig.2-20 is

correlated quantitatively with the theoretical predictions of section

(2.2) and (2.3).

In Fig.2-22, the same mobility data as shown in Fig.2-20 are pre-

sented once more for comparison with the mobility predictions based on

static wall shape calculations and the static wall shape measurements

discussed in the section on relaxation losses. The calculated mobilities

were obtained using α = 0.014 for the Landau- Lifshitz phenomenological

parameter. From the close agreement between the calculated mobility

based on Fuch's Néel wall shape measurements (Fuchs, 1962) and the

experimental values in the 100 to 900 Å thickness range, this judicious

choice of α = 0.014 is well founded. The mobility predictions based on

the linear Néel wall calculations of Middelhoek (1961) are not in agree-
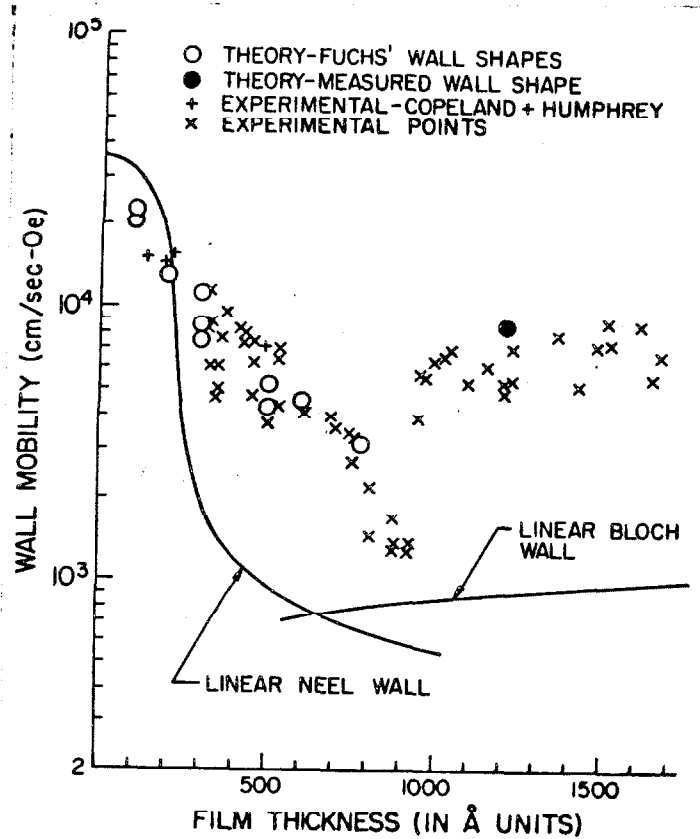
Fig.2-22. The mobility data of Fig.2-20 are shown here along with theoretical predictions based on eddy-current and relaxation losses. Calculations were performed using material parameters typical for Ni-Fe films with 80% Ni and a phenomenological damping parameter $\alpha = 0.014$.

ment with the present data. This lack of agreement is expected, since Middelhoek's calculations did not include the effect of the crosstie structures associated with Néel walls on the wall shape in increasing the wall width (and the mobility). By using measured wall shapes in the calculation, the effect of the crossties on the wall shape is included. Even so, the direct influence of the crosstie structure on the wall mobility has not been taken into account. The calculation of G_α was based on a one-dimensional wall model ($\overline{M}$ was only a function of position along wall normal) with no crossties or Bloch lines. In view of the close agreement between the data and the predictions based on Fuchs' wall shape measurements, it appears that the presence of cross-ties do not directly influence the mobility. Their only influence is indirect, in reducing the wall magnetostatic energy, thereby widening the wall. From the fit, the damping α can be taken as 0.014 and the relative contributions of relaxation losses and eddy-current losses can be calculated. In this thickness range, almost 100% of the losses limiting the wall motion are relaxation losses. Eddy-current losses are negligible, as expected from the qualitative discussion. The close fit of the theory to the data was obtained using (1) a constant value of the damping parameter α and (2) static wall shape information. The first result is important in light of the fact that the damping parameter is phenomenological. The second result appears to justify the static wall shape assumption, used extensively in the theoretical development.

For film thickness in the vicinity of 950 Å, the mobility increases by a factor of five, with increasing film thickness. A similar sharp increase in mobility near 960 Å film thickness has been reported by Il'icheva and Kolotov (1965). The photographs of Bitter patterns for wall structures for different thickness films shown in Fig.2-6 and discussed in the section on relaxation losses clearly show that some type of wall transition occurs in the vicinity of 1000 Å. As shown in Fig.2-6, for film thickness less than 1000 Å the wall is of the Néel type, characterized by the usual crosstie structure. For film thickness greater than 1000 Å, the colloid accumulation is significantly reduced, the Bitter patterns are very faint, and the crosstie structure does not appear. It is reasonable to suppose that the sharp increase in mobility near 950 Å film thickness is associated with a wall structure transition in this region.

For thicker than about 950 Å films, the mobility appears to slowly increase with increasing film thickness. Using α = 0.014 (as determined by the mobility fit for Néel walls) and the linear Bloch wall widths from Fig.2-5, the mobility was calculated and is also shown in Fig.2-22. As was the case for Néel walls, these calculated values are much lower than the actual wall mobilities because the wall model used in the calculation were one-dimensional and did not include the possibility of alternating wall sections.

Real walls do consist of alternating sections. As mentioned previously, Bloch walls with Bloch lines have been recently observed in

1200 Å films by Torok et al. (1965). However, no quantitative experimental determinations of actual wall shapes analogous to Fuch's data for Néel walls have been published, primarily because Lorentz microscopy measurements on thick films are extremely difficult. Nevertheless, by careful attention to sample preparation and by using extremely long exposure times, such measurements are possible. Lorentz microscopy observations have been performed on 1200 Å Ni-Fe films which were evaporated onto freshly cleaved sodium chloride substrates, floated on water, and mounted on copper electron microscope grids. These observations reveal a wall structure consisting of short wall sections (presumably of the Bloch type) separated by Bloch lines similar to that reported by Torok et al. (1965). A typical Lorentz microscopy photograph is shown in Fig.2-23. The Bloch lines, corresponding to the light and dark stripes along the wall length, are clearly evident. The intensity distributions of these wall images have been analyzed and the wall width has been estimated to be approximately 3000 Å for 1200 Å films. This wall structure is much wider than expected for Bloch walls in such films.

Using the above static wall width estimate and a damping parameter $\alpha = 0.014$, the mobility for 1200 Å films was calculated and is indicated in Fig.2-22 by the dark circle. As can be seen, this prediction agrees quite well with the upper bound of the experimental data. As was the case for thinner films, almost 100% of the losses limiting the theoretical mobility are relaxation losses. Eddy-current losses are again
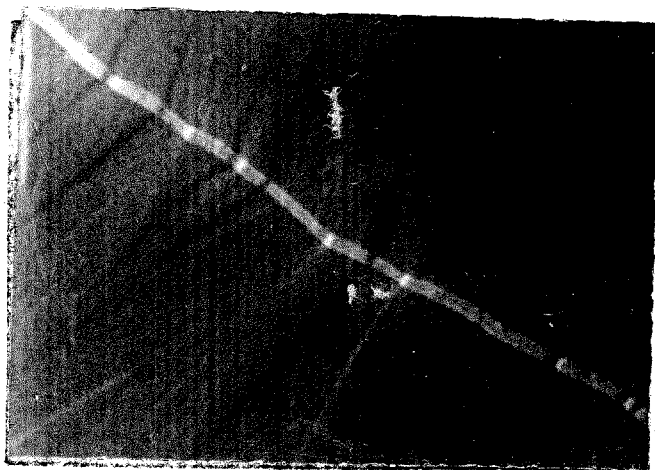
Fig.2-23. Lorentz microscopy photograph of a Bloch wall with
Bloch lines in a 1200 Å film. (Courtesy of T. Suzuki.)

negligible. In fact, almost all of the conclusions which were obtained

for Néel wall motion for films below the 900 Å transition thickness can

be extended to thicker films. The Bloch lines do not appear to

influence the mobility directly. Their only influence is indirect, by

reducing the wall magnetostatic energy and increasing the wall

width.

The present results concerning the thickness dependence of the

domain wall mobility in thin films at room temperature, in conjunction

with available static domain wall shape information, indicate: (1) Eddy-

current losses are not important for wall motion in the 100 to 1600 Å

thickness range. (2) The shapes for moving walls are very nearly equal

to those for static walls. There are no large scale changes in the

domain wall shape because of its motion. (3) Mobility can be accurately

described using a constant value of the phenomenological damping

parameter $\alpha = 0.014$ over the entire thickness range examined. (4) The

crosstie structures associated with Néel walls or the Bloch line

structures associated with Bloch walls do not directly influence the

domain wall mobility.

2.6 SUMMARY

In this chapter, an extensive investigation of domain wall motion

in thin films, both theoretical and experimental, has been presented.

In the theoretical development, two points have been emphasized: (1) The

concept of a loss-limited wall velocity, and (2) The necessity of using

the static wall shape approximation for moving walls. The first point

provided the conceptual basis for the velocity calculation while the

second made it possible to obtain numerical predictions. Both eddy-

current and relaxation losses have been considered. In the experimental

development, the primary emphasis has been on (1) obtaining reproducible

and consistent mobility data and (2) using the data to determine the

relative importance of eddy-current and relaxation losses in limiting

the wall motion. Other important problems, concerning the validity of

the phenomenological formulation for relaxation losses, the validity of

the static wall shape assumption for moving walls, and the influence of

wall shape on eddy-current losses, were also unanswered and have been

solved in the course of this investigation.

Following the course taken by previous workers, relaxation losses

have been treated phenomenologically, utilizing the Landau-Lifshitz

equation. The motivation (or excuse) for this approach rests primarily

in the fact that no physical formulation of relaxation losses has been

possible. The phenomenological treatment is based primarily on a

viscous drag model, as if the magnetization were a physical vector

moving in a fluid medium. The model can be applied to wall motion if

the domain wall shape is assumed to distort slightly. Using a

phenomenological damping parameter and the magnetization distribution

within the wall, it is possible to characterize the relaxation losses

limiting the wall motion. Static wall shape information is available

and the damping parameter was determined by fitting the theory to the data.

The eddy-current losses associated with wall motion have been calculated, taking the finite width of the domain wall into account. The analysis has been carried out for both Bloch and Néel walls and indicates that the losses are not significantly different from those predicted previously, even though the actual current distributions are significantly different.

A quasistatic technique has been developed to accurately measure domain wall velocity in thin films and to determine wall mobility from these data. One important factor in obtaining meaningful data concerns the selection of samples which exhibit uniform wall motion by straight, isolated walls. The successful use of the technique shows that time-of-flight measurements are not necessary and that the loss-limited velocity can be determined by measuring wall displacements produced by field pulses of known duration, for pulse lengths greater than 1 μsec.

Mobility data have been obtained as a function of film thickness from 300 to 1650 $\overset{o}{A}$, for Ni-Fe alloy films with 80% Ni evaporated onto glass substrates at $300°C$ in a vacuum of 10^{-6} Torr. Between 300 and 800 $\overset{o}{A}$, the mobility decreases with increasing film thickness ranging from 8 x 10^3 cm/sec Oe at 300 $\overset{o}{A}$ to 3 x 10^3 cm/sec Oe at 800 $\overset{o}{A}$. Between 900 and 1000 $\overset{o}{A}$, the mobility increases rapidly with increasing film thickness to about 7 x 10^3 cm/sec Oe. Above 1000 $\overset{o}{A}$, the mobility

increases slowly with film thickness. Bitter patterns indicate that the sharp increase in mobility between 900 and 1000 $\overset{o}{A}$ is associated with a wall structure transition. On both sides of this transition thickness range, a theoretical fit to the data was made using static wall shape information obtained from Lorentz microscopy. For films thinner than 900 $\overset{o}{A}$, published wall shape information was used but for films thicker than 1000 $\overset{o}{A}$, no static wall shape information was available. Lorentz microscopy wall shape measurements for a 1200 $\overset{o}{A}$ film yielded a width of about 3000 $\overset{o}{A}$, significantly wider than calculated wall widths. Over the entire thickness range considered, a good theoretical fit to the data was obtained for a constant value of the damping parameter, $\alpha = 0.014$. Eddy-current losses were completely negligible.

The domain wall mobility has been determined as a function of film thickness from 300 to 1650 $\overset{o}{A}$. These data can be explained on the basis of static wall shape information and the concept of a loss-limited velocity. Eddy-currents do not contribute significantly to the losses limiting wall motion. Relaxation losses dominate. The phenomenological formulation of relaxation losses for wall motion appears to constitute a useful approach; the phenomenological damping parameter required to fit the theory to the data is constant over the entire thickness range examined.

Chapter 3. FERROMAGNETIC RESONANCE

3.1 INTRODUCTION

3.1.1 Elementary Considerations

In a typical ferromagnetic resonance experiment, a sample of ferromagnetic material is placed in a uniform magnetic field large enough to magnetize the sample parallel to the field direction. If the magnetization is disturbed slightly from this equilibrium position, it does not return directly but precesses about the field direction. Energy loss associated with the magnetization motion causes the precession to be damped with eventual alignment along the field direction. In order to study this phenomenon, a small sinusoidal magnetic field is applied perpendicular to the static field. This sinusoidal field excites precessional motion but unless the frequency ω is nearly equal to the precessional frequency ω_u, the energy coupled from the excitation field to the precessing magnetization will be small. If $\omega \approx \omega_u$, the coupling is large and is limited only by the damping of the system.

The first observations of ferromagnetic resonance (FMR) were reported by Griffiths (1946) for electrolytically deposited films of iron, cobalt, and nickel. The resonances were observed to occur for values of the static external applied field H much lower than expected from the usual resonance relation for electrons, $\omega_u = g\mu_o H/\hbar$, where g

is the spectroscopic splitting factor ($g \approx 2$ for electrons) and μ_o is

the Bohr magneton. The apparent discrepancy between the theory and the

FMR data was first explained by assigning extremely large g values to

the magnetic electrons for various ferromagnetic materials. This

approach, however, yielded different g values, depending on sample

shape and field orientation. The understanding of FMR was advanced

considerably when Kittel (1948) pointed out the role of demagnetizing

fields in determining the resonance condition. Such demagnetizing

fields are connected with a nonzero magnetization divergence in much

the same way as they were in the case of domain wall stray fields. For

FMR, $\nabla \cdot \overline{M} = 0$ inside the uniformly magnetized sample and the demagne-

tizing fields are produced only by surface magnetic charge. The total

field at an electronic site in the sample can be quite different from

the applied field because of the demagnetizing fields. The usual

resonance condition with $g \approx 2$ is satisfied if the demagnetizing field

is taken into account.

Just as there are losses associated with the magnetization rota-

tion which accompanies wall motion, there are losses associated with

the magnetization precession for FMR. The precession amplitude (the

tipping angle of $\overline{M}$ away from the static field direction) is loss

limited in much the same way that the wall velocity is loss limited,

as can be understood from a simplified classical picture. An r-f field

at ω_u applied perpendicular to the static field pumps energy into the

system, increasing the precession amplitude. As the precession

amplitude grows, the losses associated with the magnetization motion also increase until the precession amplitude is such that the loss rate equals the r-f power input. For larger precession amplitudes, the loss rate exceeds the power input and the system loses energy by decreasing the precession angle. In the same way that the domain wall velocity is determined by an energy balance between losses and the net energy decrease for the system, the precession amplitude for FMR is determined by an energy balance between losses and r-f power input to the system. However, while the wall velocity can (in principle) be infinite for no losses, the precession angle is limited to π (when viewed as simple precession). Consequently, the response of the magnetic system to the transverse r-f excitation is more conveniently characterized by a transverse susceptibility $X_{\perp} = m_{\perp}/h$, rather than the precession amplitude. Here $m_{\perp}$ is the magnetization component perpendicular to the static field but along the direction of the r-f field of amplitude h. The transverse susceptibility describes the magnetic response (increase of $m_{\perp}$) per unit increase in r-f field amplitude in much the same way that G describes the wall velocity increase per unit increase in drive field. Similar to G, $X_{\perp}$ is independent of the excitation field amplitude h and diverges for no losses. For most physical situations, the r-f power level is small and the precession amplitude associated with $X_{\perp}$ (finite for nonzero losses) is extremely small. Thus, while domain wall motion involves large angle motion of $\overline{M}$ ($\overline{M}$ rotates by 180° for the situation discussed in Chapter 2), FMR involves only extremely

small deviations of $\overline{M}$ from its equilibrium position along the static

field. The magnetization dynamics in each case are quite different.

Nevertheless, both processes are loss limited and can be characterized

by a wall mobility and a transverse susceptibility respectively, both

of which are zero for infinite losses (no response) and diverge in the

limit of no losses.

In the same way that Chapter 2 was concerned with losses for wall

motion in thin films, this chapter is concerned with losses for ferro-

magnetic resonance. The resonance losses are reflected in the experi-

mental data for FMR in a very direct way. The usual technique for

observing resonance is to slowly change the applied static field while

observing the energy loss at a fixed r-f excitation frequency. As the

applied field is changed and the internal field passes through the field

value for which $\omega = \omega_u$, the magnetization will be driven to some

precession amplitude determined by the loss rate and energy will be

absorbed from the r-f field. For no losses, $X_\perp$ is infinite at $\omega = \omega_u$

and the energy absorption diverges for a vanishingly small excitation

field amplitude h. Off resonance, however, the r-f excitation does not

have a fixed phase relationship with the precession so that very little

energy absorption is expected. For no losses, then, the absorption

curve for resonance (a plot of r-f energy absorption vs applied static

field) could be described by a delta function centered at the value of

the applied field for which the internal field satisfies the resonance

condition. For nonzero losses, the amplitude of the absorption curve is

finite and its width is also nonzero. The difference between the field

values $H_o \pm \Delta H/2$ at which the energy absorption is one-half the maximum

absorption at H_o is used to define the half power linewidth ΔH. Since

the line broadens with increasing losses, the linewidth is a measure of

the losses associated with resonance. In the same way that the wall

mobility represents a measure of the losses associated with wall motion

(losses $\propto 1/G$), ΔH represents a measure of resonance losses (losses

$\propto \Delta H$).

Several approaches are possible for calculating the resonance

linewidth in thin films. A phenomenological equation of motion for

$\overline{M}$ (such as the Landau-Lifshitz equation or the Gilbert equation) can be

used to calculate the linewidth and a resonance loss parameter just as

the Landau-Lifshitz equation was used to calculate the wall mobility

and the damping parameter α. The main interest in the FMR linewidth

for thin films, however, is not because of any possible phenomenological

interpretation but because of the fact that, for resonance, some under-

standing of the physical relaxation processes is possible. The

phenomenological formulation of relaxation losses for wall motion was

necessary because no technique for calculating such losses from physical

principles has yet been developed. For FMR, however, the magnetization

motion consists of extremely small angle precession at a single

frequency and in some cases fundamental relaxation loss calculations

are possible. In Chapter 2, relaxation losses were defined (for

esthetic reasons) in terms of elementary interactions involving the magnetic normal modes (magnons) and the normal modes of the lattice (phonons). For FMR, this is a working definition for relaxation losses. For many insulating ferromagnets, the contributions of various magnon and phonon processes to the linewidth have been calculated and are in good quantitative agreement with experimental data. For conducting ferromagnets, progress has not been so rapid. At present, the most exciting aspect of resonance linewidth investigations in thin films is the opportunity to understand, at least qualitatively, what physical loss processes are really relevant and which are not. The investigation and results described in this chapter represent an initial step in the direction of such an understanding.

3.1.2 Uniform Mode Relaxation

The starting point for calculating resonance losses is with the precessing spin system. The simplest possible situation is one in which the field for resonance is uniform over the sample and the r-f excitation field is uniform in amplitude, direction, and phase throughout the sample. If these conditions are satisfied, the magnetization precession is also uniform both in amplitude and phase over the entire volume of the sample. This resonance mode is appropriately called the uniform mode. Throughout this chapter, it is the uniform mode which is assumed to be excited by the r-f field and the discussion will be concerned with relaxation processes for uniform mode resonance. The

assumption of uniform mode resonance is not a trivial one, even if the fields (static and r-f) are uniform throughout the sample. Considerable controversy exists concerning the effect of the sample surfaces on the internal fields for FMR and magnetization motion near the surfaces. This controversy represents another aspect of resonance phenomena in thin films which is not of direct interest in the present investigation of loss processes for resonance. It is sufficient to say that the measured fields for resonance satisfy the original Kittel resonance condition (Kittel, 1948) for uniform mode resonance.

Once the uniform mode has been excited, the precession amplitude and the susceptibility are determined by the various processes by which energy can be transferred from the precessing spin system to the lattice. The uniform mode is not the only normal mode of the magnetic system. Other spin wave modes are possible for which the precession angle and phase vary periodically through the lattice. Spin waves will be discussed in section (3.3). The uniform mode can be viewed as a spin-wave mode with wave number k equal to zero (infinite wavelength and no spatial variation in $\overline{M}$). In the same way that the normal modes for lattice vibrations can be quantized into phonon states and treated as particles, the normal modes of the magnetic system (spin waves) can be quantized into magnon states with particle properties. In particle language, it is relatively easy (at least in principle) to discuss relaxation losses in terms of scattering processes. Uniform mode relaxation processes can be viewed as scattering interactions between

the magnetic modes (spin waves) and the other modes of the system (electrons, phonons).

There are many possible scattering reactions by which the energy pumped into the precessing spin system (uniform mode magnons) may finally be transferred to the lattice vibrations (phonons) as joule heating. The existence of losses in the first place means that uniform mode magnons scatter into phonon states (lattice heating) by one path or another. Uniform mode magnons may relax directly into phonons or scatter into other magnon states which eventually relax into lattice vibrations. For complicated scattering sequences where several processes may be operative, the concept of a relaxation time for each scattering interaction is convenient in correlating the FMR linewidth with fundamental loss processes. Any individual scattering reaction can be characterized by a relaxation time which is a measure of the average lifetime of the initial state before it suffers a transition to the final state. If the total relaxation time for uniform mode magnons is long, for example, they decay into other states very slowly; the relaxation rate and the linewidth are both small. The linewidth is inversely proportional to the total relaxation time for uniform mode magnons.

Individual scattering interactions which may contribute to the total relaxation time are summarized in the block diagram of Fig.3-1 and may be characterized by their individual relaxation times. The
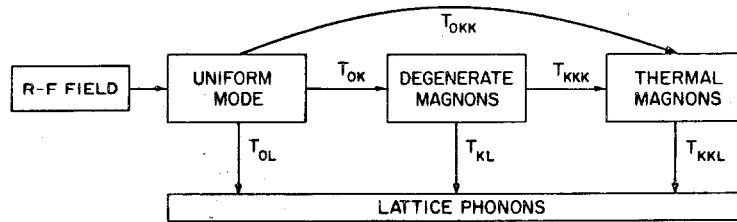
Fig.3-1. Relaxation channels for uniform mode resonance. The processes included are as follows:

T_{ok} two-magnon.

T_{ol} magnon-phonon, eddy-current, temperature-peak.

T_{okk} and T_{kkk} three-magnon.

T_{kl} and T_{kkl} multiple magnon-phonon.

uniform mode resonance is excited by the r-f field and uniform mode

magnons eventually relax into lattice phonons by various channels. For

processes which occur sequentially, such as (uniform mode) → (degenerate

magnons) → (phonons), the individual relaxation times add (only

approximately valid unless $T_{ok} >> T_{kl}$). For parallel processes which

occur simultaneously (such as the above sequence and the (uniform

mode) → (phonon) process), each process represents a separate loss

channel and the linewidths (or reciprocal relaxation times) add. For

the processes mentioned above, then

$$\Delta H \propto 1/T_{total} = 1/T_{ol} + 1/(T_{ok} + T_{kl}).$$

The complete expression, including all the loss channels indicated in

Fig.3-1, is extremely complicated. Such an expression can in concept

be constructed on the basis of the above information and Fig.3-1.

A large number of calculations have been made concerning the

various relaxation channels sketched in Fig.3-1. The aspects of these

calculations which are directly relevant to thin films have been

summarized by Comly (1965) and a detailed discussion of these calcula-

tions is not directly relevant to the present discussion. It is,

however, important to indicate briefly some of the physical ideas

involved and the large range of linewidths which have been obtained.

Corresponding to the classification scheme of Fig.3-1, these calcula-

tions may be grouped according to the nature of the scattering. Two

magnon (T_{ok}), multiple (three or more) magnon (T_{okk} and T_{kkk}), magnon-phonon (T_{ol}, T_{kl}, and T_{kkl}), temperature-peak (T_{ol}), and magnon-conduction electron (T_{ol}) processes have all been considered and will be touched on briefly.

Clogston et al. (1956) first pointed out the role of $k \neq 0$ magnons degenerate with uniform mode magnons in FMR relaxation, due to sample inhomogeneities which couple non k-conserving pairs of magnons together. Scattering involving only two magnon states (corresponding to T_{ok} in Fig.3-1) is not possible in a perfect lattice since the magnons correspond to normal modes which do not interact. Thin films, however, are very imperfect structures. The stray fields around localized imperfections and inhomogeneities produce a mode mixing so that the true normal modes consist of various combinations of the normal modes of the perfect lattice. This mode-mixing approach is useful for illustrating the point that two-magnon scattering is controlled by the imperfection or inhomogeneity distribution in the film.

Processes involving three or more magnons (denoted by T_{okk} and T_{kkk}) have been calculated by many workers. Three magnon scattering calculations by Sparks et al. (1961) and Schlömann (1961) yield numerical values for linewidth (from this process only) of 0.5 to 5.0 Oe (Comly, 1965) for parallel resonance in Ni-Fe films with 80% Ni at room temperature and 9 Gc/sec. Pincus, Sparks, and LeCraw (1961) have summarized calculations for four-magnon scattering, which give

linewidths from 5.0×10^{-4} to 1.5 Oe (Comly, 1965) depending on the details of the process.

The first proposal for magnon-phonon relaxation (denoted by T_{op}) was made by Akhieser (1946) who used an averaging procedure over all spin-wave states. His calculation is not appropriate for relaxation concerning only uniform mode or small k magnon relaxation. Kittel and Abrahams (1953) have estimated that the largest linewidth resulting from the magneto-elastic scattering of magnons into phonons for nickel at room temperature is 10^{-5} Oe. Kasuya and LeCraw (1961) have considered a two-magnon-one-phonon process which gives $\Delta H = 0.1$ Oe for Ni-Fe films (Comly, 1965).

In several classes of insulating ferromagnets, namely the ferrites and garnets, a characteristic linewidth maximum as a function of temperature occurs. For YIG (yttrium iron garnet), this behaviour is extremely sensitive to the substitution of various rare-earth ions for yttrium (Yager et al., 1955). For the ferrites, the behaviour has been associated with an electron hopping process between Fe^{2+} and Fe^{3+} ions in the ferrite (Teale and Tweedale, 1962). Because of the characteristic linewidth maximum, these processes are termed temperature peak processes. The maximum usually occurs below $100^{o}K$. No similar processes, however, have been observed or calculated for metals.

Several calculations have been made for magnon relaxation due to coupling between the magnetic and conduction electrons. These calcula-

tions (Kasuya, 1954; Abrahams, 1955; Kittel and Mitchell, 1956) give

linewidths which depend on some inverse power of spin wave number (for

nonzero-k magnons), and are between 3 Oe and 700 Oe.

In spite of the large amount of theoretical work on FMR relaxation,

very little consistent information exists. By proper (if arbitrary)

selection of processes, almost any linewidth can be explained. In line

with the old saying that one cannot see the forest for the trees, in the

present situation it is not possible to understand resonance relaxation

because of the large number of possible relaxation processes and the

even larger number of contradictory calculations pertaining to these

processes.

In spite of (or perhaps because of the confusion in) the large

amount of theoretical work on resonance relaxation, only a small number

of experimental investigations of the FMR linewidth in thin films have

been carried out. The bulk of these investigations were performed at

room temperature, at only a few frequencies, and using only a limited

number of film samples. For the most part, the results of these

investigations have been interpreted only phenomenologically (Smith,

1958; Smith and Harte, 1962; Rossing, 1963; Nelson, 1964) using the

Gilbert equation. Values of the damping parameter for resonance were

found to be significantly smaller than that for wall motion. Beyond

the phenomenological interpretation, very little progress has been made

in connecting the resonance linewidth for thin films with physical

processes or film properties. Rossing (1963) and Nelson (1964) found
that the linewidth is larger for films which show large fluctuations
in the magnitude of the uniaxial anisotropy constant K (large disper-
sion) than for films with a well-defined uniaxial anisotropy. Goser
(1965a) has investigated the thickness dependence of the parallel
resonance linewidth at frequencies from 1-9 Gc/sec in order to under-
stand the role of eddy-current losses. He concluded that eddy-current
losses were not important for any film thickness and that the linewidth
is independent of film thickness. Only two physical relaxation
processes have been proposed in connection with parallel resonance
linewidth data for thin Ni-Fe films. Inhomogeneity two-magnon
scattering of the sort originally proposed by Clogston et al. (1956)
has been used by Callen (1958) Comly and Penney (1963), and Berteaud
and Pascard (1965) to qualitatively explain an observed monotonic
increase of the parallel resonance linewidth with film thickness. A
similar monotonic increase of the parallel resonance linewidth with
thickness has been reported by Soohoo (1964) which he attributed to
magnon-conduction electron relaxation based on the Kittel-Mitchell
(1956) calculation. Soohoo ignores the possibility of inhomogeneity
two-magnon scattering and his adaption of the Kittel-Mitchell result
assumes that the relaxing magnons have wave numbers $k \approx 2\pi/D$ and not
$k = 0$ which is appropriate for the uniform mode. It is not clear why
this assumption is valid. Moreover, the original Kittel-Mitchell
result that $\Delta H \propto 1/k$ is not consistent with the data on linewidth as

a function of k by Comly (1965) which indicate that ΔH is not inversely proportional to k. The main problem concerning these linewidth investigations is in the complete disagreement between Goser's conclusion that ΔH is independent of D and the work of Belson (unpublished but mentioned by Callen (1956)), Comley and Penney (1963), Soohoo (1964), and Berteaud and Pascard (1965) which indicate that ΔH increases with thickness. If the monotonic increase with thickness is correct, Soohoo's explanation using the Kittel-Mitchell interaction can be excluded on the basis of Comly's data (since ΔH is not proportional to 1/k) but there is still no quantitative justification for accepting the two-magnon inhomogeneity scattering explanation. In addition, no work has been reported on the temperature dependence of the resonance linewidth. Such an investigation would be of great value in understanding the role of eddy-current losses (since the conductivity is temperature dependent) and the role of temperature-peak processes (such as the rare earth impurity process) in determining the resonance linewidth.

As is evident from the above discussion, the present day understanding of resonance relaxation in thin films is in a confused state, both theoretically and experimentally. Many calculations have been published and there is no lack of relaxation processes from which to choose. The experimental situation is no better. The data which have been published are contradictory and in the few cases where the data are in agreement, the interpretations are not in agreement. The

theoretical situation will continue to be confused until there is

sufficient experimental information to provide an indication as to the

relevant loss processes. What is needed, then, is a thorough investi-

gation of the parallel resonance linewidth for thin films as a function

of frequency, temperature, and thickness with careful attention to

minimizing the contribution of dispersion to the linewidth. The data

on ΔH as a function of thickness at room temperature can be used to

determine whether there is any dependence and if so, whether the thick-

ness dependence is really consistent with two-magnon inhomogeneity

scattering. The temperature dependence of ΔH can be used to examine

the importance of eddy-current losses and the possible existence of

magnon-phonon or temperature-peak processes.

Such an investigation is the objective of the work reported in

this chapter. The parallel resonance linewidth has been measured for

over two hundred Ni-Fe alloy films with approximately 77% Ni evaporated

under the same conditions described in Chapter 2 on wall motion. Film

thickness ranged from 150 to 3200 Å. These linewidths have been

measured at frequencies from 1-9 Gc/sec and temperatures from $2^{o}K$ to

$300^{o}K$. Such an extensive investigation represents a significant

advance in the understanding of FMR relaxation in thin metal films.

The most important results of this study are: (1) Evidence for the

monotonic increase of linewidth with thickness above a critical thick-

ness. (2) Evidence for a two-magnon inhomogeneity scattering process

associated with this thickness dependence. (3) Evidence that eddy-current losses do not contribute significantly to the resonance linewidth for film thickness less than 1500 Å, but do contribute for somewhat thicker films. (4) Evidence for a temperature-peak process in thin Ni-Fe films. The first three of these results represent confirmations of earlier proposals. The fourth result is completely new, one which was unexpected and is not yet fully explained.

In the next section (3.2), a short discussion of the phenomenological formulation of resonance losses will be presented. This will serve as a basis for comparing linewidth data with the wall motion results of the last chapter and for discussing earlier linewidth results. In addition it will serve as further motivation for investigating physical loss processes, without recourse to the phenomenological formulation. The inadequacy of the phenomenological formulation for resonance losses will be made evident. In order to make an effective connection between the experimental data and the conclusions concerning physical loss mechanisms summarized above, it will be necessary to briefly review the relevant mechanisms in more detail. In section (3.3), two-magnon scattering will be considered. In the first part of this section, the relevant material concerning spin waves in thin films will be reviewed, and two-magnon scattering proper will be discussed in the second part. In section (3.4) temperature-peak processes and eddy-current losses will be considered. Each of

these two mechanisms, if operative, give the linewidth a definite

temperature dependence and will be important in discussing the line-

width vs temperature data. These three sections serve to provide the

theoretical background for the discussion of the present experimental

results. The theoretical ideas are developed within the context of

existing experimental information. In section (3.5) the apparatus

which was used to obtain the present linewidth data will be described

in detail. In section (3.6), the data will be presented and discussed

in terms of the various ideas developed in the earlier sections.

Using the phenomenological formulation of section (3.2), values of the

damping parameter α appropriate for FMR will be obtained which can be

compared to the α for wall motion. More important, the data will also

be shown to be consistent with the assumption that two-magnon

scattering is associated with the linewidth thickness dependence.

Linewidth data as a function of temperature will be presented which

demonstrate the existence of a temperature-peak process for FMR

relaxation in thin films. Possible origins for this temperature-peak

process will be discussed. In section (3.7) the results of this

investigation of FMR relaxation in thin films will be summarized.

3.2 PHENOMENOLOGICAL LOSS FORMULATION

In the introduction, the emphasis was on physical loss mechanisms

for FMR. While a physical understanding is the primary objective of

this chapter, there are several reasons for considering a phenomeno-

logical approach. Physically, both domain wall motion (considered in

the last chapter) and FMR represent a damped precessional motion of the

magnetization, a large amplitude precession about the Becker field in

the case of wall motion and a small angle precession about the internal

field in the case of resonance. If the phenomenological formulation

really provides a reasonable description of the losses for magnetiza-

motion, the values of the damping parameter α should be similar for

both phenomena. In order to obtain α from linewidth data for

comparison with the α for wall motion, a phenomenological calculation

based on the Landau-Lifshitz or Gilbert equation is necessary. A

second reason for having a phenomenological formulation of resonance

linewidth is simply that a large amount of data has been interpreted

phenomenologically by other workers (Smith, 1958; Smith and Harte, 1962;

Rossing, 1963; Nelson, 1964) and a basis for comparison with these

earlier results would be convenient. The final reason for devoting the

present section to the phenomenological treatment of resonance losses

is that it provides a further motivation for considering physical loss

processes. After the phenomenological formulation has been presented,

it will be shown that such a treatment is inadequate. A phenomenologi-

cal formulation is most useful for situations in which the loss

parameter is approximately constant as was shown to be the case for wall

motion. If the loss parameter for resonance turns out to be dependent

on a number of experimental parameters, the simplicity of the approach

is sacrificed and the formulation is no longer justified. Such is the

situation for FMR in thin films, as will be discussed shortly. In some

contexts, the phenomenological formulation is still useful but it cannot be expected to provide an adequate basis for any quantitative description of resonance losses.

In the section on relaxation losses for wall motion, the physical motivation for the phenomenological equations of motion for the magnetization (such as the Landau-Lifshitz equation or the Gilbert equation) was discussed extensively. The equations were based on a viscous damping model in which a rotating vector experiences a drag torque during motion in a fluid medium. The Landau-Lifshitz equation was then used to calculate the domain wall mobility in terms of a phenomenological damping parameter α which was later determined experimentally to be 0.014, independent of film thickness and domain wall shape. The calculation of the resonance linewidth is usually done using the Gilbert equation rather than the Landau-Lifshitz equation. In the Gilbert equation,

$$d\overline{M}/dt = -\gamma(\overline{M} \times \overline{H}_i) + (\alpha/M)(\overline{M} \times d\overline{M}/dt), \qquad (3.1)$$

the loss term is written using $d\overline{M}/dt$ rather than the triple cross product $\overline{M} \times (\overline{M} \times \overline{H})$ as in the Landau-Lifshitz equation, and is more convenient for handling time-harmonic fields and magnetization components.

Consider a right-handed x:y:z coordinate system with the static magnetic field $\overline{H}$ in the z-direction, and a small amplitude r-f excitation field $he^{i\omega t}$ ($h << \Delta H$) at frequency ω and in the x-direction. For this discussion, it is not necessary to assume thin film geometry. Let (N_x, N_y, N_z) be the sample demagnetizing factors in the (x,y,z) directions respectively. For small r-f amplitudes, the precession amplitude will be much less than M and to first order the z-component of the magnetization in the static field direction is equal to M. If the transverse components of $\overline{M}$ are denoted by $m_x e^{i\omega t}$ and $m_y e^{i\omega t}$, the total field and the total magnetization can be written as:

$$\overline{H}_i = (H - N_z M)\overline{e}_z + (-N_y m_y e^{i\omega t})\overline{e}_y + (he^{i\omega t} - N_x m_x e^{i\omega t})\overline{e}_x, \qquad (3.2a)$$

$$\overline{M} = M\overline{e}_z + (m_y e^{i\omega t})\overline{e}_y + (m_x e^{i\omega t})\overline{e}_x, \qquad (3.2b)$$

where ($\overline{e}_x$, $\overline{e}_y$, $\overline{e}_z$) denote unit vectors. These expressions for $\overline{H}_i$ and $\overline{M}$ can be substituted into the Gilbert equation, the x- and y-components of which then yield two simultaneous equations for m_x and m_y. The susceptability $\chi_\perp = m_x/h$ can be obtained from the solution for m_x and is given by

$$\chi_\perp = m_x/h = \gamma M(1/X - i\alpha\omega/\omega_u^2)/\{(1-\omega^2/\omega_u^2) - i\alpha\omega(X+Y)/\omega_u^2\} \qquad (3.3)$$

where $X = \gamma\{H - (N_x - N_z)M\}$, $Y = \gamma\{H - (N_y - N_z)M\}$, and $XY = \omega^2$. The

Kittel resonance condition (Kittel, 1948) for uniform mode resonance at
a frequency ω_u in an applied field H can be obtained from $XY = \omega_u^2$. As
can be seen from the denominator of the R.H.S. of Eq.(3.3), $\chi_\perp$ is
maximum for $\omega = \omega_u$ and diverges if $\alpha = 0$, which is consistent with the
previous qualitative discussion.

Equation (3.3) gives the x-component of the transverse suscepti-
bility (in the field direction) of the ferromagnetic sample as a func-
tion of applied field (since X, Y, and ω are defined in terms of H).
The quantity of experimental interest is not the susceptibility $\chi_\perp$ but
the energy absorption rate as a function of field. The power loss for
the system (i.e. the r-f power input) can be calculated as the time
average of $dE/dt = -\overline{M} \cdot d\overline{H}/dt$. Only the $(m_x e^{i\omega t})(h e^{i\omega t})$ term in dE/dt
gives a real contribution whose time average is not zero. If the
standard definition $\chi_\perp = \chi_\perp'' - i\chi_\perp''$ is used to separate the real and
imaginary parts of $\chi_\perp$, the time average power loss can be calculated
to be

$$(dE/dt)_{time\ av} = -\omega h^2 \chi_\perp''/2. \qquad (3.4)$$

In other words, the FMR absorption curve (power absorption as a
function of applied field) is proportional to the imaginary part of
the transverse susceptibility. The linewidth ΔH is the difference
between the field values for which χ'' (the imaginary part of Eq.(3.3))

has half its maximum amplitude. Half-amplitude points occur at field

values (approximately) for which $(1-\omega^2/\omega_u^2) = \alpha\omega(X+Y)/\omega_u^2$ which are

approximately equal to $H(\omega = \omega_u) \pm \alpha\omega_u/\gamma$ so that the linewidth is

given by $\Delta H = 2\alpha\omega_u/\gamma$.

Assuming that α is a constant, three properties of the linewidth
are predicted from the above phenomenological treatment. First, no
shape demagnetizing factors or vector quantities appear in ΔH, so that
the linewidth is expected to be independent of sample shape and field
orientation. Second, the linewidth is expected to increase linearly
with r-f excitation frequency, and finally, ΔH should be zero in the
limit $\omega_u = 0$. Only the second of these expectations has been confirmed
experimentally (Smith, 1958). Tannewald and Seavey (1957) and Berteaud
and Pascard (1965) have reported that the linewidth is a function of
field orientation with respect to the film plane. Soohoo (1964) and
Berteaud and Pascard (1965) also find that the parallel resonance
linewidth increases linearly with film thickness so that ΔH is dependent
on the sample dimensions. Smith (1958), Smith and Harte (1962), Rossing
(1963), and Nelson (1964) report that the linewidth is linear in
frequency but does not extrapolate to zero for zero frequency. Rather
than $\Delta H = 2\alpha\omega_u/\gamma$, they find that the linewidth is better described by

$$\Delta H = (\Delta H)_o + 2\alpha\omega_u/\gamma \tag{3.5}$$

If Eq.(3.5) is to be consistent with the thickness dependence of the

linewidth reported by Soohoo (1964) and Berteaud and Pascard (1965),

α must be taken to be thickness dependent. The linewidth, however, has

been found to be dependent on other parameters besides film thickness

and excitation frequency. The original data reported in conjunction

with Eq. (3.5) by Smith (1958),were correlated with dispersion in the

uniaxial anisotropy field magnitude $H_K = 2K/M$. Further research by

Rossing (1963) and Nelson (1964) indicated that both $(\Delta H)_o$ and α

increase with magnitude dispersion of the uniaxial anisotropy. This

situation is in considerable contrast with the situation for wall

motion, where α remains constant independent of film thickness and wall

shape.

From the previous discussion two points are evident. First, a

phenomenological description of resonance losses is straightforward

and simple. The resonance linewidth may be characterized by two

parameters, $(\Delta H)_o$ and α. Second, and more important, it should be

evident that such a description is not adequate. A phenomenological

formulation is most useful in situations for which the loss parameter

is approximately constant (as for wall motion). The primary justifi-

cation for such an approach is in its simplicity. If the loss

parameter turns out to be dependent on film thickness, field direction,

excitation frequency, and dispersion (as for FMR), the simplicity of

the approach is sacrificed and the phenomenological formulation is no

longer justified. In some contexts, the phenomenological formulation

is still useful (such as for comparison of FMR with wall motion or in discussing earlier FMR data) but it cannot be expected to provide an adequate basis for any quantitative physical description of resonance losses.

3.3 TWO-MAGNON SCATTERING

3.3.1 Spin Waves in Thin Films

In the introduction (section 3.1), relaxation processes were described in terms of scattering interactions between two or more different magnons or between magnons and other normal modes of the system (such as phonons). As is the case for phonons and electrons, all combinations of ω and $\bar{k}$ are not allowed for spin waves. Only definite spin-waves states are possible which are described by a characteristic spin-wave dispersion relation $\omega = \omega(\bar{k})$, just as phonons and electrons have their own characteristic dispersion relations. Before discussing two-magnon scattering, it is necessary to know which magnon states are allowed, and a brief discussion of the dispersion relation for spin waves in thin films is required. The spin-wave dispersion relation for thin films can be best understood by first considering the dispersion relation for spin waves in bulk material, which can be obtained formally by a method introduced by Holstein and Primakoff (1940). Rather than present the tedious mathematics of this calculation, the normal modes will be constructed

from a plausibility argument (Sparks, 1964) which demonstrates the physical origin of spin waves and their dispersion relation.

The starting point for the development is the hamiltonian for the magnetic system, including only the Zeeman and exchange energies.

$$H = -g\mu_o \sum_i \overline{S}_i \cdot \overline{H} - 2J \sum_{i,j} \overline{S}_i \cdot \overline{S}_j \tag{3.6}$$

The $\overline{S}_i$ are the spins of the magnetic electrons, $\overline{H}$ is the magnetic field, and J is the exchange integral. The j summation in the exchange term is over the nearest neighbors of $\overline{S}_i$ and the i summations are over the N spins of the system. The ground state (the state of minimum energy) is the state in which every spin in the sample is aligned parallel to the applied d-c magnetic field. Both the Zeeman and exchange energy are minimum for this configuration. One initial guess as to the first excited state would be to flip one spin antiparallel to the magnetic field. However, this state with one flipped spin corresponds to a very high exchange energy. Since the exchange energy is proportional to $-\cos\delta$, where δ is the angle between neighboring spins, it can be kept small by keeping δ small. Thus, a judicious twist on the spin system gives a much smaller exchange energy than the flip of an individual spin. The most economical twist is shown in Fig.3-2. Each spin is tipped at the same angle β with respect to the applied field. For small β, the Zeeman energy is small. This disturbance on the spin system is called a spin wave and is a normal mode of the system. The detailed quantum-
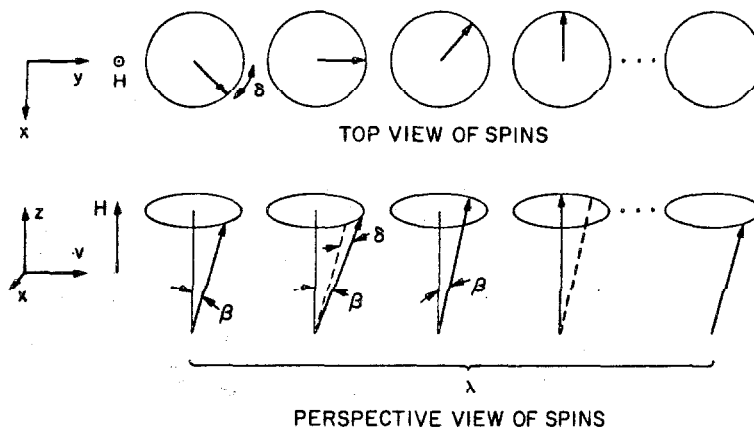
Fig.3-2. Spin wave propagating along the y-axis. The angle β between a spin and the applied field $\overline{H}$ is the same for each spin. The angle δ between adjacent spins is the same for each pair of neighboring spins. Each spin precesses at frequency ω_k and all the spins in any plane perpendicular to $\overline{e}_y$ are parallel.

mechanical calculation (Holstein and Primakoff, 1940) is in agreement

with this simple picture. In particular, the precession angle β is the

same for each spin and the angle between neighboring spins along a

given direction is the same for all spins. The shortest distance

between parallel spins (except in the plane containing all parallel

spins, the x:z plane in Fig.3-2) defines the propagation direction

(y-direction in Fig.3-2) and the wavelength λ. The wave vector $\overline{k}$ has

magnitude $2\pi/\lambda$ (the conventional definition) and is directed along the

propagation direction.

From an understanding of the spin-wave picture discussed above and

sketched in Fig.3-2, the general shape of the dispersion relation

$\omega = \omega(k)$ can be obtained. The exchange energy of a magnon with

frequency ω is $(\hbar\omega)_{exch}$.

$$(\hbar\omega)_{exch} \propto \overline{S}_i \cdot \overline{S}_{i+1} \propto -\cos\delta \approx -(1 - \tfrac{1}{2}\delta^2). \tag{3.7}$$

Since δ is inversely proportional to $\lambda (\delta \approx 2\pi(a/\lambda)$ if a is the spin-

separation distance) and k is also inversely proportional to λ, δ is

proportional to k. Thus, the exchange energy of a magnon (ω, k) is

$$(\hbar\omega)_{exch} = Bk^2 \tag{3.8}$$

neglecting constant terms. The coefficient B is given by $2SJa^2$, where

S is the electron spin, and a is the nearest neighbor distance in the magnetic lattice. (B is related to the exchange constant A of Chapter 2 by $B = 2A\gamma\hbar/M$.) From the rigorous calculation, it can be shown that for a single magnon corresponding to a spin-wave (ω, k) with an energy of $\hbar\omega_k$ (i.e. the magnon occupation number n_k is 1), each spin is tipped by an angle β from the field such that the total change of the magnetic moment in the field direction is the same as if one spin were completely flipped. For one magnon $(\omega, k, n_k = 1)$, $(\hbar\omega)_{Zeeman} = g\mu_o H$ and the total magnon energy is

$$\hbar\omega_k = g\mu_o H + Bk^2. \tag{3.9}$$

This dispersion relation, however, is still incomplete. The direction of propagation for the magnon has not been taken into account (the above equation has no directional dependence on $\overline{k}$). In the same way that a nonzero $\nabla \cdot \overline{M}$ produced a demagnetizing field energy term for domain walls, the magnetization divergence associated with spin waves propagating at right angles to the applied field raises the energy for these transverse directed spin waves. For spin waves propagating parallel to the applied field (and $\overline{M}$), $\nabla \cdot \overline{M} = 0$ and there is no additional demagnetizing field energy. The effect of the demagnetizing field energy, therefore, is to add a term to $\hbar\omega_k$ which is proportional to $\overline{H} \times (\overline{k}/k)$. If the angle between the wave vector $\overline{k}$ and the applied field $\overline{H}$ is denoted by θ, the spin wave dispersion relation $\omega = \omega(k, \theta)$

can be displayed as shown in Fig.3-3, including Zeeman, exchange, and
volume demagnetization energies. The set of dispersion curves for all
values of θ, $0 < \theta < \pi/2$ are contained in the region between the
$\theta = 0$ and the $\theta = \pi$ dispersion curves. Considered collectively, these
curves represent a continuum of magnon states (θ can have any value
between 0 and $\pi/2$) which is called the magnon or spin-wave manifold.
The exact expression for $\omega = \omega(k,\theta)$ is given by (Holstein and Primakoff,
1940):

$$\hbar\omega_k = \left[(Bk^2 + \hbar\omega_i)(Bk^2 + \hbar\omega_i + \hbar\omega_m \sin^2 \theta_k)\right]^{\frac{1}{2}} \qquad (3.10)$$

where $\hbar\omega_m = 4\pi\hbar\gamma M$ and $\hbar\omega_i = \hbar\gamma H_i$. The internal field $\overline{H}_i$ (in the
z-direction) is equal to $H - 4\pi N_z M$ (the sample is assumed to be satur-
ated in the direction of the applied field) where H is the applied
field and N_z is the sample demagnetizing factor along the z-axis. For
FMR in thin films with the applied field in the plane of the film
(parallel resonance), $N_z = 0$ and $\overline{H}_i = \overline{H}$.

It should be noticed that the sketch of the spin-wave manifold in
Fig.3-3 does not extend to $k = 0$. The dispersion relation of Eq.(3.10)
and Fig.3-3 is not valid for very small values of k where the spin-wave
wavelength is greater than the film thickness because of surface
demagnetization fields which are induced by the divergence of $\overline{M}$ at the
surfaces of the sample. The surface demagnetization field of a magnon
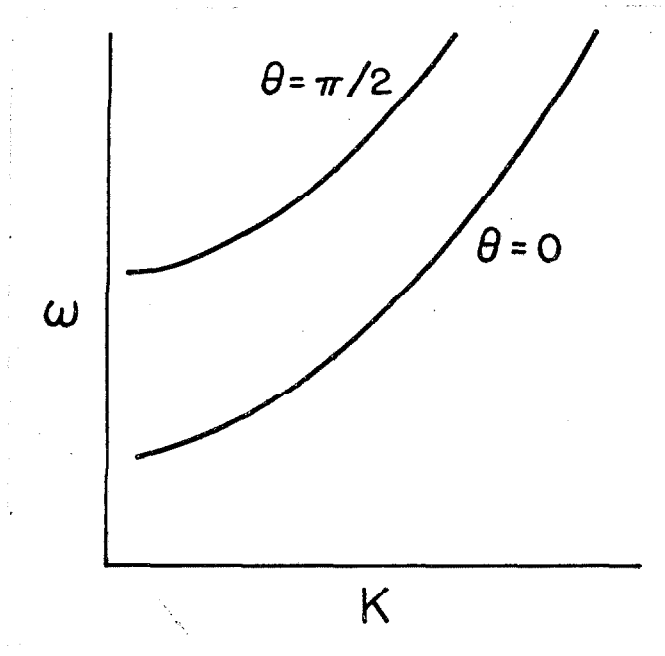whose wavelength is much smaller than the dimensions of the sample can

Fig.3-3. Spin-wave dispersion relation including Zeeman, exchange, and volume demagnetization energy terms. The lower bound of the manifold (θ = 0) corresponds to spin waves with k along the field direction while θ = π corresponds to k perpendicular to the field direction.

be neglected because the divergence of $\overline{M}$ oscillates very rapidly along the surface of the sample, thus integrating to zero except for the magnetostatic component which produces the static shape demagnetizing field. However, when the wavelength of the magnon is no longer much smaller than the sample size, this surface demagnetization must be taken into account. Walker (1957) has calculated the normal modes for a spherical sample when this surface demagnetization field is included. The resulting modes, called magnetostatic modes, were discovered in experiments by White and Solt (1956a, 1956b; Dillon, 1956) prior to Walker's calculations. Walker solved the problem for modes with $k \approx 0$ and neglected exchange. Damon and Eshbach (1961) have repeated Walker's calculations for thin film geometry, again neglecting exchange. Both of these calculations are therefore valid only for $k \approx 0$ where the exchange contribution to the dispersion and the slope $d\omega/dk$ are small. Harte (1964) has recently calculated the spin-wave spectrum for thin films taking into account Zeeman, exchange, volume demagnetization, and surface demagnetization energies. Although the detailed predictions of these three calculations vary, they all predict that the dispersion relation is very similar to the bulk dispersion for λ less than the film thickness, but for wavelength such that $\lambda \gtrsim D$ the dispersion is modified significantly. The magnetostatic mode modification of the spin-wave dispersion relation for thin film is sketched in Fig.3-4. The modified magnon manifold is shown for three situations, an extremely thick film ($D \approx 10,000 \text{ Å}$), a thin film ($D \approx 1000 \text{ Å}$), and a very thin

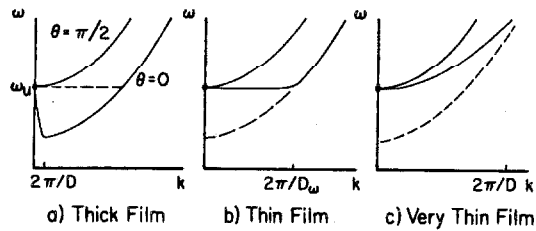a) Thick Film   b) Thin Film   c) Very Thin Film

Fig.3-4. Magnetostatic mode modification of the spin-wave dispersion relation for thin films with the applied field $\bar{H}$ parallel to the film plane. (a) Thick film where $D >> D_\omega$. (b) Thin film where $D = D_\omega$. (c) Very thin film where $D << D_\omega$. The critical thickness D_ω is about 1000 Å for 80-20 Ni-Fe films and FMR from 1 to 9 Gc/sec.

film ($D \approx 100$ Å). For the thick film case, the dispersion is very similar to the relation for bulk material for $k \gtrsim 2\pi/D$. For $k < 2\pi/D$, however, the dispersion does not follow the bulk relation. Instead, the boundaries of the manifold converge to the uniform mode resonance frequency ω_u at $k = 0$. The situation is the same for thinner films (Case (b) and (c) in Fig.3-4) except that the convergence begins at larger k (the transition point $k_D = 2\pi/D$ moves to larger k with decreasing thickness). The thickness dependence of the thin film dispersion relation, qualitatively sketched in Fig.3-4, is the primary result of this discussion. The physical origin of the bulk dispersion relation and the thin film magnetostatic modifications have been discussed and mathematical details have been avoided. The information in Fig.3-4 will be of considerable importance in discussing two-magnon scattering.

3.3.2 Two-Magnon Scattering

One scattering interaction which will prove to be of interest in connection with the experimental data is the process in which a uniform precession magnon (at frequency ω_u with $k = 0$) scatters into another magnon at the same frequency ($\omega_u = \omega_k$) but with $k \neq 0$. In the relaxation scheme of Fig.3-1 discussed in the first section (3.1), this is a T_{uk} process. It is important to realize that this u $\rightarrow$ k process is only one reaction in the total relaxation scheme and will influence the linewidth significantly only if the subsequent relaxation channels following (u $\rightarrow$ k) have fast relaxation times compared to T_{uk} and

parallel relaxation channels which do not involve $(u \rightarrow k)$ have slow

relaxation times compared to T_{uk}. The T_{uk} process can be viewed as

the destruction of a uniform mode magnon (so that the uniform mode

magnon occupation number n_u goes to n_u-1) and the creation of a magnon

with $k \neq 0$ (so that some n_k goes to n_k+1). By this process, one

quantum of energy is removed from the uniform mode and appears in some

other spin-wave state.

On the basis of the spin-wave dispersion for thin films, discussed

above and sketched in Fig.3-3, an understanding of two-magnon scatter-

ing is possible. Suppose that uniform precession is excited in a thin

film containing a spherical pore, imperfection, or some other magnetic

inhomogeneity. The magnetization vector will have a transverse

component which rotates with time and the resultant demagnetization

field $\overline{H}_D$ is a dipole field (for a spherical inhomogeneity). Suppose

that in addition to the uniform precession there is also another magnon

$\overline{k}$ excited in the film. In addition to the dipole field $\overline{H}_D$ from the

uniform precession, there is a magnetization $\overline{M}_k$ from the k magnon.

Classically, there is energy transferred from the uniform mode into

$\overline{k}$ magnons at a rate given by $\int d\overline{r}\; \overline{H}_D \cdot (d\overline{M}_k/dt)$. Using quantum-

mechanical transition probability theory, Sparks (1961) has calculated

the relaxation time for such a process. The energy transfer mechanism

described above, however, is an oversimplification. The transition

probability per unit time TP_k (i.e. the rate) for going from a given

state $\left| n_k, n_u \right\rangle$ to a state $\left| n_k + 1, n_u - 1 \right\rangle$ containing one less uniform mode magnon and one more $k \neq 0$ magnon is given by

$$TP_k = (2\pi/\hbar) \left\langle n_k+1, n_u-1 \left| H' \right| n_k, n_u \right\rangle \delta(\hbar\omega_u - \hbar\omega_k) \qquad (3.11)$$

where the quantum-mechanical scattering hamiltonian H' is $-\int d^3 r \bar{H}_D \cdot \bar{M}_k$. Even this formulation is an oversimplification. In the actual calculation the magnetization $\bar{M}_k$ must be taken as the total magnetization when all magnons are present, the demagnetization field must be taken to be the total demagnetization field for all magnons present, and a self-energy factor of $\frac{1}{2}$ must be included in H'; also, the inverse process in which a uniform precession magnon is created and a $\bar{k}$ magnon is annihilated must be included in Eq.(3.11). The total time rate of change of uniform precession magnons is then given by the sum of Eq.(3.11) over all $\bar{k}$.

Spark's original calculation was carried out for a spherical sample, assuming spherical pores and an applied field large enough to hold the magnetization in the field direction even in the vicinity of the pores where demagnetizing fields are quite large. The details of the calculation are not appropriate for parallel resonance in thin films at 1-9 Gc/sec, for two reasons. (1) The inhomogeneity distribution and geometry are not precisely known. (2) For parallel resonance at 1-9 Gc/sec, $H \ll 4\pi M$. However, several of the qualitative results are

of general validity and are directly applicable to two-magnon scatter-
ing for resonance in thin films. The first result is immediately
evident from Eq.(3.11). Because of the $\delta(\hbar\omega_u - \hbar\omega_k)$ term, scattering
can occur only between degenerate states with $\omega_u = \omega_k$. In order for
two-magnon scattering to contribute to the linewidth, magnon states
must exist which are degenerate with ω_u. Because of the magnetostatic
mode modification of the spin-wave dispersion relation for thin films,
such a degeneracy is possible only for sufficiently thick films. As
discussed previously and shown in Fig.3-4, for a thick film
$(D > 10,000$ Å, Case (a) in Fig.3-4) there are many magnon states
degenerate with ω_u (indicated by the dotted line). For extremely thin
films $(D < 100$ Å, Case (c) in Fig.3-4) there are no magnon states
degenerate with ω_u and two-magnon scattering cannot contribute to the
linewidth. The thickness D_ω corresponding to the dispersion of Case (b)
in Fig.3-4, $(D \approx 1000$ Å) represents a critical value. For $D > D_\omega$, two-
magnon scattering is allowed and for $D < D_\omega$, two-magnon scattering is
not allowed. The ability to eliminate two-magnon scattering from the
relaxation scheme by selecting films with $D < D_\omega$ will be very important
in the interpretation of the experimental data to follow in section
(3.6).

If two-magnon scattering actually does contribute to ΔH, some
change in the linewidth as a function of thickness should be evident
near $D = D_\omega$. For $D > D_\omega$, where two-magnon scattering is allowed, two
factors determine whether or not a $(u \rightarrow k)$ process will actually occur.

The first of these concerns the nature of the scattering centers (the voids, pores, or other magnetic inhomogeneities). This factor is only of academic interest primarily because the geometry and distribution of these scattering inhomogeneities in thin films are not well understood. As shown by Sparks (1961), scattering will occur from uniform pre-cession magnons to degenerate magnons corresponding to spin waves with wavelengths on the order of the dimensions of the scattering centers. Since the degenerate magnons (corresponding to the dotted line in Case (a) of Fig.3-4) exist for $0 < k < 10^5 \, cm^{-1}$ for FMR at 1-9 Gc/sec, the only scattering centers which can be of importance for two-magnon scattering must be larger than about 1000 $\overset{o}{A}$ in size. Evaporated Ni-Fe films are known to contain a large number of imperfections (non-magnetic inclusions, voids, grain boundaries, dislocations) so that some inhomo-geneities greater than 1000 $\overset{o}{A}$ in size are certain to exist.

The density of magnon states degenerate with ω_u is the other factor which determines whether or not a $(u \rightarrow k)$ process will actually occur. It is this density which can provide a qualitative prediction of the linewidth thickness dependence based on two-magnon scattering. Since two-magnon scattering is possible between the uniform mode and any degenerate magnon state (assuming scattering centers with the appropriate dimensions exist), the total relaxation rate is the sum of the individual rates for single scattering interactions (given by TP_k in Eq.(3-4)) over all magnon $\overline{k}$ states degenerate with ω_u. The relaxation rate due to two-magnon scattering and the resultant line-

width will be a function of the density of magnon states degenerate

with ω_u. No quantitative calculation for the density of states

degenerate with the uniform mode for parallel resonance in thin films

has been reported (except, of course, for the point that there are no

degenerate states for $D < D_\omega$, as discussed above). Nevertheless, a

qualitative idea of the thickness dependence of this density of states

can be obtained by again considering the thin film dispersion relations

shown in Fig.3-4. The portions of the magnon manifold corresponding to

bulk material spin-wave states (i.e. for $k > 2\pi/D$) represent a high

density of states since θ can take almost any value $0 < \theta < \pi/2$. The

portions of the manifold corresponding to magnetostatic modes (i.e. for

$k < 2\pi/D$) do not even approximately correspond to continuum states. For

$k < 2\pi/D$, only discrete $(\omega, \bar{k})$ combinations (corresponding to the allowed

magnetostatic modes) are allowed and only a relatively small number of

these states are degenerate with ω_u. As the film thickness increases

beyond D_ω (for $D < D_\omega$ there are no continuum states degenerate with ω_u),

the continuum region of the manifold containing states degenerate with

the uniform mode increases, as $k_D = 2\pi/D$ becomes smaller. In other

words, the density of magnon states degenerate with ω_u is zero for

$D < D_\omega$ and increases with thickness for $D > D_\omega$. This dependence of

the density of states degenerate with ω_u should be reflected in the

linewidth-thickness dependence if two-magnon scattering is important.

For $D < D_\omega$, the linewidth should be independent of thickness

(assuming none of the other processes contributing to ΔH are

thickness dependent) and should increase with thickness for

$D > D_\omega$.

On the basis of the above discussion, experimental linewidth data can be used to determine whether two-magnon scattering is operative to any large extent. The first step is to positively identify (or eliminate) a two-magnon scattering process in the FMR relaxation scheme for parallel resonance in thin films. In this regard, progress has already been made, as previously discussed, but some of the results are contradictory. Goser (1965b) has reported that ΔH is independent of D (which indicates that no two-magnon process is operative). On the other hand, Callen (1958), Comly and Penney (1963), Soohoo (1964), and Berteaud and Pascard (1965) have observed a linear increase in linewidth with thickness for parallel resonance in 80-20 Ni-Fe films at 9 Gc/sec and thickness from 500 to 6000 Å (consistent with two-magnon scattering). In addition, Berteaud and Pascard (1965) have measured linewidths on the same samples for resonance with the applied field perpendicular to the film plane. For this field orientation ω_u falls at the $k = 0$ extrapolation of the bottom of the spin-wave manifold of Fig.3-4, where there are no degenerate magnon states for any thickness so that two-magnon scattering is eliminated for all thickness values. Consequently, the perpendicular resonance linewidth would be expected to be independent of thickness, which is exactly what Berteaud and Pascard observed. Except for Goser's data, all of the experimental work which has been reported support the two-magnon scattering hypothesis. The crucial test would lie in the experimental observation of the

critical thickness effect for parallel resonance; ΔH should be indepen-
dent of thickness for $D \lesssim D_\omega$ and increase with thickness for $D \gtrsim D_\omega$.
As can be seen from the dispersion relations in Fig.3-4, D_ω can be
estimated by solving for k_ω, the value of k for which $\theta = 0$ and
$\omega_k = \omega_u$ since $D_\omega = 2\pi/k_\omega$. The bulk dispersion relation (Eq.3-10)) can
be used for this calculation and D_ω will be obtained as a function of
uniform mode excitation frequency. If the critical thickness effect
can be observed experimentally and empirical D_ω values extracted from
the linewidth data, the dependence of D_ω on r-f excitation frequency
will provide a crucial test of the two-magnon scattering hypothesis.
The experimental results will be discussed in section (3.4) concerning
the room-temperature linewidth data.

3.4 TEMPERATURE DEPENDENT RELAXATION PROCESSES

The two-magnon process discussed in the last section has no
significant temperature dependence for FMR at room temperature and
below because of the high Curie temperatures for Ni-Fe alloys (from
about 350°C for 100% Ni to about 750°C for 100% Fe). The data, however,
indicate that the thin film linewidth does exhibit a significant
temperature dependence. In preparation for a discussion of these data,
it is important to discuss several processes which appear to be
relevant. The major portion of this section will be concerned with
eddy-current losses. If important, these losses should result in a
linewidth contribution which has a temperature dependence related to

the temperature dependence of the conductivity of the sample. For Ni-Fe alloys, this conductivity increases with decreasing temperature from about $16\mu\Omega$-cm at 300°K to $9\mu\Omega$-cm at 77°K and then levels off. The linewidth data indicate that, in addition to eddy currents, another process may be important. In some cases, the linewidth shows a peak as a function of temperature. Several processes which are well known in connection with relaxation in insulating ferromagnets and which predict a linewidth temperature dependence similar to the present data will be considered briefly.

In FMR, as in wall motion, eddy-current losses simply denote the joule heating of the system by the eddy currents which are generated because of the magnetization motion. An understanding of the eddy-current contribution to the linewidth will be important in the discussion of the data, to follow in section (3.6). Two previous investigations, an order of magnitude calculation by Smith (1963) and an experimental study by Goser (1965a,b), will be discussed briefly and the results of a very recent calculation by Schlömann (1967) will be presented.

Smith (1963) calculated that the linewidth in thin films due to eddy currents should vary linearly with conductivity and frequency, and quadratically with film thickness. He predicted that the eddy-current contribution to the linewidth would be comparable to the relaxation loss contribution for $D \approx 3,000$ $\overset{\circ}{A}$. On the other hand, Goser (1965a,b) has

observed FMR in thin films 200 $\overset{o}{A}$, to 150,000 $\overset{o}{A}$ thick and reported no change in linewidth. He concluded that eddy currents do not influence the linewidth for any thickness. Smith assumed that the r-f field was uniform throughout the film sample even though the on-resonance skin depth is on the order of 1000 $\overset{o}{A}$ (to be discussed shortly). He also assumed that the magnetization precession cone consisted of a flat ellipse with $\overline{M}$ essentially in the film plane, which is justified at 1 Gc/sec where the eccentricity of the elliptical precession cone is almost unity but is not valid at higher frequencies. At 9 Gc/sec, for example, the ratio m_x/m_y is greater than 1/3. On the other hand, the linewidths reported by Goser are an order of magnitude greater than previous measurements on Ni-Fe films (Smith, 1958; Nelson, 1964). His measurements were carried out for films which were electrolytically deposited on brass tubes, quite a different situation from vacuum deposited films on glass substrates. Various additives in the electrolyte for the electro-deposition of Ni-Fe films are necessary to obtain good films (uniform composition, low dispersion, low coercive force) as reported by Luborsky (1966) and these additives may well result in line broadening. In any case, Goser's linewidths are an order of magnitude greater than reported in the literature for vacuum deposited films on glass. Neither Smith's predictions or Goser's data, therefore, can be used to obtain any general definitive conclusions concerning the eddy-current linewidth for thin films.

Schlömann (1967) has calculated the eddy-current loss contribution
to the linewidth without invoking the assumptions which limited the
validity of Smith's earlier treatment. He considers the situation in
which the thin film forms part of the side wall of a microwave cavity
or transmission line (such as a ground plane of a stripline). The
microwave excitation field and the static magnetic field were taken to
be orthogonal and in the plane of the film. The extent to which the
electromagnetic field penetrates the film (the skin depth δ) depends
upon the applied field strength, since the microwave permeability μ
goes through a maximum at resonance ($\delta \propto \mu^{-\frac{1}{2}}$). Off resonance, the
penetration depth is larger than near resonance. The absorption is
therefore reduced near resonance (less of the film feels the microwave
excitation) and the net effect is a broadening of the absorption line.
For film thickness such that D is always much less than the skin depth
δ, eddy-current broadening is not important. For $D << \delta$, then, the
linewidth is determined almost completely by relaxation losses and the
absorption curve is Lorentzian, as predicted from the phenomenological
formulation of relaxation losses in section (3.2). When the film
thickness approaches or becomes greater than the on-resonance skin
depth, the absorption curve is broadened and is no longer Lorentzian.
The influence of film thickness on the shape and width of the FMR
absorption curve was obtained, in Schlömann's calculation, by
simultaneously solving Maxwell's equations with the proper boundary
conditions and the Landau-Lifshitz equation of motion for the magneti-

zation. Once the solutions for the electromagnetic modes of the

system were obtained, the absorption curve was extracted as the

imaginary part of the frequency for the solution which corresponds to

the uniform mode in the limit $D \to 0$ (in this limit, the r-f field is

uniform through the film so that the uniform mode criteria are

rigorously satisfied).

The algebraic details of the calculation are not of direct

interest here but the results will be important in the discussion to

follow in section (3.6). Schlömann obtains an absorption curve of the

form:

$$Im(\omega) = \{p \sinh(dp) - q \sin(dq)\}/\{\cosh(dp) - \cos(dq)\} \qquad (3.12)$$

where

$$p = \{(f^2+1)^{-\frac{1}{2}} + (f^2+1)^{-1}\}^{\frac{1}{2}},$$
$$q = \{(f^2+1)^{-\frac{1}{2}} - (f^2-1)^{-1}\}^{\frac{1}{2}},$$
$$d = D/D_o,$$
$$f = 2(H-H_{res})/\Delta H_o;$$

Here H_{res} is the field for resonance, ΔH_o is the linewidth in the

$D = 0$ limit (no eddy-current losses), and D_o is a characteristic thick-

ness given by

$$D_0 = (c/2)(2\pi\sigma\omega U)^{-\frac{1}{2}}$$

with
$$U = (4\pi M/\Delta H_0)\left\{1 + \left[1 + (2\omega/\omega_M)^2\right]^{-\frac{1}{2}}\right\}$$

where $\omega_M = 4\pi\gamma M$. Since the resonance losses are proportional to $Im(\omega)$,

the absorption curve is given by $Im(\omega)$ as a function of applied field.

From the absorption curve, the half-power linewidth can be determined

as the field separation of the points on the curve at half maximum.

Experimentally, a more convenient linewidth parameter for the present

purposes is the field separation for inflection points on the absorption

curve. Both are indicated as a function of normalized film thickness in

Fig.3-5. For very thin films, ΔH is quadratic in film thickness and the

lineshapes are Lorentzian. For thick films, the linewidth approaches

a constant value of about 2.4 times ΔH_0 (for the half-power linewidth).

For 80-20 Ni-Fe alloy films and resonance at 1-9 Gc/sec, $D_0 \approx 1000$ Å.

These predictions will be discussed in more detail in conjunction with

the experimental data in section (3.6).

In section (3.6), another aspect of the data will be discussed

which is directly relevant to the present discussion of eddy-current

losses. For thick films ($D \approx 5000$ Å), the observed linewidth is

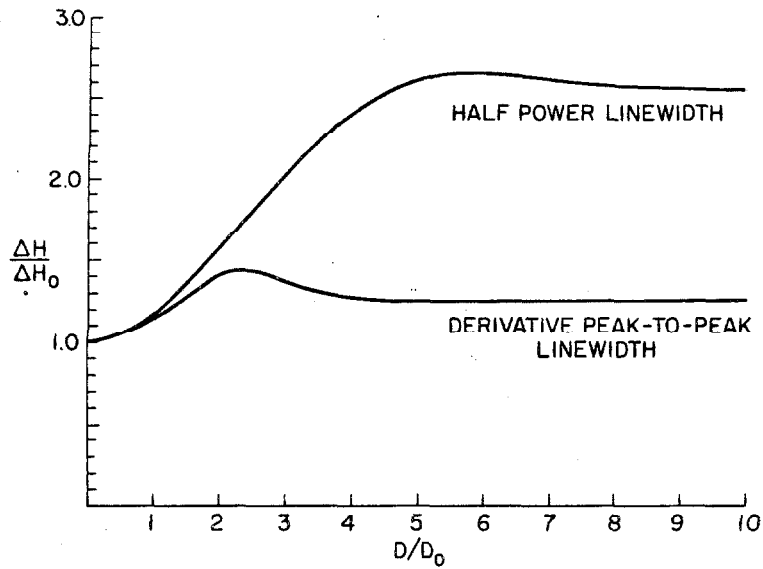sometimes highly asymmetric. A similar asymmetry in the resonance line-

Fig.3-5. Linewidth as a function of film thickness including eddy-current losses. The zero thickness linewidth ΔH_0 corresponds to no eddy-current losses. Both the half power linewidth and the derivative peak-to-peak linewidth are shown. The thickness parameter D_0 is about 1000 Å for 80-20 Ni-Fe alloy films and FMR from 1-9 Gc/sec.

shapes, observed for FMR in metal single crystals, has been associated

with the Ament and Rado (1955) exchange conductivity mechanism

(Rodbell, 1965). The Ament-Rado theory indicates that the asymmetric

broadening is a result of the exchange field produced by nonparallel

spins within the skin depth. Since exchange was neglected in

Schlomann's calculation, no asymmetry is predicted. Based on present

indications, however, it is entirely possible that exchange is important

for thick films $(D > 5000 \text{ Å})$. Both Schlömann's calculation and line-

width asymmetry will be discussed further in section (3.6). In closing

this discussion of eddy-current losses for FMR in thin films, it is

important to repeat the point, stated earlier, that for any eddy-

current process the linewidth should exhibit a temperature dependence

related to the temperature dependence of the conductivity.

Another class of loss mechanisms give rise to a linewidth tempera-

ture dependence in which the linewidth shows a peak as a function of

temperature. Two such processes, valence exchange and slowly-relaxing

impurity, are well known in connection with linewidth data in ferrites

and garnets (Yager et al., 1955; Teale and Tweedale, 1962) which exhibit

a large maximum below $100^{o}K$. These particular processes are of interest

because, as will be shown later, linewidth data for thin Ni-Fe films

exhibit a similar temperature dependence. It is appropriate to

summarize briefly the aspects of these processes which are relevant to

the present results.

Both processes depend on a coupling between the uniform mode and the electronic levels of the system. Valence exchange is important in high conductivity spinel ferrites where the coupling is primarily a combination of spin orbit coupling and crystalline electric field interactions between Fe^{2+} and Fe^{3+} ions. Impurity relaxation appears to be important for rare earth impurities in yttrium iron garnet where the coupling is exchange coupling between the iron lattice and the rare earth impurity ion. A quantitative analysis yields a contribution to the linewidth of the form (Sparks, 1964)

$$\Delta H_{TP} = C\omega t_r/(1 + \omega^2 t_r^2) \tag{3.13}$$

where C depends on the details of the particular process. The time constant t_r has a temperature dependence

$$1/t_r \propto e^{-\Delta E/KT}$$

where ΔE is a measure of the level splitting due to the coupling described above (0.1 eV $\leq \Delta E \leq 0.5$ eV for valence exchange; Smit, 1959, p.235). The maximum occurs at the temperature for which $\omega t_r = 1$. On the basis of the above discussion, two properties of the linewidth temperature dependence can be obtained. (1) The amplitude of the temperature dependence is constant, independent of frequency. (2) The peak in the linewidth is expected to shift to slightly higher temperature for increasing frequency. It has been mentioned several times previously

that effects similar to the predictions of these theories have been found in metal Ni-Fe alloy thin films. Several points must be kept in mind in applying these ideas to metals. First, it is necessary to establish the presence of the appropriate impurities or ions involved in the temperature peak process. Second, the role of the conduction electrons must be taken into account. The above discussion is appropriate for electronic transitions in insulators. In metals, the sea of conduction electrons which surrounds the relaxing ions or impurities conceivably has an effect on the relaxation process. These points will be considered in the discussion of the experimental results.

This section has been concerned with those processes which result in a temperature dependent linewidth and which appear to be relevant to the present data. Eddy-current processes have been considered in detail and both the thickness dependence and temperature dependence of the eddy-current linewidth have been discussed. In addition, several processes which result in a linewidth which exhibits a maximum as a function of temperature have been discussed briefly.

3.5 EXPERIMENTAL DETERMINATION OF THE LINEWIDTH

In this section, the experimental techniques and the instrumentation used in making the linewidth measurements will be described. This section will be considerably more brief than the corresponding experimental section in Chapter 2 on domain wall motion. The section on wall mobility measurements represented a major part of the previous chapter

because similar attempts at such measurements had proved unsuccessful. In contrast, linewidth measurement techniques for various resonance phenomena have become rather standard over the past decade and it is important only to present the aspects of the technique which are peculiar to this particular investigation.

A block diagram of the instrumentation is shown in Fig.3-6. A microwave oscillator drives a nonresonant stripline section containing the film. As the field is swept through resonance, the absorption curve is obtained using phase sensitive detection. The system can be discussed conveniently in three parts, concerning the microwave instrumentation, the field instrumentation, and the phase sensitive detection scheme.

Microwave power (about 5 mw) was supplied to the stripline from a bank of klystron sources covering the frequency range from 0.8 Gc/sec to 9.3 Gc/sec. Frequency was measured using a transfer oscillator and a high frequency counter. The stripline was designed to provide a good 50 Ω match with the input transmission line. A cross section of the stripline is shown in Fig.3-7. The ground plane spacing and the stripline dimensions were chosen to provide a 50 Ω impedence and a microwave excitation field uniform to better than 0.1% over the 1 cm diam film sample, which was placed directly under the center conductor against one ground plane. The impedance match provides for a large excitation field for resonance and r-f field uniformity is necessary to satisfy the

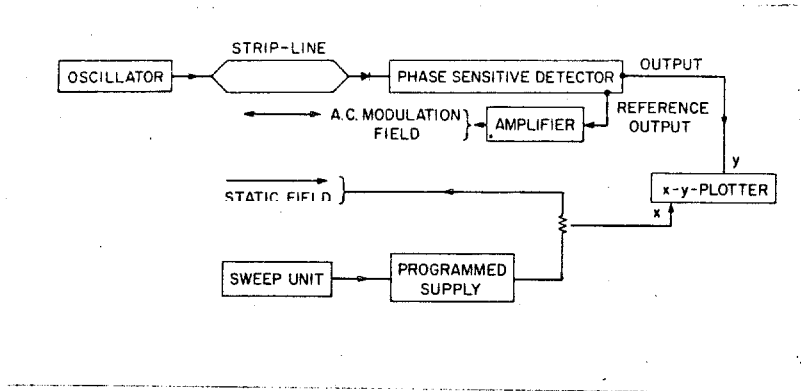

-150-

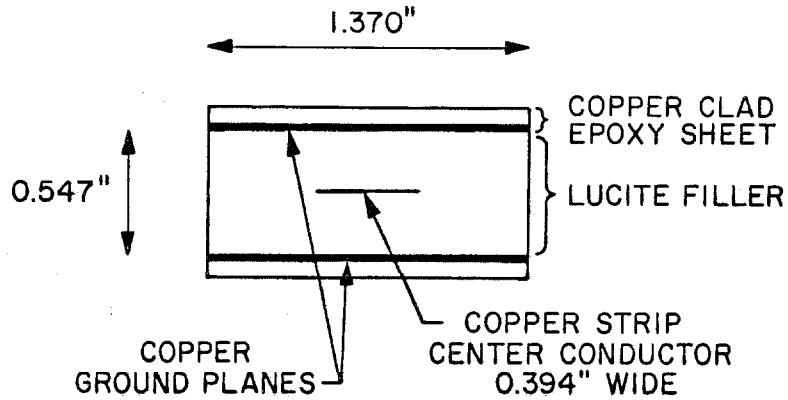Fig.3-6. Block diagram of the instrumentation for linewidth measurements.

Fig.3-7. Cross-section of the stripline section used to provide microwave excitation.

criteria for uniform mode resonance.

The static magnetic field for resonance was applied using a Helmholtz coil pair with a calibration constant of 53.0(±0.1) Oe/amp. Field calibration and homogeneity measurements were accomplished using a rotating coil gaussmeter. The homogeneity was better than 0.01% over the film. The static field was swept using a voltage ramp generator and a high current (20 amp) programmable power supply. The voltage across a 0.1 Ω 150 watt resistor in series with the field coils was used to sweep the field axis of the recorder used to plot the absorption curve. A second Helmholtz pair applied the 1 kc modulation field for use in the phase sensitive detection scheme. The peak-to-peak amplitude of the modulation field was nominally 0.5 Oe, much less than the smallest measured linewidth (3 Oe at 1 Gc/sec for D < 1000 Å).

The microwave power transmitted through the stripline was measured using a crystal detector and the output from the crystal was fed to a phase sensitive detector. The voltage output from the phase sensitive detector is proportional to the derivative of the absorption curve. This voltage was recorded as a function of static applied field using an X-Y recorder and a plot of the derivative of the resonance absorption curve was obtained. The time constant on the filter for the phase sensitive detector was nominally 100-300 msec and the sweep time for the field range covering the absorption line (nominally 5 to 50 Oe) was on the order of 3 minutes. Absorption curves taken for smaller time

constants and slower sweep rates were identical to those taken under the above conditions, so that these parameters did not introduce any significant distortion into the data.

The system shown in Fig.3-6 and described above can be seen to satisfy three requirements which are important in the present experiment. (1) The system involves few critical adjustments so that linewidth measurements can be made for a large number of films efficiently and rapidly. (2) The system is broadband and linewidth measurements can be made over a large frequency range. (3) The stripline section is compact and can be easily contained in a cyrogenic system so that low temperature linewidth measurements can be made. These points are concerned primarily with the stripline design which was touched on briefly in conjunction with the microwave instrumentation. The stripline is shown in Fig.3-8 with one ground plane removed. Several points are evident from the figure. First, changing films is a relatively simple operation. All that is required is the partial removal of one ground plane. (The film seats in the square slot in the center of the stripline in Fig.3-8.) Second, the film is mounted on a rotatable platform which forms part of the stripline dielectric and the platform can be rotated by means of an attached lever arm. Because the film samples exhibit a uniaxial anisotropy, the field for resonance is a function of film orientation with respect to the applied field and a mechanism to rotate the film _in situ_ by 90° is useful (the uniaxial anisotropy constant can be measured by FMR at different film orientations). Using the
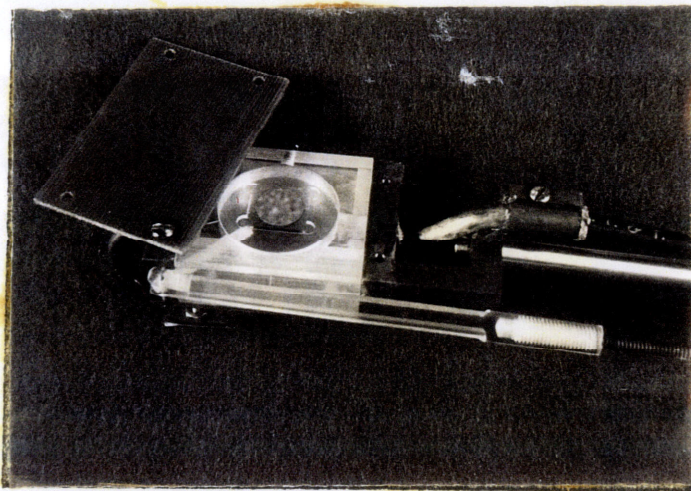
Fig.3-8. Photograph of stripline with one ground plane removed. A thin film is mounted in the square slot in the center of the stripline.

stripline design discussed above, FMR linewidth measurements were possible at frequencies up to 9 Gc/sec and for easy-axis orientations from 0° to 90° with the applied field. The sensitivity of the entire system was such that linewidth measurements could be obtained for films thinner than 100 $\mathring{A}$.

For measurements at low temperatures, the stripline sketched in Fig.3-7 and shown in Fig.3-8 was suspended in a double dewar cyrogenic system. Measurements could be performed from $2^{\circ}K$ to room temperature. Temperature measurements were made using a calibrated carbon resistor and a pulsed resistance bridge. For measurements between $300^{\circ}K$ and $77^{\circ}K$, the outer dewar was filled with liquid nitrogen and measurements could be made while cooling since the rate of cooling was only about $1.5^{\circ}K$ per minute. Similarly, measurements between $4.2^{\circ}K$ and $77^{\circ}K$ could be made as the system warmed up, since the warming rate after the helium level fell below the stripline was only about $1^{\circ}K$ per minute. Measurements below $4.2^{\circ}K$ were made by pumping on the liquid helium.

The usual linewidth measurement is the width of the absorption curve at half power (as discussed in the introduction). As indicated above, the instrumentation was such that the derivative of the absorption curve was obtained as a function of static applied field. From the data, the most convenient width measurement is the field separation between the peaks of the absorption derivative. This width measurement will be taken as what is meant by "linewidth" in the

remaining portion of this chapter. This linewidth can be converted to
the usual half-power linewidth by multiplying ΔH by $\sqrt{3}$, if the absorp-
tion curve is Lorentzian. For broader non-Lorentzian line shapes, the
correction factor is larger. The derivative peak-to-peak linewidth,
obtained using the instrumentation described in this section, is the
parameter on which the discussion of results in the next section is
based. Experimental linewidth determinations will be presented and
discussed in conjunction with the theoretical background developed in
the three previous sections.

3.6 LINEWIDTH AND RELAXATION PROCESSES

In this section linewidth data obtained using the instrumentation
described in section (3.5) are presented and discussed in terms of the
theoretical material developed in the previous three sections. This
investigation is one of the first to obtain and interpret thin film
linewidth data over a wide range of temperature, frequency, and film
thickness, even though the conclusions concerning physical relaxation
processes for FMR which are obtained from the present data are qualita-
tive. The details of the various physical processes which appear to
contribute to the linewidth are not developed since the primary purpose
of the present study is to obtain some indication as to what processes
are important. Such information should be extremely useful in evalu-
ating the validity of existing calculations, of which there are many,
and in guiding new (and hopefully correct) calculations. The discussion

centers around the three physical relaxation processes, two-magnon scattering, eddy-current losses, and temperature-peak processes. The phenomenological formulation of relaxation losses, two-magnon scattering and eddy-current losses are discussed in conjunction with the room-temperature data. Eddy-current losses and temperature-peak processes are discussed further in conjunction with the low temperature data. The results of the investigation are summarized in section (3.7).

3.6.1 Room Temperature Linewidth

Linewidth data for two hundred samples at 2 Gc/sec are shown as a function of thickness in Fig.3-9. One striking feature of the data is the large scatter in the measured linewidths for films which were all evaporated under nearly identical conditions as described in Chapter 2, section (2.4). Briefly, the films were evaporated from a melt of 80% Ni and 20% Fe using r-f induction heating, onto glass substrates at $300^{\circ}C$ in a moderate vacuum of 10^{-6} Torr, in the presence of a uniform magnetic field in the plane of the substrate. Film thickness was determined magnetically, using a 20-cps hysteresis loop tracer, and optically, utilizing the Tolansky multiple-beam interference technique (Tolansky, 1948). Linewidth measurements were made using the technique described in the previous section and the linewidths could be determined to better than 5%. The scatter evident in Fig.3-9 cannot be due to experimental error.
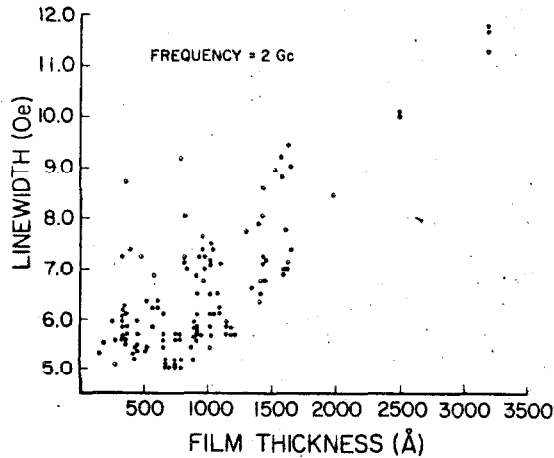
Fig.3-9. Ferromagnetic resonance linewidth as a function of film thickness for Ni·Fe alloy films at 2 Gc/sec with the static field in the film plane.
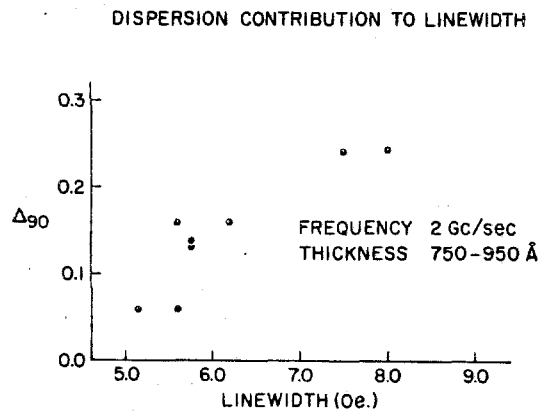

Fig.3-10. Correlation between the dispersion parameter Δ_{90} and the 2 Gc/sec FMR linewidth for films 750 to 950 Å thick.

Recently, Nelson (1964) has performed an extensive investigation of
the influence of anisotropy dispersion on the linewidth for thin films.
His results indicate that the quality of individual film samples is
extremely important. In order to examine the influence of anisotropy
dispersion on the scatter in the present data, measurements of the
magnitude dispersion of the uniaxial anisotropy were made for a number
of films with thickness between 750 $\overset{o}{A}$ and 950 $\overset{o}{A}$, the range in Fig.3-9
where the largest amount of linewidth scatter is evident
(5 Oe $< \Delta H <$ 9.5 Oe). An approximate measure of the dispersion was
obtained using a torque magnetometer (Humphrey and Johnston, 1963) and
a technique developed by Hasegawa et al. (1964). In Fig.3-10, Δ_{90}
(a dispersion parameter which is roughly a measure of the fractional
film volume with a local H_k different from the average H_k by more than
10%) is displayed as a function of linewidth for films 750 to 950 $\overset{o}{A}$
thick. The correlation is quite good. Films with large anisotropy
dispersion have broad resonance linewidths. Extrapolated to Δ_{90} = 0
(no anisotropy dispersion), from Fig.3-10 the zero dispersion linewidth
can be seen to correspond to about 5 Oe, which is the smallest linewidth
indicated in Fig.3-9. It therefore appears that the scatter in the
linewidth data of Fig.3-9 can be explained on the basis of anisotropy
dispersion.

At the start of this discussion it was emphasized that the film
samples were prepared under nearly identical conditions. If the films
are nearly identical, except for thickness, what is the origin of the

large linewidth fluctions and the large range of anisotropy dispersion with which these fluctuations have been connected? No definite or conclusive answer to this question is presently possible but several remarks are in order. First, for a number of films in the same range of thickness the linewidths for older films tend to be larger than the linewidths for freshly evaporated samples. Second, for the films corresponding to the data in Fig.3-9, small reductions in the linewidths ($\approx$ 1 0e) for those films with the larger linewidths could be accomplished by annealing the samples in a hydrogen atmosphere at 150°C with a 50 0e easy-axis field. Linewidth increases resulted from similar treatments in air. From the first remark, it is evident that the linewidth and dispersion are related to some film aging process. From the second, this aging process is apparently connected with oxidation-reduction effects. These hydrogen and oxygen annealing treatments will be discussed in more detail in the next part, in connection with the low temperature data.

In order to minimize the contribution of dispersion to the linewidth, samples which exhibited the smallest linewidth were selected for each thickness. These linewidths correspond to the lower boundary of the experimental data in Fig.3-9. This selection is analogous to the procedure in Chapter 2 on wall motion where the upper boundary of the mobility data was taken to represent the relaxation-loss-limited mobility. Both selection procedures attempt to eliminate the contribution of film imperfections to the dynamic process under investigation.

By virtue of the large number of films examined, the selection
procedure provided an accurate determination of the linewidth in the
ideal film limit. The remaining portion of this section will be con-
cerned with films corresponding to the lower boundary of the data in
Fig.3-9, the so-called minimum linewidth samples.

As discussed in section (3.2), a phenomenological formulation
based on the Landau-Lifshitz or Gilbert equation can be applied to FMR
and the damping parameter can be obtained from

$$\Delta H = (\Delta H)_o + (2\alpha\omega/\gamma)(1/\sqrt{3}).$$
(3.14)

The $(1/\sqrt{3})$ factor is due to the fact that the data yield derivative
linewidths and not half-power linewidths. Linewidth measurements have
been made for the minimum linewidth samples as a function of frequency
from 1 to 9 Gc/sec. Data for a 280 Å film are shown in Fig.3-11. The
linewidth increases linearly with frequency and extrapolates to $\approx$ 1 Oe
for zero frequency. This frequency dependence is in good agreement
with Eq.(3.1). Similar data have been obtained for all of the minimum
linewidth samples corresponding to the lower boundary of the data in
Fig.3-9. By fitting the data to Eq.(3.1), the damping parameter α was
evaluated as a function of film thickness and the results of this
evaluation are shown in Fig.3-12. The phenomenological damping parame-
ter for ferromagnetic resonance with the static magnetic field in the
plane of the film increases linearly with film thickness from 0.005 at
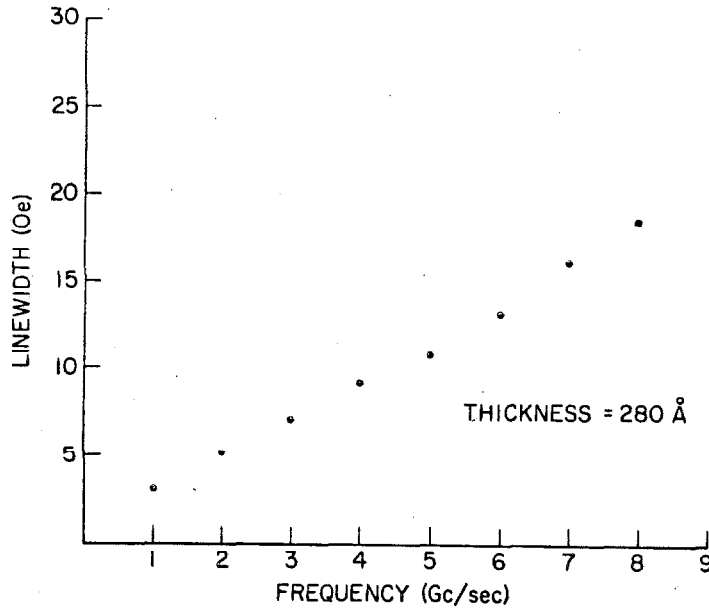250 Å to 0.009 at 2500 Å. It should be emphasized that these numerical

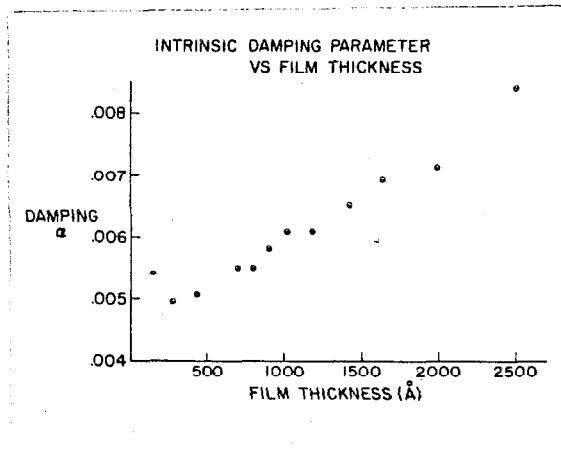Fig.3-11. Linewidth as a function of frequency at 300°K.

Fig.3-12. Damping parameter as a function of film thickness determined from Eq.(3.5).

values for α (resonance) are significantly lower than the value for wall motion, $\alpha = 0.014$. Moreover, α (resonance) exhibits a definite increase with thickness while α (wall motion) in independent of thickness. (See Chapter 2.) Therefore, the physical relaxation processes involved in wall motion are not identical with those which are important for FMR relaxation.

The minimum linewidth data indicate that the losses for FMR in thin films increase with thickness. This conclusion is apparent from the minimum linewidth data in Fig.3-9 and the thickness dependence of the phenomenological damping parameter extracted from the frequency dependence of the data (Fig.3-12). Two-magnon scattering and eddy-current losses are physical loss processes which correspond qualitatively to this behaviour. Both mechanisms predict an increase in the resonance losses with thickness.

The minimum linewidth data of Fig.3-9 is not in agreement with the quantitative predictions of Schlömann's eddy-current calculation. For FMR at 2 Gc/sec in 80-20 Ni-Fe films with a resistivity of 16 $\mu\Omega$-cm (corresponding to a conductivity of 0.45×10^{17} sec^{-1}), the transition thickness D_0 in Schlömann's calculation of section (3.4) is 800 Å. From Fig.3-9, the zero thickness linewidth ΔH_o is 5 Oe. From these parameters and Schlömann's linewidth vs thickness curve in Fig.3-5, the linewidth is expected to exhibit a peak at about 2600 Å film thickness and level off at about 6.25 Oe for thicker films. The lower boundary

of the linewidth data increases monotonically from 5 Oe at 800 $\overset{o}{A}$ to a

value greater than 11 Oe at 3000 $\overset{o}{A}$, in complete contradiction with the

behaviour expected on the basis of eddy-current losses. Eddy-current

losses clearly cannot explain the present data.

A more reasonable explanation of the data is based on two-magnon

scattering, which was discussed in detail in section (3.3). Two-magnon

scattering is a process in which a uniform mode magnon at frequency ω_u

scatters into another magnon at the same frequency but with $k \neq 0$. For

film thickness less than some frequency dependent critical value D_ω,

magnons with $k \neq 0$ at ω_u do not exist and two-magnon scattering is not

allowed. For thicker films, the density of magnon states degenerate

with the uniform mode increases with thickness and approaches the bulk

limit for extremely thick films ($D > 6000 \overset{o}{A}$). On the basis of two-

magnon scattering, the linewidth should be independent of film thickness

for $D < D_\omega$ and increase monotonically with thickness for

$D_\omega < D < 5000 \overset{o}{A}$. For thicker films, the linewidth should be indepen-

dent of film thickness.

As can be seen from Fig.3-9 the thickness dependence of the

minimum linewidth data is qualitatively consistent with the dependence

predicted by two-magnon scattering. To further investigate this

point, linewidth data for the minimum linewidth samples were obtained

at frequencies from 1 to 7 Gc/sec. These data are shown in Fig.3-13.

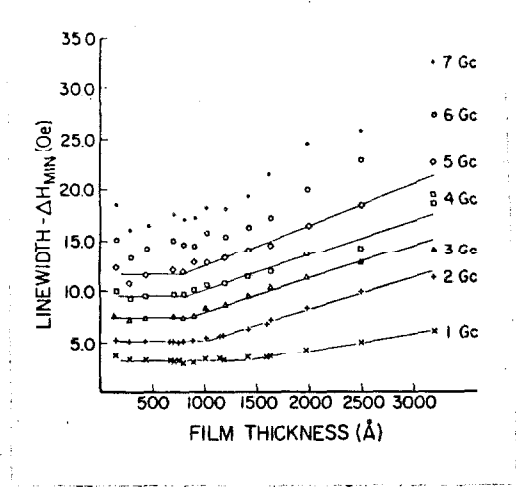As indicated by the solid lines, the linewidth is independent of thick-

Fig.3-13. Minimum linewidth for a specified film thickness as a function of film thickness for Ni-Fe alloy films with the static field in the film plane, for FMR from 1 to 7 Gc/sec.
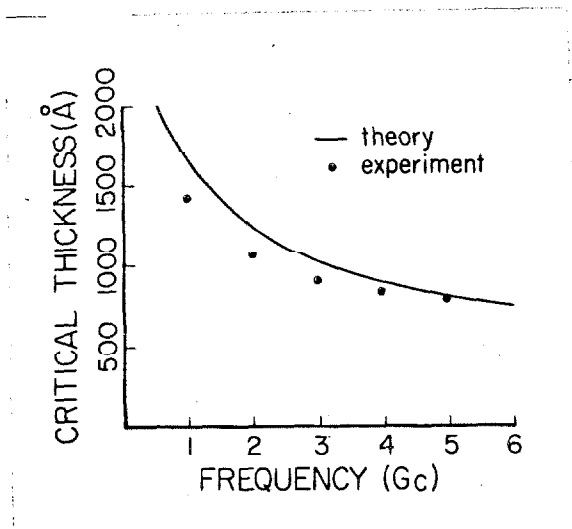

Fig.3-14. Calculated and experimental values of the critical thickness for two-magnon scattering as a function of uniform mode frequency. The theoretical curve was calculated using an exchange constant $A = 10^{-6}$ erg/cm and a saturation flux density $4\pi M$ of 10^4 Gauss.

ness for D less than some critical thickness and increases with thickness for thicker films. The critical thickness is clearly frequency dependent and shifts to smaller values for increasing frequency. The theoretical critical thickness D_ω can be calculated from the spin-wave dispersion relation for thin films, as discussed in section (3.3), and compared with the experimental values corresponding to the break points in the data of Fig.3-13. This comparison is shown in Fig.3-14. The theoretical and experimental values of the critical thickness are displayed as a function of frequency. The agreement between the break-points for the minimum linewidth data and the predictions based on two-magnon scattering is quite good.

Scattering will occur from uniform precession magnons to degenerate magnons corresponding to spin waves with wavelengths on the order of the dimensions of scattering centers. The only scattering centers which can be of importance for two-magnon scattering must be larger than about 1000 Å in size. Berteaud and Pascard (1965) have proposed that the edges of the film serve as scattering centers for two-magnon scattering, in much the same way that surface pits are scattering centers for FMR in YIG spheres. This proposal has been tested in a very straightforward manner by selecting a film thickness and a frequency where two-magnon scattering gives a large contribution to the linewidth, and scratching through the film with a diamond scribe to increase the effective edge length in the sample. The results of such an experiment are shown in Fig.3-15. By scratching through a 1600 Å film with a diamond scribe,

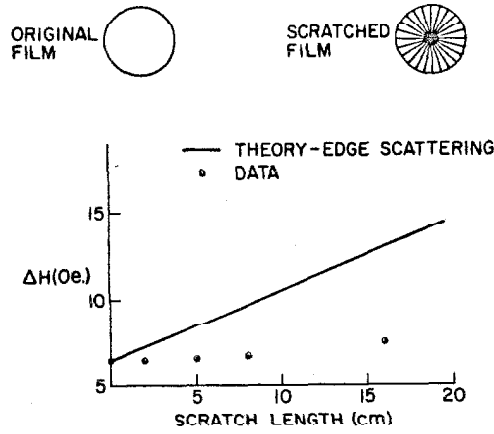Fig.3-15. Linewidth for a 1600 Å film at 2 Gc/sec as a function of
effective edge (or scratch) length in the film. The edge length was
increased by scratching through the film with a diamond scribe.

the effective edge length was increased by 600% with only a 15% increase in the linewidth at 2 Gc/sec. Therefore the two-magnon process connected with the linewidth thickness dependence is not associated with inhomogeneous scattering at the film edges. If edge scattering is not important, as these results indicate, the inhomogeneities which are responsible for the scattering are not understood. The obvious film inhomogeneities (such as surface irregularities, crystallites, grain boundaries, and dislocations) are all much smaller than required for a large scattering amplitude. However, the density of these inhomogeneities is extremely high in polycrystalline, evaporated films, and it is entirely possible that the total scattering amplitude is large, in spite of the small probability for a single interaction. In any case, the important point to be made here is that the nature of the inhomogeneities responsible for two-magnon scattering is not completely understood.

It would be misleading to close this discussion of the room temperature data without noting that: (1) the theoretical basis for two-magnon scattering is not as sound as indicated by Fig.3-14, and (2) it appears, on the basis of preliminary data, that two-magnon scattering is not the only contribution to the linewidth thickness dependence. Although the evidence for two-magnon scattering is extremely convincing, several minor difficulties still exist. The evidence consists primarily of the good agreement between the calculated critical thickness values and the observed break points in the thickness dependence of the

minimum linewidth data. The theoretical D_ω values were calculated on the basis of a very crude model. Recently, Harte (1964) has calculated a modified spin-wave manifold for thin films which could form the basis for a precise density-of-states calculation for degenerate two-magnon scattering. Qualitatively, Harte's results indicate that the theoretical D_ω values should be lower than indicated by the theoretical curve in Fig.3-13 and that the transition should be considerably less sharp than indicated by the solid lines in Fig.3-13. Both of these points are supported by the present data. The D_ω data indicate that the transition is lower than shown by the theoretical curve (Fig.3-14). The minimum linewidth data show that the transition from no thickness dependence to a monotonic increase with thickness is not sharp.

Preliminary data indicate that the linewidth does not continue to increase with thickness for films thicker than 6000 Å but levels off and is essentially constant. These results are consistent with two-magnon scattering, except that the lineshapes are sometimes asymmetric. Such asymmetry is characteristic of lineshapes for FMR in bulk single crystal iron whiskers and nickel platelets which have been successfully correlated with the Ament-Rado (1955) exchange conductivity mechanism (Rodbell, 1965). In other words, eddy-current effects appear to be important for extremely thick films. Exchange-conductivity will be discussed further in the next part. While the present data clearly constitute sound evidence for the importance of a two-magnon relaxation process for FMR in thin films, other processes also appear to be impor-

tant.

3.6.2 Linewidth Temperature Dependence

By measuring the linewidth as a function of frequency for different temperatures, the temperature dependence of the damping parameter α can be obtained. In Fig.3-16, linewidth data as a function of frequency are shown at 300°K, 77°K, and 4.2°K. At all frequencies, the linewidth is larger at 77°K than at the two extremes. The data in Fig.3-15 are typical of films from 150 $\overset{\circ}{A}$ to 3000 $\overset{\circ}{A}$ thick. The linewidth increase at 77°K was generally larger in thinner films, but in all cases the slope of the linewidth vs frequency curve was nearly temperature independent. Since α is proportional to the slope of the data (Eq.(3.1)), it appears that the damping is extremely insensitive to temperature between 4.2°K and 300°K even though the linewidth exhibits a definite temperature dependence.

These data indicated that the linewidth exhibits a significant temperature dependence which is not reflected in the damping parameter α of Eq.(3.1). In order to obtain a more accurate picture of this dependence, the linewidth for a 150 $\overset{\circ}{A}$ film was obtained as a function of temperature from 4.2°K to room temperature, at 2, 4, and 6 Gc/sec. These data are shown in Fig.3-17. Linewidth data at 2 Gc/sec could not
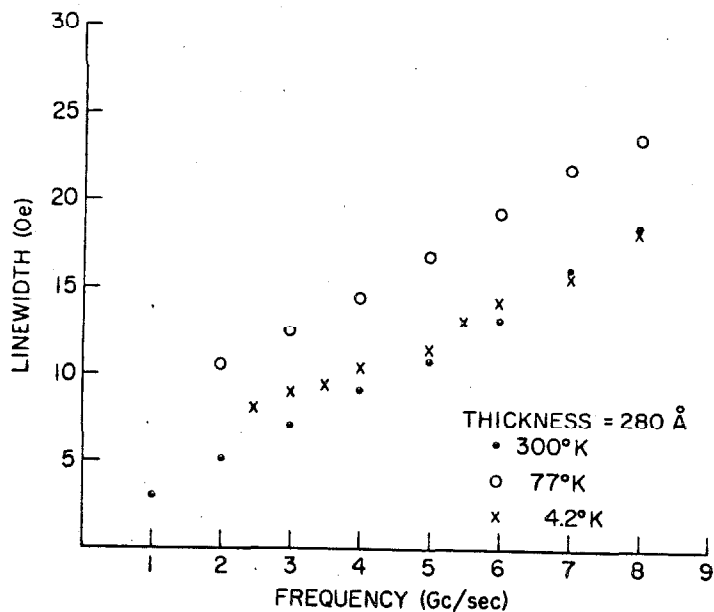
Fig.3-16. Linewidth as a function of frequency for a 280 Å film at 300°K, 77°K, and 4.2°K.
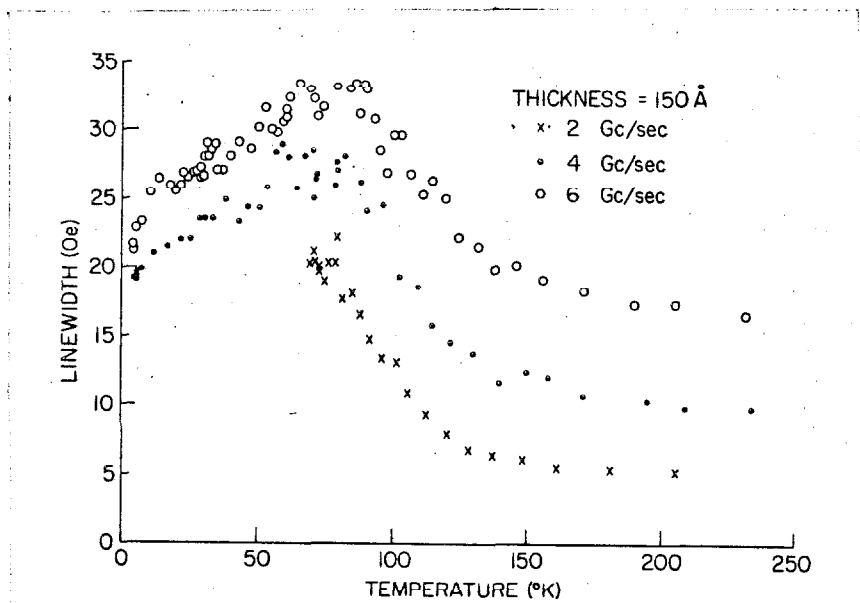

Fig.3-17. Linewidth as a function of temperature for a 150 Å film at 2,4, and 6 Gc/sec.

be obtained below 70°K.* For the other two frequencies, the linewidth

exhibits a maximum in the vicinity of 80°K. For all frequencies, the

linewidth is almost independent of temperature down to about 150°K,

increases rapidly below 150°K to a maximum in the vicinity of 80°K,

and decreases again for lower temperatures. It should be noted that the

amplitude of the linewidth peak is almost constant, independent of

frequency. Also, the temperature at which the maximum occurs appears

to shift to slightly higher temperature with increasing frequency.

These two features are characteristic of the linewidth temperature

dependence predicted by two well known temperature peak-processes,

valence exchange and impurity relaxation, discussed in section (3.4).

Before considering temperature-peak processes, however, it is

important to dismiss eddy-current losses as a possible explanation of

these data. From Schlömann's calculation of the eddy-current losses for

FMR, in the situation where the film thickness is much less than the

skin depth, the resonance linewidth due to eddy-current losses is

linearly proportional to the frequency and film conductivity, and is

quadratic in film thickness. None of these dependences are consistent

---

* The disappearance of the 2 Gc/sec resonance below 70°K may be
associated with the anomalous increase in the anisotropy field at low
temperatures reported by Mitchel and Briscoe (1966). However, the
anisotropy increase should shift the hard-direction resonance to higher
field and it should still be observable. Both the easy- and hard-direc-
tion resonances disappeared off the low end of the field sweep at
temperatures below 70°K.

with the present data. If the temperature dependence were due to eddy-current losses, the linewidth change between two fixed temperatures should increase with frequency. In addition, if eddy-current losses were important, the linewidth vs temperature curve should have the same shape as the conductivity vs temperature curve, which is inversely proportional to temperature down to about $100^{\circ}K$ and levels off for lower temperature. The conductivity does not exhibit a maximum as a function of temperature as do the present data. Finally, the change in linewidth with temperature should be larger for thicker films, not smaller. These data substantiate the conclusion obtained from the room temperature data. Eddy-current losses do not contribute significantly to the linewidth for thin films thinner than about 3000 $Å$.

The linewidth temperature dependence of Fig.3-16 is quite similar to that predicted by valence exchange and slowly relaxing impurity processes. Several difficulties occur in applying either of these two theories to the present data. If an impurity-relaxation mechanism is to be taken seriously, a quantitative understanding of the contribution of specific impurities to the peak in linewidth is required. In previous applications of this process to relaxation in ferromagnetic insulators, the only relevant impurities (in the theoretical treatments) have been rare earth ions. The presence of rare earth impurity ions in the proper crystalline environment to make an impurity-relaxation process possible appears to be highly unlikely. Admittedly, evaporated Ni-Fe alloy films are very imperfect and dirty structures,

containing many foreign substances. In order to make any conclusive
connection between the present data and a slowly relaxing impurity
process, it will be necessary to isolate the relevant impurities and
determine their role in the relaxation. On the other hand, an explana-
tion based on valence exchange must provide for the formation of the
appropriate ions in the proper crystalline environment for charge
transfer to occur. In addition to these problems, possible modifica-
tions of the theory for the various temperature-peak processes due to
the presence of conduction electrons must be considered. It is one
thing to passively call attention to the similarity between the present
linewidth data and the linewidth predictions based on known temperature-
peak processes and it is quite another to substantiate quantitatively
any connection between the two. To do so would involve a much better
knowledge of the film properties which influence the temperature depen-
dence of the linewidth than is now available.

A starting point in obtaining a better understanding of the specif-
ic film properties which influence the temperature-peak effect is with
the observation that the effect is larger for thinner films. Another
influential factor is the age of the film. A larger increase in from
$300^{\circ}K$ to $77^{\circ}K$ occurs in old films (several years) than in freshly
evaporated samples. These two observations indicate that some form of
surface contamination may be connected with the linewidth behaviour,
such as oxidation or diffusion of impurities through the film surface.
For this reason, the influence of two annealing treatments on the line-

width change from $300^{\circ}K$ to $77^{\circ}K$ $(\Delta H_{77^{\circ}K} - \Delta H_{300^{\circ}K})$ was investigated. The initial objective was to attempt to control the contamination in such a way that some understanding of the process could be obtained from the annealing data.

The first annealing treatment consisted of simply heating the film to $150^{\circ}C$ in a poor vacuum of 10^{-3} Torr, with an applied field of 50 Oe in the plane of the film along the easy axis. It was hoped that this vacuum annealing procedure would slow the contamination sufficiently, compared to annealing at atmospheric pressure, so that the increase of $(\Delta H_{77^{\circ}K} - \Delta H_{300^{\circ}K})$ could be observed at progressive stages of the process. If the linewidth enhancement were due simply to volume diffusion through the film surface, from a simple analysis of diffusion through a plane surface of fixed impurity concentration, one would expect the time required for the enhancement to saturate to vary as the square of the film thickness. In Fig.3-18, the linewidths at $77^{\circ}K$ and $300^{\circ}K$ are shown as a function of annealing time for films 190, 290, and 1350 $\mathring{A}$ thick. The enhancement in the $77^{\circ}K$ linewidth above the room temperature value is greatest for the thinnest sample, but the saturation time for the enhancement is about 80 hours for all three films. The saturation time is clearly not quadratic in thickness. The change in linewidth in going from $300^{\circ}K$ to $77^{\circ}K$ is enhanced by vacuum annealing but the enhancement is not the result of a volume diffusion process. If the enhancement is due to contamination, a surface effect, not a volume effect, must be important.
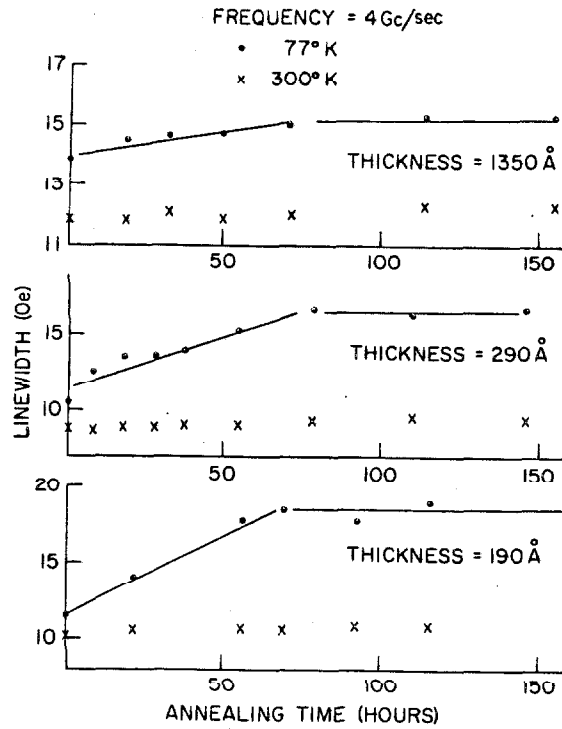
Fig.3-18. Linewidth data (4 Gc/sec) at 77°K and 300°K for three films, 190 Å, 290 Å, and 1350 Å thick, as a function of annealing time at 150°C in a vacuum of 10^{-3} Torr with a 50 Oe field along the easy axis.

The second annealing procedure which has been investigated could be better termed an oxidation-reduction treatment. The film was heated to about $150^{\circ}C$ in a hydrogen atmosphere (reduction) or in air (oxidation) with an applied field of 50 Oe along the easy axis. In Fig.3-19, the linewidths at $77^{\circ}K$ and room temperature are shown after successive oxidation and reduction treatments. The first oxidation treatment for 12 hours increased $\Delta H_{77^{\circ}K}$ by over 2.0 Oe and had a much smaller influence on $\Delta H_{300^{\circ}K}$. Next the film was reduced for 10 hours. After this treatment, $\Delta H_{300^{\circ}K}$ and $\Delta H_{77^{\circ}K}$ were equal and almost 0.5 Oe lower than the initial room temperature linewidth. Heating the film in a hydrogen atmosphere at $150^{\circ}C$ for 10 hours, therefore, made the FMR linewidth independent of temperature and the temperature-peak effect was completely eliminated. As shown in the figure, repeated oxidation and reduction treatments produced the same result. Oxidation reproducibly enhanced the linewidth change from $300^{\circ}K$ to $77^{\circ}K$ and reduction made the effect vanish. The ease with which the linewidth enhancement can be accomplished and removed by alternate oxidation and reduction at low temperatures indicates that a surface effect is involved, consistent with the conclusions based on vacuum annealing. These data clearly indicate that the contamination process which causes the temperature-peak in the linewidth data reported here is associated with a surface layer, presumably an oxide layer.

Two possible mechanisms are suggested by the apparent importance of surface oxidation in producing the linewidth maximum as a function of
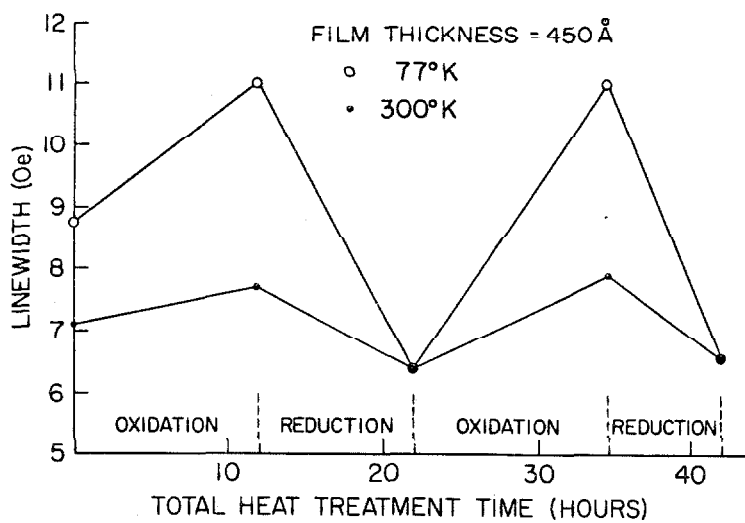
Fig.3-19. Linewidth data (4 Gc/sec) at 77°K and 300°K for a
450 Å film after successive oxidation and reduction treatments at 150°C
and atmospheric pressure in a 50 Oe easy-axis field.

temperature. Valence exchange, or the Fe^{2+} - Fe^{3+} charge transfer

mechanism, as discussed previously, is known to be an important relaxa-

tion process in high conductivity spinel ferrites which contain both

Fe^{2+} and Fe^{3+} ions on a single type of crystalline site. In Ni-Fe alloy

films, surface oxidation may well result in a similar situation. More-

over, if the relevant ions do result from the surface oxide layer, the

conduction electrons in the bulk of the metal film may have little

effect on the charge transfer relaxation. An alternate explanation of

the present temperature-peak data may be connected with an effect

which has not been mentioned heretofore and which, up to the present,

has been in no way associated with resonance relaxation —exchange

anisotropy. The motivation for making such an association here is two-

fold. First, the oxidation-reduction treatments discussed above are

very similar to the treatments discussed by Hagedorn (1967) in conjunc-

tion with his observation of anomalous hysteresis loops in Ni-Fe alloy

films at low temperatures. Hagedorn proposed the formation of an

antiferromagnetic oxide on the film surface and attributed the loop

behaviour to exchange anisotropy. Second, in several alloy systems, a

maximum in the rotational hysteresis loss as a function of temperature

is observed below $100^{O}K$ which has also been connected with exchange

anisotropy (Kouvel and Graham, 1959). The rotational hysteresis loss

for the Fe-FeO system also exhibits a rapid increase below $120^{O}K$

(Meiklejohn, 1958), similar to the increase in linewidth in Fig.3-15.

However, complete data at low temperatures are not available to show

whether there is a peak. It is entirely possible that exchange

anisotropy may also be connected with the linewidth data reported here.
It should be emphasized that this discussion of the possible importance
of these two processes for ferromagnetic relaxation in metal films is
only qualitative. The most important results of the present tempera-
ture study are: (1) the discovery of a temperature dependent linewidth
in thin films which exhibits a maximum in the vicinity of $80^{\circ}K$ and
(2) the identification of this dependence with a surface oxidation
process.

3.7 SUMMARY

In this chapter, the results of an extensive investigation of
ferromagnetic resonance linewidths and relaxation processes in thin
Ni-Fe films have been presented. The experimental results are pre-
sented and discussed in terms of the previous theoretical development.
It has been found that dispersion in the uniaxial anisotropy
has a considerable influence on the thin film linewidth. This disper-
sion contribution was minimized by simply selecting films in each
thickness range which exhibited the smallest linewidth. For these
minimum linewidth samples, the phenomenological damping parameter for
resonance at $300^{\circ}K$ increased with thickness, from about 0.005 at 400 Å
to 0.009 at 2500 Å, in contrast with the damping for wall motion which
was a constant (0.014) independent of thickness. The linewidth for the
minimum linewidth samples exhibits a very definite thickness dependence.
For film thickness less than a frequency dependent critical thickness
D_{ω}, ΔH is independent of thickness. For thicker films, ΔH increases

linearly with thickness. The observed D_ω values (about 1000 Å) are in good agreement with predictions based on magnon scattering involving spin waves degenerate with the uniform mode. Because of the magneto-static mode modification of the spin-wave dispersion relation for thin films there are very few spin wave states degenerate with the uniform mode for $D < D_\omega$ and magnon scattering cannot contribute significantly to the linewidth. The present data indicate that two-magnon scattering is important. Moreover, eddy-current losses cannot explain the observed room temperature linewidth data for $D < 3000$ Å. Preliminary evidence does indicate that eddy-current effects may be important for thicker films.

While the room temperature data provided some conclusions concerning relaxation mechanisms which had been previously proposed in connection with FMR in thin films, the low temperature data has provided some entirely new information concerning thin film resonance relaxation. The damping parameter extracted from the linewidth temperature dependence does not have any significant temperature dependence. The linewidth, however, does exhibit a distinctive and unexpected temperature dependence. The linewidth exhibits a maximum in the vicinity of 80°K and the effect is generally larger in thinner films. The amplitude of the linewidth temperature dependence is independent of frequency and the maximum shifts to slightly higher temperatures with increasing frequency. The amplitude can be enhanced by heating the film at 150°C in air (oxidation) and removed by a similar treatment in hydrogen

(reduction). The enhancement removal cycle can be repeated reproducibly. The time required for saturation of the enhancement when the oxidation treatment was performed in a poor vacuum of 10^{-3} Torr was observed to be independent of film thickness, indicating that a volume diffusion process is not involved. The apparent importance of surface oxidation suggests two possible mechanisms, valence exchange and exchange anisotropy, which may contribute to the linewidth temperature dependence. The relevant aspects of these processes are discussed. The discovery of a temperature dependent linewidth in thin films which exhibits a maximum in the vicinity of 80°K and the identification of this dependence with a surface oxidation process are the primary results of this low temperature study.

Chapter 4. <u>WALL</u> <u>MOTION</u> <u>AND</u> <u>FERROMAGNETIC</u> <u>RESONANCE</u> - <u>A CONNECTION</u>

From the phenomenological formulation of the losses for wall motion
and FMR presented in the previous two chapters, it would appear that the
correlation between the two processes is extremely poor. Damping param-
eters at room temperature for the two processes are shown as a function
of film thickness in Fig.4-1. For wall motion, the damping parameter is
a constant, independent of film thickness. For resonance, the damping
is a linear function of thickness and is significantly smaller than the
wall motion damping parameter. In spite of this apparent lack of corre-
lation, at least some of the losses which contribute to the FMR line-
width also influence the domain wall mobility. The correlation is only
qualitative and in no sense can be taken to imply that the total relaxa-
tion process is the same for both phenomena. The fact that the phenomeno-
logical approach gives different results for wall motion and FMR is
dramatic proof that the losses are not identical. Some, but not all, of
the relevant relaxation processes contribute to both phenomena.

The basis for the present correlation is the temperature dependence
of the FMR linewidth. As discussed in Chapter 3, the linewidth at 77°K
could be significantly enhanced over the room temperature value by means
of an oxidation treatment. In addition, a reduction treatment could be
used to render the linewidth temperature independent. In other words,
a procedure was available to make the resonance losses greater at 77°K
than at 300°K or to make the losses at both temperatures identical. A
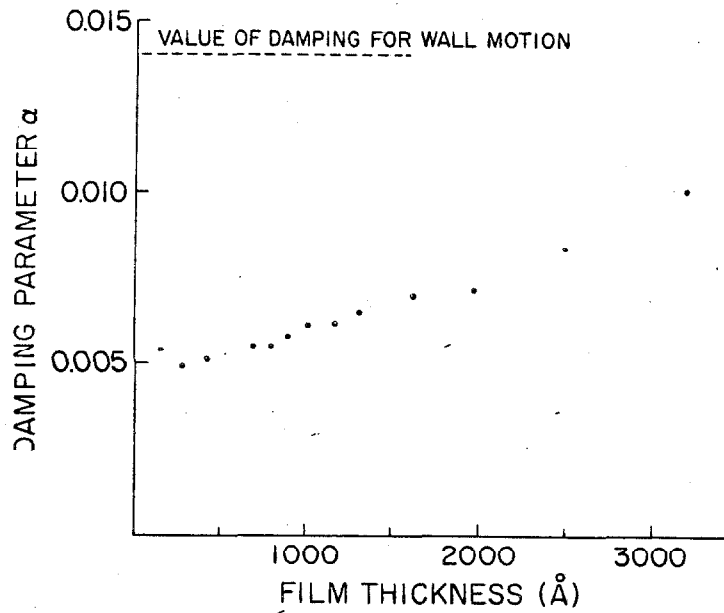
Fig.4-1. Damping parameter as a function of film thickness for domain wall motion and ferromagnetic resonance.
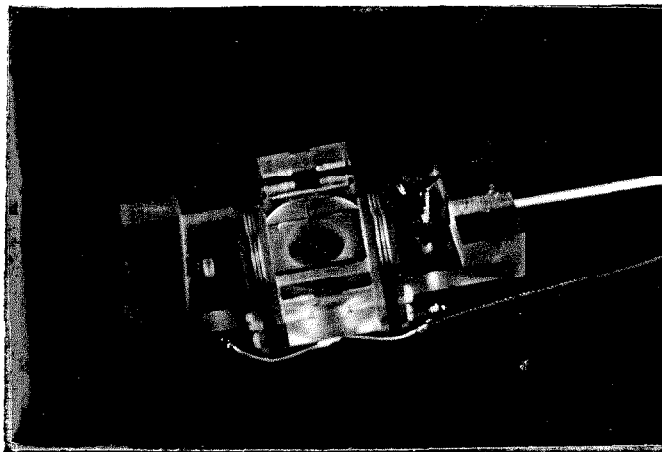

Fig.4-2. Switching apparatus for mobility measurements at low temperature.

clear test for a correlation between the losses for wall motion and the

losses for resonance would be to measure the domain wall mobility for

a number of films in both categories at 300°K and 77°K. If there is a

correlation between the losses associated with the two phenomena, films

which exhibited a significant linewidth enhancement at 77°K compared to

the room temperature value should show a reduced wall mobility at 77°K

compared to the mobility at 300°K, and films for which the linewidth

did not change should have the same mobility at both temperatures.

In Chapter 2, a technique for measuring domain wall velocity in

thin films was described in detail. The technique was based on static

wall observations utilizing the Kerr magneto optic effect. Such an

optical technique is not easily adaptable to use at 77°K where the film

must be immersed in liquid nitrogen. On the other hand, a considerable

amount of information pertaining to wall motion can be obtained without

directly observing the domain walls using the Kerr effect. As shown by

Copeland and Humphrey (1963), switching data for flux reversal by domain

wall motion can be related to the wall mobility if the wall configura-

tion during flux reversal is known. If switching data is taken at

different temperatures, the ratio of the wall mobilities at the two

temperatures can be obtained directly from the data. No knowledge of the

wall configuration is necessary. A modification of this technique was

first used by Patton and Humphrey (1964) in an investigation of the

effect of hard direction fields on the Néel wall mobility in 300 Å films.

The same technique is used in the present investigation, with temperature

as the variable instead of hard direction field.

Since the emphasis in this concluding chapter is on the connection between wall motion and resonance, the details of the technique used for low temperature mobility determinations will not be discussed. Only the general aspects of the technique will be touched on briefly. Even though the present description is quite brief, the successful use of it in making low temperature mobility measurements is a significant accomplishment, comparable to the technique described in Chapter 2 and many of the ideas presented in the section on wall mobility measurements in Chapter 2 are directly applicable.

The apparatus for such an experiment is shown in Fig.4-2. The small Helmholtz pair is used to apply a long duration easy-axis field pulse which switches the film from saturation antiparallel to this field to saturation along the field. For field amplitudes slightly larger than the coercive force, flux reversal will occur by wall motion. As this reversal proceeds, a voltage is induced in the pick-up coil beneath the film, similar to the winding discussed in section (2.4). An additional coil is connected in series to cancel pick-up due to the flux change during the rise time of the field pulse. The amplitude of the ramp function obtained by integrating the voltage pulse is proportional to the total magnetization reversed during the switching. The switching time can be conveniently defined as the 10% to 90% rise time for the integrated pick-up voltage. As reported by Copeland and Humphrey (1963),

plots of the inverse switching time as a function of easy-axis field

amplitude exhibit linear regions for small intervals of field amplitude

and the slopes of these linear sections are proportional to the wall

mobility. The proportionality constant involves the film geometry and

a knowledge of the wall configuration during flux reversal which, in

general, is not known. The ratios of slopes for switching curves taken

for a single film under slightly different conditions should correspond

to the ratio of wall mobilities for the two different conditions, if

the wall configurations were the same in both cases. A qualitative test

for this last requirement is to compare the shapes of the unintegrated

voltage pulses for flux reversal in each case. If the shapes are

similar, the wall configurations in each case are also similar. By

mounting the switching apparatus of Fig.2-2 in a dewar, measurements

could be made at 77°K as well as 300°K and the mobility ratio

$G(77^{\circ}K)/G(300^{\circ}K)$ could be obtained from the slopes of the two curves.

Since $G(300^{\circ}K)$, the mobility at room temperature, is known from the

investigation described in Chapter 2, it is a simple matter to calcu-

late $G(77^{\circ}K)$.

Using the above technique, switching data at 77°K and 300°K were

obtained for a number of films which exhibited linewidth increases at

77°K over the 300°K linewidth by amounts ranging from 2 to 16 Oe

(for $\Delta H_{77^{\circ}K} - \Delta H_{300^{\circ}K}$). From these switching data, the ratio of the

mobility at 77°K to the mobility at 300°K was obtained. The mobility

at 77°K was evaluated using this ratio and the room temperature mobility

data of Chapter 2. The correlation between the change in losses from $300^{\circ}K$ to $77^{\circ}K$ for wall motion and resonance is shown in Fig.4-3. The losses for wall motion are inversely proportional to the mobility so that $(1/G(77^{\circ}K) - 1/G(300^{\circ}K))$ represents the increase in the losses from $300^{\circ}K$ to $77^{\circ}K$. The losses for resonance are directly proportional to the linewidth so that $(\Delta H(77^{\circ}K) - \Delta H(300^{\circ}K))$ represents the increase in the losses from $300^{\circ}K$ to $77^{\circ}K$. The correlation between the loss increase in the two cases is quite good. Those films which exhibit an increase in the losses for resonance (in the form of a larger linewidth at $77^{\circ}K$) also exhibit an increase in the losses for wall motion (in the form of a reduced mobility at $77^{\circ}K$).

It appears, then, that the physical processes which contribute to the linewidth change also influence the domain wall mobility. In Chapter 3, the various physical mechanisms which may contribute to the linewidth increase were described in detail and it is not necessary to discuss them further here. The important point to be emphasized is that these same mechanisms, be they valence exchange, exchange anisotropy, or whatever, also appear to contribute to the losses limiting domain wall motion. Such a result is both surprising and satisfying. It is surprising because the form of the magnetization motion for wall motion and resonance are quite different. Wall motion is a large angle process in which a localized moving boundary (the wall) propagates through the film accompanied by a sequential rotation of the magnetization by 180°. Ferromagnetic resonance, on the other hand, represents an extremely small but uniform precessional

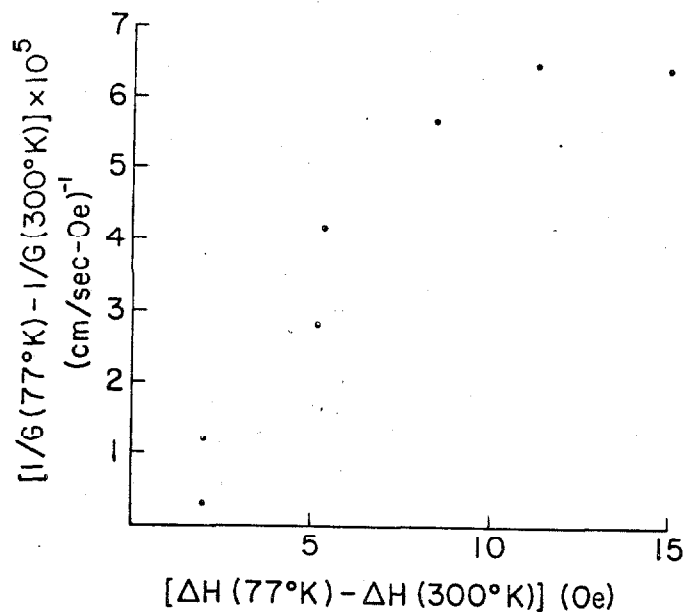Fig.4-3. Correlation between the change in the losses for wall motion $(1/G(77^\circ K) - 1/G(300^\circ K))$ and the change in the losses for resonance $(\Delta H(77^\circ K) - \Delta H(300^\circ K))$ between $300^\circ K$ and $77^\circ K$.

perturbation on a magnetic system which is completely saturated in the direction of an applied static magnetic field. It is surprising that some of the same physical relaxation mechanisms are important in both situations. The connection between the two processes is satisfying because it affords the possibility of understanding, in terms of physical relaxation phenomena, the mechanisms which limit wall motion as well as other modes of large angle flux reversal where previous understanding has been limited to a phenomenological formulation.

Chapter 5. <u>SYNOPSIS</u>

The objective of the present investigation has been three-fold:
(1) To characterize domain wall motion in thin ferromagnetic films
experimentally and to determine what film properties influence wall
mobility. (2) To investigate ferromagnetic resonance relaxation in
thin films over a wide range of temperature, frequency, and thickness
and to determine what physical relaxation processes contribute to the
resonance linewidth. (3) To correlate, as far as possible, the losses
for wall motion with relaxation processes for ferromagnetic resonance.

The domain wall mobility for Ni-Fe alloy films has been measured
over a wide range of film thickness (300 to 1600 $\overset{\circ}{A}$). The velocity mea-
surements were made using a quasistatic technique successfully for
the first time. The mobility determinations have been interpreted on
the basis of theoretical eddy-current loss calculations and a phenome-
nological formulation of relaxation losses, utilizing available static
wall shape information for domain walls in thin films. It has been
found that the eddy-current losses associated with wall motion are too
small to explain the observed wall mobilities and that only relaxation
losses are important. Furthermore, it has been found that the mobility
data can be explained on the basis of static wall shape information and
a constant value of the damping parameter in the phenomenological
equation of motion. Moving domain walls have very nearly the same
magnetization distribution as stationary walls. The present results

also indicate that the crossties and Bloch lines associated with domain walls in thin films have a negligible influence on the wall mobility. The initial results of this study indicated that Bloch walls in films are much wider than expected on the basis of simple calculations. This indication has been confirmed experimentally and correlated to the mobility data.

Ferromagnetic resonance linewidth data have been obtained in thin films over a wide range of temperature (4.2 - 300°K), frequency (1 - 9 Gc/sec), and thickness (100 to 3000 $\overset{o}{A}$). The linewidth has been successfully correlated with anisotropy dispersion in thin films. Treated phenomenologically, the linewidths are best described in terms of a damping parameter which increases with film thickness and is temperature independent. From the thickness and temperature dependence of the linewidth, it appears that eddy currents do not contribute to the losses for resonance, for films less than several thousand angstroms thick. The present data indicate the importance of two-magnon scattering in resonance relaxation. Several features of the linewidth thickness dependence are explained remarkably well on the basis of such scattering. For thicker films, eddy-current effects appear to be important. For a large number of films, the linewidth exhibits a peak as a function of temperature at about 80°K and the effect is larger for thicker films. Annealing experiments indicate that the temperature dependence is connected with the formation of an oxide layer on the film surface. Two possible mechanisms for this dependence are proposed,

valence-exchange and exchange anisotropy. The most important results of this resonance study are (1) the extensive amount of experimental linewidth data which are now available, and (2) the conclusions concerning the importance of two-magnon scattering, eddy-current losses, and temperature peak processes in resonance relaxation.

In addition to these two parallel but separate investigations of wall motion and resonance phenomena, an attempt has been made to connect the relaxation mechanisms for the two processes. An experiment has been devised to correlate the temperature dependence of the resonance linewidth with the temperature dependence of the wall mobility. Films which exhibit an increase in the losses for resonance from $300^{o}K$ to $77^{o}K$ also exhibit an increase in the losses for wall motion. The temperature-peak process connected with resonance relaxation is involved in the losses for domain wall motion as well. This connection between the two processes affords the possibility of understanding large angle flux reversal in terms of the physical relaxation mechanisms for ferromagnetic resonance where previous efforts have been limited to a phenomenological characterization.

APPENDIX

Solution for J_x: It is necessary to solve Eq.(2.17a) subject to two boundary conditions, one given by $(\partial J_x/\partial y)_{\text{film surfaces}} = h(x)$, and the other that J_x vanishes at $x = \pm\infty$. Since the range of the variable is $\pm\infty$ and the function vanishes at these limits, one can make use of Fourier transforms. Taking the Fourier transform of Eq.(2.17a) with respect to x, one obtains

$$\{\partial^2 \overline{J}_x(\zeta,y)/\partial y^2\} - \zeta^2 \overline{J}_x(\zeta,y) = 0. \tag{A.1}$$

Eq.(A.1) has a solution of the form

$$\overline{J}_x = A(\zeta)^{-\zeta y} + B(\zeta)e^{\zeta y}, \tag{A.2}$$

where $A(\zeta)$ and $B(\zeta)$ are arbitrary functions of ζ.

Applying the above boundary condition, and solving for $A(\zeta)$ and $B(\zeta)$, one obtains

$$A(\zeta) = -\overline{h}(\zeta)(e^{\zeta D}-1)/2\zeta \sinh(\zeta D) \tag{A.3}$$

and

$$B(\zeta) = -\overline{h}(\zeta)(e^{-\zeta D}-1)/2\zeta \sinh(\zeta D), \tag{A.4}$$

where

$$\overline{h}(\zeta) = \int_{-\infty}^{+\infty} h(x')e^{i\zeta x'}dx'.$$

Eq.(2.18a) is obtained by taking the inverse transform of $\overline{J}_x(\zeta,y)$.

Solution for J_y: It is necessary to solve Eq.(2.17b) subject to the boundary conditions that $\overline{J}_y$ vanishes at $y = 0$, $y = D$, and $x = \pm\infty$. A common technique of solving inhomogeneous partial differential equations is to obtain the Green's function which satisfies the equation

$$(\partial^2\Omega/\partial x^2) + (\partial^2\Omega/\partial y^2) = \delta(x-x') \tag{A.5}$$

subject to the given boundary conditions.

The solution is

$$\Omega(x,x',y) = \sum_{\text{odd } n} -(2D/n^2\pi^2)e^{-n\pi x'/D}e^{n\pi x/D} \sin(n\pi y/D) \text{ for } x < x'$$

$$\tag{A.6}$$

$$\Omega(x,x',y) = \sum_{\text{odd } n} -(2D/n^2\pi^2)e^{n\pi x'/D}e^{-n\pi x/D} \sin(n\pi y/D) \text{ for } x > x'.$$

Consequently, one obtains the solution to Eq.(2.17b).

$$J_y(x,y) = \int_{-\infty}^{+\infty} f(x')\Omega(x,x',y)dx'. \tag{A.7}$$

Eq.(2.18b) is obtained by substituting Eq.(A.6) into Eq.(A.7).

BIBLIOGRAPHY AND AUTHOR INDEX

E. Abrahams, Phys. Rev. 98, 387 (1955).

A.I. Akhieser, J. Phys. (USSR) 10, 217 (1946).

W.S. Ament and G.T. Rado, Phys. Rev. 97, 1558 (1955).

R. Becker, Proceedings of Grenoble Conference (1950).

R.E. Behringer and R.S. Smith, J. Franklin Inst. 272, 14 (1961).

A.J. Berteaud and H. Pascard, J. Appl. Phys. 36, 970 (1965).

F. Bitter, Phys. Rev. 38, 1903 (1931).

F. Bloch, Z. Physik 74, 295 (1932).

W.F. Brown and A.E. LaBonte, J. Appl. Phys. 36, 1380 (1965).

H.B. Callen, J. Phys. Chem. Solids 4, 256 (1958).

A.M. Clogston, H. Suhl, L.R. Walker, and P.W. Anderson, J. Phys. Chem. Solids 1, 129 (1956).

J.B. Comly, Scientific Report No. 5 (Series 3), Cruft Laboratory, Harvard University, Cambridge, Massachusetts, August, 1965.

J.B. Comly and T. Penney, Scientific Report No. 8 (Series 2), Cruft Laboratory, Harvard University, Cambridge, Massachusetts, December, 1963.

J.A. Copeland and F.B. Humphrey, J. Appl. Phys. 34, 1211 (1963).

R.W. Damon and J.R. Eshbach, J. Phys. Chem. Solids 19, 308 (1961).

R.W. DeBlois and C.D. Graham, Jr., J. Appl. Phys. 29, 931 (1958).

H.D. Dietze and H. Thomas, Z. Physik 163, 523 (1961).

J.F. Dillon, Jr., Bull. Am. Phys. Soc. 1, 125 (1956).

N.C. Ford, Jr., J. Appl. Phys. 31, 300S (1960).

C.A. Fowler and E.M. Fryer, Phys. Rev. 100, 746 (1955).

E. Fuchs, Z. Angew. Phys. 14, 203 (1962).

J.K. Galt, Phys. Rev. $\underline{85}$, 664 (1952).

T.A. Gilbert, Armour Research Foundation, Rept. No. 11, January 25, 1955 (unpublished).

K. Goser, Z. Angew. Phys. $\underline{18}$, 511 (1965a).

K. Goser, Arch. Elek. Ubertragung $\underline{19}$, 384 (1965b).

J.H.E. Griffiths, Nature $\underline{158}$, 670 (1946).

F.B. Hagedorn, J. Appl. Phys. $\underline{38}$, (1967).

K.J. Harte, Technical Report No. 364, Lincoln Laboratory, M.I.T., Lexington, Massachusetts, August 27, 1964.

R. Hasegawa, S. Uchiyama, and Y. Sakaki, Japan. J. Appl. Phys. $\underline{3}$, 671 (1964).

T. Holstein and H. Primakoff, Phys. Rev. $\underline{58}$, 1098 (1940).

E.E. Huber, D.O. Smith, J.B. Goodenough, J. Appl. Phys. $\underline{29}$, 294 (1958).

F.B. Humphrey and A.R. Johnston, Rev. Sci. Instr. $\underline{34}$, 348 (1963).

E.N. Il'icheva and I.S. Kolotov, Bull. Acad. Sci. USSR $\underline{29}$, 559 (1965).

T. Kasuya, Progr. Theoret. Phys. (Kyoto) $\underline{12}$, 802 (1954).

T. Kasuya and R.C. LeCraw, Phys. Rev. Letters $\underline{6}$, 223 (1961).

C. Kittel, Phys. Rev. $\underline{73}$, 155 (1948).

C. Kittel and E. Abrahams, Rev. Mod. Phys. $\underline{25}$, 233 (1953).

C. Kittel and A.H. Mitchell, Phys. Rev. $\underline{101}$, 1611 (1965).

J.S. Kouvel and C.D. Graham, Jr., J. Phys. Chem. Solids $\underline{11}$, 220 (1959).

A.E. LaBonte, thesis, University of Minnesota, Minneapolis (1966).

L. Landau and E. Lifshitz, Physik Z. Sowjetunion $\underline{8}$, 153 (1935).

F.E. Luborsky, Report No. 66-C-437, Information Sciences Laboratory, General Electric Company, Schenectady, New York, December, 1966.

W.H. Meiklejohn, J. Appl. Phys. $\underline{33}$, 1328 (1962).

N. Menyuk, J. Appl. Phys. <u>26</u>, 692 (1955).

S. Methfessel, S. Middelhoek, and H. Thomas, IBM J. Res. Develop. <u>4</u>, 96 (1960).

S. Middelhoek, thesis, University of Amsterdam, Holland (1961).

S. Middelhoek, IBM J. Res. Develop. <u>10</u>, 4 (1966).

E.N. Mitchell and C.V. Briscoe, J. Appl. Phys. <u>37</u>, 1489 (1966).

L. Néel, Compt. Rend. <u>241</u>, 533 (1955).

R.H. Nelson, J. Appl. Phys. <u>35</u>, 808 (1964).

H.J. Oguey, Rev. Sci. Instr. <u>31</u>, 701 (1960).

C.E. Patton and F.B. Humphrey, J. Appl. Phys. <u>35</u>, 921 (1964).

C.E. Patton and F.B. Humphrey, J. Appl. Phys. <u>37</u>, 1270 (1966a).

C.E. Patton, T.C. McGill, and C.H. Wilts, J. Appl. Phys. <u>37</u>, 3594 (1966b).

C.E. Patton and F.B. Humphrey, J. Appl. Phys. <u>37</u>, 4269 (1966c).

P. Pincus, M. Sparks, and R.C. LeCraw, Phys. Rev. <u>124</u>, 1015 (1961).

D.S. Rodbell, Physics <u>1</u>, 279 (1965).

T.D. Rossing, J. Appl. Phys. <u>34</u>, 995 (1963).

E. Schlömann, Phys. Rev. <u>121</u>, 1312 (1961).

E. Schlömann, APS Spring Meeting, Chicago, March 27-30, 1967.

J. Smit and H.P.J.Wijn, <u>Ferrites</u>, (John Wiley & Sons, Inc., New York, 1959).

D.O. Smith, J. Appl. Phys. <u>29</u>, 264 (1958).

D.O. Smith, <u>Magnetism</u>, G.T. Rado and H. Suhl, eds. (Academic Press, New York, 1963), Vol. III, Chap. 10, pp.506-7, 517.

D.O. Smith and K.J. Harte, J. Appl. Phys. <u>33</u>, 1399 (1962).

R.F. Soohoo, Proc. International Conf. on Mag., Nottingham 1964, p.852.

M. Sparks, thesis, University of California, Berkeley (1961).

M. Sparks, Ferromagnetic Relaxation Theory (McGraw-Hill, New York, 1964).

M. Sparks, R. Loudon, and C. Kittel, Phys. Rev. 122, 791 (1961).

P.E. Tannewald and M.H. Seavey, Jr., Phys. Rev. 105, 377 (1957).

R.W. Teale and K. Tweedale, Phys. Letters 1, 298 (1962).

S. Tolansky, Multiple Beam Interferometry of Surface Films (Oxford University Press, London, 1948).

E.J. Torok, A.L. Olson, and H.N. Oredson, J. Appl. Phys. 36, 1394 (1965).

L. Walker, Phys. Rev. 105, 390 (1957).

P. Weiss, J. Phys. 6, 661 (1907).

R.L. White and I.H. Solt, Phys. Rev. 104, 56 (1956a).

R.L. White, I.H. Solt, and J.E. Mercereau, Bull. Am. Phys. Soc., Sect.II 1, 12 (1956b).

H.J. Williams, W. Shockley, and C. Kittel, Phys. Rev. 80, 1090 (1950).

W.A. Yager, J.K. Galt, and F.R. Merritt, Phys. Rev. 99, 1203 (1955).